TÉCNICO LISBOA

Integration of Polymerase Chain Reaction in a Magnetoresistive Biochip

Mariana Soares Martins Antunes

Thesis to obtain the Master of Science Degree in

Bioengineering and Nanosystems

Examination Committee

Chairperson: Professor Luís Joaquim Pina da Fonseca

Supervisors: Professor Paulo Jorge Peixeiro de Freitas

Doctor Filipe Arroyo Cardoso

Members of committee: Professor João Pedro Estrela Rodrigues Conde

Professor Gabriel António Amaro Monteiro

June 2013

Agradecimentos

Em primeiro lugar ao Professor Paulo Freitas pela oportunidade de integrar a sua equipa de investigação no INESC MN e pôr em prática o conhecimento adquirido durante o meu Mestrado. Á Professora Susana Freitas pela orientação e conhecimento que me transmitiu ao longo deste trabalho. Ao Filipe Cardoso por todos os ensinamentos e paciência perante as minhas dúvidas. Obrigada pela boa disposição, optimismo e motivação constantes.

Gostaria de agradecer a todo o grupo do INESC MN. A todos os técnicos com os quais aprendi e iniciei a minha investigação em microfabricação. A todos os colegas investigadores do grupo. Aos que partilharam comigo o meu local de trabalho durante este último ano, o João, a Carolina, o António, os Ricardos, o Miguel, o Zé Amaral, a Diana, Ana, Tomás, obrigada pela boa disposição. Aos que me ajudaram a crescer como investigadora.

Aos meus amigos que me acompanharam durante estes dois anos. Aos amigos que criei no GASTagus com os quais passo grande parte dos meus dias. Ás minhas queridas amigas Dani e Nina que me acompanham desde a Covilhã. Á Inês Ferreira pela amizade, partilha e bondade.

Não posso deixar de agradecer ao António Sousa, pelo apoio e incentivo incansável.

Ao meu namorado Robe por todo a paciência, dedicação, carinho e amizade. Obrigada por todo o apoio, calma que me transmitiste nestes últimos dias, até ao último minuto.

Por fim quero agradecer à minha Mãe, por todo amor, força, ternura e suporte incondicional. Á minha Mana por todo o amor, alegria, dedicação, força e coragem para mais uma grande etapa da minha vida. Obrigada por estares sempre comigo, a meu lado.

Ao meu Pai de quem tenho muitas saudades e que me ajudou e inspirou a cada segundo.

Obrigada Pai.

Resumo

A Nanotecnologia e a microfabricação têm surgido como poderosos métodos que prometem inovadoras soluções para a miniaturização e integração de processamento da amostra, realização de ensaios biológicos, amplificação de ácidos nucleicos e sistemas de detecção de analitos. As soluções lab-on-a-chip (LOC) têm trazido a oportunidade de desenvolver sensíveis plataformas de diagnóstico e controlo de doenças. Estes sistemas são dotados de inúmeras vantagens, tais como, descartabilidade, elevada sensibilidade, baixo custo, facilidade de uso, análise de pequenos volumes de amostra e portabilidade. Os ensaios baseados na técnica de reacção em cadeia da polimerase on chip (PCR) têm sido extensivamente aplicados no diagnóstico e controlo de doenças genéticas moleculares e infeciosas. Para a fabricação e optimização do processo de microfabricação do biochip, diferentes estudos foram realizados, incluindo o estudo de diferentes materiais de substratos, camadas de passivação e o design e arquitectura do biochip. Os sensores magnetoresistivos, válvulas de spin foram calibrados como sensores de temperatura, sendo necessário um rigoroso estudo dos parâmetros térmicos do sistema com o objectivo de garantir um ciclo térmico preciso para uma óptima reacção de PCR. Para calibrar os sensores e garantir o controlo térmico, com uma rápida e eficaz resposta térmica com pouco consumo de energia, foi utilizado um controlador de modulação de largura de pulso. A integração da técnica de PCR num biochip magnetoresistivo inserido e controlado por uma plataforma portátil tem sido intensivamente investigada nos últimos anos e representa hoje em dia um motivador desafio para o melhoramento de aplicações LOC no mundo da Nanotecnologia.

PALAVRAS CHAVE

Reacção em cadeia de polimerase Biochip magnetoresistivo Válvulas de Spin

Integração Plataforma portátil Controlo de ciclo térmico

Abstract

Nanotechnology and microfabrication have emerged as powerful methods that promise exciting and integrated solutions for miniaturization and integration of sample processing, assay performance, nucleic acid amplification and analyte detection systems. The lab-on-a-chip (LOC) solutions have become an opportunity to bring accurate and sensitive point of care diagnostic tests and monitoring platforms. The disposability, sensitivity, cost-effectiveness, user-friendliness, small volume analysis and portability are the main advantages of these LOC systems. Polymerase chain reaction (PCR) assays on chip have been extensively applied for the diagnosis and monitoring of molecular genetic and infectious diseases. For the improvement of biochip microfabrication, a recent research of different substrates materials, passivation layer optimization and architecture designs have been reported. The calibration of magnetoresistive (MR) sensors, spin valves, as temperatures sensors have been studied in order to evaluate the system thermal parameters and to ensure a temperature cycling system required for an optimal PCR reaction. A Pulse Width Modulation controller has been also developed to assure the sensors calibration, the thermal control, promoting a fast and accurate thermal response and very low power consumption. The integration of a PCR in a MR biochip controlled by a portable platform has been intensively investigated and has emerged as a motivating challenge for improvement of point of care and LOC applications in the nanotechnology world.

KEYWORDS

Polymerase chain reaction Magnetoresistive Biochip Spin Valve Sensors

Integration Portable platform Thermo cycling control

Index

List of Figures

List of Tables

List of Abbreviation

AIDS	Acquired Immunodeficiency Syndrome
AMR	Anisotropic Magnetoresistance
BSA	Bovine Serum Albumin
CVD	Chemical Vapour Deposition
CVS	Comma Separated Value
DI	Deionised Water
DNA	Deoxyribonucleic acid
dNTPs	Desoxynucleotide Trisphosphates
dsDNA	Double-stranded DNA
DSP	Digital Signal Processor
DWL	Direct Write Laser
ELISA	Enzyme-linked immunossorbent assay
FM	Ferromagnetic
GMR	Giant Magnetoresistance
GPIB	General Purpose Interface Bus
GUI	Graphical User Interface
HDMS	Hexamethyldisilane
HEK	Human Enbryonic Kidney
HIV	Human Immunodeficiency Virus
IBD	Ion Beam Deposition
IPA	Isopropyl Alcohol
LOC	Lab-on-a-chip
M	Metallic
MEMS	Micro Electric Mechanical System
MR	Magnetoresistive
PB	Phosphate Buffer
PBS	Phosphate Buffer Saline
PCB	Printed Circuit Board
PCR	Polymerase Chain Reaction
PDMS	Polymethylsiloxane
PID	Proportional Integral Derivative
PMMA	Polymethylmethacrylate
POC	Point of care
PR	Photoresist
PVD	Physical Vapour Deposition
PWM	Pulse Width Modulation
RT	Room Temperature

rt-PCR	Real Time Polymerase Chain Reaction
SEM	Scanning Electron Microscope
Si	Silicon
SPM	Sensing and Processing Module
ssDNA	Single-stranded DNA
SV	Spin Valve
SVG	Silicon Valley Group
TCR	Temperature Coefficient of Resistance
TMR	Tunneling Magnetoresistance
UHVII	Ultra High Vacuum
UV	Ultra Violet
UVO	Ultra Violet Ozone
VRC	Virtual Reaction Machine
WHO	World Health Organization
XML	Extensible Markup Language

1. General Introduction

1.1 Motivation

Appropriate diagnostic and monitoring tools play a critical role in the evaluation and improvement of global health. In the developed and developing countries the diagnostic is an essential component for correctly detecting of disease, both at individually or population level, as well as the treatment monitoring. Fast diagnosis provides proper and prompt treatment for patients, limiting the spread of diseases during the determination of drug resistance and/or recurrence of existing diseases and minimizing the waste of public resources on ineffective treatments (1-3).

The developing world and in low-resources settings have no access to many of the best medical diagnostic and monitoring technologies and current diagnostic tools are largely inadequate for meeting health needs (2). Infectious diseases continue to be a main cause of death in such countries (4, 5). Over 95% of these deaths are caused by a crucial factor: the lack of proper diagnosis and treatment as well as the difficulty in accessing adequate health care infrastructures by most of the global population (1, 4). A study reported by World Health Organization (WHO) estimates that in many countries in sub-Saharan Africa, more than 20% of pregnant women are infected with human immunodeficiency virus (HIV). Without intervention, more than 25% of infant born from infected women will be infected with HIV during the first year of life. In 2005, an estimated 2.3 million children worldwide were living with HIV or acquired immunodeficiency syndrome (AIDS), 2 million of whom in sub-Saharan Africa (4). The number of adults and children estimated to be living with HIV in 2011 is presented in Figure 1-1 (6).

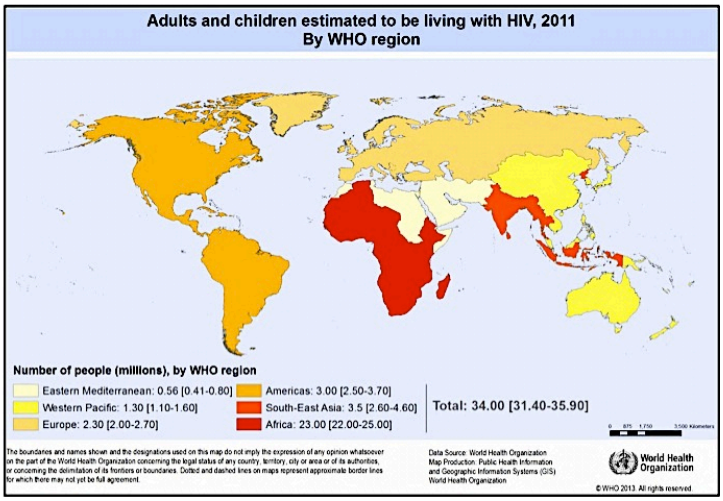

Figure 1-1: Data reported by WHO: Number estimated of adults and children to be living with HIV, 2011 (6).

Point of care (POC) diagnostics offers great potential for detection and monitoring of infectious diseases at resource-limited environments, at high-income countries as well as in the developing

world, although in this last case the potential is probably even greater. This happens due to the fact that POC diagnostics can be taken to remote locations, decreasing the need for large decentralized diagnostics facilities (1, 5). The WHO has emphasized the need to develop POC devices for HIV/AIDS on chip diagnosis and monitoring, at resource limited setting. Nano/microfluidic technologies have been successfully integrated with POC devices promoting an accurate, inexpsensive and disposable platform, which enables the enumeration of CD4+ T-lymphocytes an HIV viral load (5).

The WHO has established a set of guidelines to develop diagnostic and monitoring platforms for infectious diseases in order to enhance the overall quality of life of global population: (i) AFFORDABLE by those at risk of infection, (ii) SENSITIVE ensuring few false-negative results, (iii) SPECIFIC promoting few false-positive results, (iv) USER friendly, simple to manipulate by persons with limited training, (v) RAPID treatment at the first visit and robust use without the need for special storage, (vi) EQUIPMENT-free, no large electricity-dependent instruments needed to perform the test (note that portable handheld battery-operated devices are acceptable) and (vii) DELIVERED to those who need it, leading to the acronym 'ASSURED' (4, 5).

In the developed world, other factors are responsible for scientific and technological advances, such as genome mapping and sequencing and high throughput antigen screening (7). LOC devices have revealed a major impact in a variety of fields of life sciences, such as, the genotyping of individuals, environmental sensing and monitoring, food quality management, forensic sciences, controlling of epidemic diseases, clinical diagnostic including molecular detection of hereditary and infectious disease and therapeutic compounds development (3, 7-10). So, the unraveling of disease pathogenesis at a molecular level and the detection of the pathogen and disease biomarkers has been accelerated (1).

Microfluidics and nanotechnology are emerging powerful methods that promise exciting and integrated solutions for sample processing, assay performance and analyte detection (3). These LOC solutions have become an opportunity to bring accurate and sensitive POC diagnostic and monitoring platforms (1). The disposability, cost-effectiveness, ease to use, small volume analysis and portability are the main advantages of these POC technologies. Several aspects have to be considered in order to decrease the cost of these diagnostic tests, such as, minimal use of expensive reagents, inexpensive manufacturing and quality control and miniaturization (1).

Besides that, nano/microfluidic technologies have enabled the generation of on chip immunoassays for POC application for detection and monitoring of diseases such as cancer and viral infections. These diseases are commonly detected using enzyme-linked immunossorbent assays (ELISA). However this approach has a number of limitations due to its cross-reactivity, long assay time requirement, cumbersome liquid handling, need for large amounts of expensive reagents and equipment (5). Therefore, the real time polymerase chain reaction (rt-PCR) has been used on the specific detection of gene mutations and DNA biomarkers related to cancer, or mRNA in the case of

virus detection (11). Although very sensitive, this system remains bulky, expensive and not easily multiplexable (12).

In this project we highlight an application of on chip POC diagnostics and monitoring platform focusing on DNA amplification. Following the specific guidelines imposed by WHO the aim of this project is to perform a portable POC platform that consists in the integration of the polymerase chain reaction (PCR) in a magnetoresistive biochip. This system will therefore combine the advantage of rt-PCR on the specificity of the detection with the high sensitivity, specificity, rapidity and portability, multiplexability and low cost of the magnetoresistive biochips.

1.2 State of the Art

In this subchapter three main subjects used in this thesis will be handled: Magnetoresistive (MR) Sensors, Biosensors and PCR and will be also referred their previous applications and its contribution in this work.

1.2.1 Magnetoresistive Sensors

Magnetoresistance is the property of a material exhibits a change in electrical resistance in presence of an external magnetic field (13-15). Thin film technologies allow the fabrication of three main MR mechanisms:

- Anisotropic Magnetoresistance (AMR)
- Giant Magnetoresistance (GMR)
- Tunneling Magnetoresistance (TMR)

In this thesis, the MR sensors integrated in the detection system consist in spin valves (SV) sensors, which are based on the GMR effect. Baibich discovered the GMR effect in 1988 (16). In 1998, Baselt and co-workers introduced the GMR sensors in molecular biorecognition field, combining them with magnetic labeled molecules (17). The GMR effect is based on the spin-depend transmission of conduction electrons crossing ferromagnetic – nonmagnetic (metallic (M)) – ferromagnetic (FM) multilayer structures. This transmission depends on the relative orientation of the moments, parallel or antiparallel alignment of the FM layers. The spin valve consists of two FM layers, separated by a M spacer of a non magnetic conductive material, FM1/M/FM2. One of the two magnetic layers, called free layer, is free to rotate between parallel and antiparallel alignments with an external magnetic field. The antiferromagnetic layer allows the magnetization pinning of other ferromagnetic layer, called pinned layer (15, 18, 19).

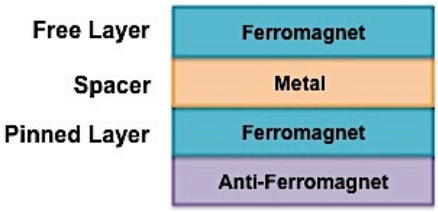

Figure 1-2: Spin valve sensor typical structure that comprises a free layer, a pinned layer and a metallic spacer.

An applied magnetic field is used to change the relative orientation of the magnetic layers magnetizations. The angle between the magnetization directions dictates the resistance of the sensor. With the rotation of the free layer the resistance changes and could lead to different responses, a square response, suitable for memories or a linear response, which is appropriate for sensors. In a square response the transitions from a '0' into a '1' state and vice-versa are accomplished, without a measurable value between this transitions states. In a linear response, the output value can reflect the gradual change of the magnetic field intensity. In this thesis, a linear response should be accomplished. The linear response comes from the rotation of the free layer with respect to the pinned layer. Therefore, is crucial to know the easy axis of both the free layer and pinned layer prior to the microfabrication steps. With the easy axis of the free layer (the direction of magnetization) at a 90º angle (in-plane) with respect to the easy axis of the pinned layer it is possible to achieve the desired linear response, in which the free layer rotation will be performed by a gradual change in the magnetic field. If the FM layers become aligned in a parallel configuration, the resistance is minimal. However, if FM layers were aligned in an antiparallel configuration, a maximal resistance is produced (13, 15, 18). In Figure 1-3 is shown a transfer curve of a spin valve sensor, which presents a linear response, and the parallel and antiparallel configuration of FM layers, correspondent to minimal resistance and maximal resistance.

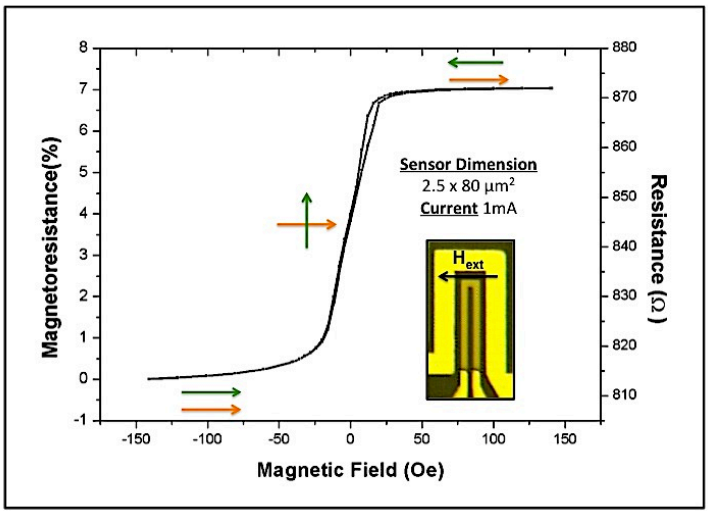

Figure 1-3: Typical transfer curve of a SV sensor taken at a bias current of 1mA. The image shows the U-shaped spin valve 2.5x80µm^2 surrounded by a U-shaped current line, which was used as the heating element. When the FM layers are aligned in a parallel configuration, the resistance is minimal. When the FM layers are aligned in a antiparallel configuration, a maximal resistance is obtained.

In past years, GMR sensors have become a potential element integrated in magnetic biosensors for detection or identification of biomolecules due to its sensitivity to small magnetic fields, high signal to noise ratio and their simplified fabrication process (14, 15, 20-24). In these biosensors applications, magnetic particles can be used as markers of target biomolecules and the GMR elements detected the presence of the particles that are immobilized to the sensors through intermolecular interactions, e.g. DNA hybridization (13, 15, 25, 26).

1.2.2 Biosensors

The magnetoelectronics has emerged as a promising technology for biosensor and biochip development, which consists in the detection of the magnetic fringe field of a magnetically labelled biomolecule interacting with a complementary biomolecule bound to a high sensitive microfabricated MR sensor. MR sensors combined with biologically functionalized magnetic labels have been used to demonstrate the ability to detect the biomolecular recognition by offering high sensitive detection, a stable labelling system, low magnetic background and cheap device components (15, 19). This detection has been playing an important role in the DNA hybridization. Based on these systems, real-world bio-applications, such as genetic disease diagnostic, gene expression quantification, mutation and microorganism detection have been investigated (18).

A typical biosensor can be defined as a 'compact analytical device or unit incorporating a biological or biologically-derived sensitive element (bioreceptor) integrated or associated with a physical and/or chemical transducer and an output system' (27) . First, the bioreceptor recognizes a target performing a physical and/or chemical change, which is converted into an electric/electronic signal at the transducer. Then, the signal is measured and interpreted by the output system. The biorecognition between the target and the bioreceptor can occur through a reaction, specific adsorption, or other physical or chemical process. Biosensors can be integrated with different biological target, for instance, enzymes, cell receptors, nucleic acids, microorganisms and antibodies (15).

For MR biosensors, presented in Figure 1-4, the biomolecule to be detected (target or analyte) is magnetically labeled and passed over an array of specific biological probes, which are immobilized over on chip MR sensors. First, the target molecule labeled with a small biochemical label, e.g. biotin, is hybridized with probe molecules immobilized over the MR sensor. The magnetic labels functionalized with streptavidin (the complementary molecule to biotin) are used to recognize the probe hybridized with biotinylated target molecule. When the magnetic labels interact with the probe molecule bound to the surface, an external magnetic filed is applied to magnetize the labels and the magnetoresistive sensor detects the magnetic fringe field, via a change in sensor resistance at a fixed bias current. Finally, unbound target biomolecules are washed away. If the signal remains after this washing step, this indicates that the magnetically labeled target interacts successfully with the complementary probe molecules bound to the surface (15, 19, 22).

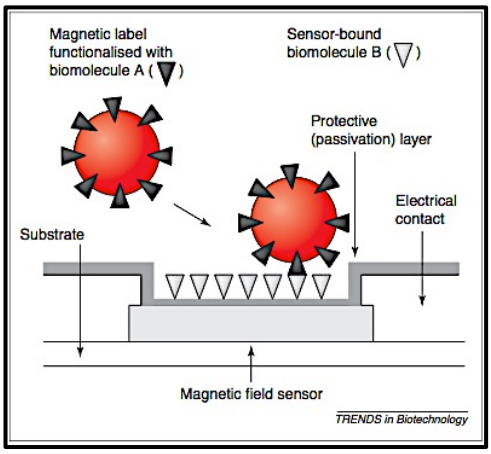

Figure 1-4: The biomolecule to be detected is magnetically labeled (immobilized on a magnetic label) and injected over an array of specifically patterned probe, which are immobilized over on chip MR sensors. The sensors detect the presence of magnetic labels via a change in sensor resistance at a fixed bias current. The unbound target molecules are then washed away and sensor signals are obtained at sensor sites where magnetically labeled target and the complementary probe bound to the surface have successfully interacted (15).

These biosensors have been integrated by several studies in fully controllable biochip platforms including control and acquisition electronics and microfluidics systems for sample handling (13, 15, 19, 21, 22, 24, 28). In this thesis, a LOC platform will be achieved by integration of MR sensor with an PCR on chip device. In future work, the genomic deoxyribonucleic acid (DNA) which specific genes are amplified using a PCR technique have to be labeled with a biotin and hybridized with probe molecules immobilized over MR sensor, performing DNA hybridization.

1.2.3 Polymerase Chain Reaction

PCR technology, which was introduced by Mullis in 1985, is a powerful research tool for DNA amplification and quantification and, has become the method of choice to exponentially amplify specific DNA sequences of interest in a sample through repetitive temperature cycling (29-31). There are many different methods to perform PCR, such as conventional PCR, rt-PCR and PCR on chip that will be described and discussed in subchapter 5.2.

A typical PCR process, illustrated in the Figure 1-5, consists of three main steps conducted at different optimal reaction temperatures (32). The temperatures that are typically used in PCR include: heating up the sample to 95°C for denaturation of the double-stranded DNA (dsDNA) providing single-stranded DNA (ssDNA) for primer annealing; cooling down to annealing temperature (58°C to 68°C) to renature the specific primers with the ssDNA template and finally increasing the temperature to 72°C-74°C for enzymatic extension of the primers with thermo stable DNA polymerase, such as Taq polymerase (extension step). The annealing and extension steps can be combined into one and performed at a temperature of about 60°C (29, 30, 33). Ensuring repeated thermal cycling, typically 20-40 cycles, an exponential increase in the number of copies of a specific DNA sequence relative to the original DNA template is successfully achieved. The ability to amplify a single DNA template into

millions or billions of copies of the same sequence has revolutionized the field of molecular biology (7). Recently, there has been increasing demand for the development of POC diagnostic kits or platform combining the integration of PCR technology. Several studies have emerged in this biomedical research (7, 12, 30, 32-36).

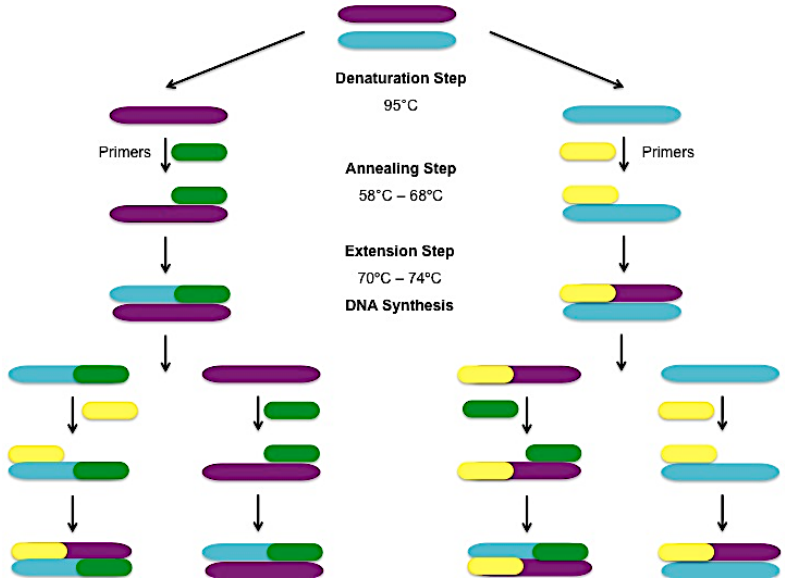

Figure 1-5: Scheme of PCR: Denaturation step (95ºC): dsDNA denaturation; Annealing step (58ºC-68ºC): Binding of the specific primers to their target sites; Extension Step (70ºC-74ºC): Extension of the primers with the thermo stable DNA polymerase.

1.3 Aim of Studies

The purpose of this project is to perform the integration of PCR in a MR biochip. This system will combine the advantage of PCR on the specificity of the detection with the high sensitivity, portability, multiplexability and low cost of the MR biochips to perform biorecognition assays by detecting magnetically labeled target.

The first part of the work will be dedicated to the microfabrication process of biochip following a Run Sheet designed and tested previously by Filipe Cardoso and Verónica Martins (18). Microfabrication process includes several techniques such as photolithography, thin film deposition techniques and etching and lift-off methods that will be described. After that, the chip design optimization and specific characterization of the materials constituting the biochip, specifically the passivation layer that protects the surface, will be evaluated in order to achieve good and uniform temperature control and to avoid instability and corrosion in microelectronic when the biorecognition assays are performed. The MR sensors will be characterized as temperature sensors and the thermal parameters, heating and cooling methods will be mentioned in detail. Finally, a DNA sample prepared following a specific protocol will be introduced in a microfluidic channel placed over the integrated biochip and connected to a portable platform. Then a PCR on chip will be performed through the temperature control by

Pulse Width Modulation (PWM) controller in order to achieve an optimal thermal cycling as fast and efficient as possible.

1.4 Thesis Outline

The experimental work is divided in five different chapters dedicated to the integration of PCR in a MR biochip. Each chapter is accompanied with: a brief overview used to contextualize the reader with the different steps of the project, a description of different methods involved in each approach and additionally the obtained results and respective discussion.

- **Chapter 2** comprises the experimental work realized at INESC MN clean room for microfabrication process of the MR biochip following a specific runsheet designed by Filipe Cardoso and Verónica Martins (18). Respective description of all the steps and methods of microfabrication, the characterization techniques and machines operation mode will be described.
- **Chapter 3** includes the optimization of the original runsheet, described in Chapter 2, and the biochip microfabrication following these improved processes. Three different tests were performed: substrate material selection to ensure a good thermal uniformity; photoresist profile optimization in order to avoid the rabbit ears after lift-off process and consequently a short circuit behaviour when the fluid is put into contact with the biochip and finally the optimization of passivation layer by testing all oxides present at INESC MN, and respective selection of oxide that presents the optimal characteristics in order to avoid the corrosion of microfabricated elements (sensors, contacts) when biological assay will be performed.
- **Chapter 4** describes the characterization of SV sensors as temperature sensors, regarding the calibration method, thermal parameters study (thermal conductivity, thermal capacitance and thermal time constant), and the temperature control using PWM controller.
- **Chapter 5** involves three different approaches used to accomplish the PCR (conventional PCR, rt-PCR and PCR on chip) and the integration of PCR in a MR biochip in order to amplify DNA sample successfully.
- **Chapter 6** culminates with general conclusions, in which are reported the most important achievements accomplished during this work and it is finalized with the main suggested steps for future work aiming to ensure the success of this biomedical application.

2. Magnetoresistive sensors: Spin Valve Biochip

2.1 Overview

In this chapter, a microfabrication process was performed in order to obtain a magnetoresistive (MR) biochip for the polymerase chain reaction (PCR) integration. The microfabrication process consisted in combining of several lithography, thin films deposition, etching and lift-off techniques. The characterization of materials was also accomplished, ensuring a successful performance of the devices. This MR biochip was integrated in a portable platform that includes all hardware components required to temperature control, real time signal processing and PCR on chip.

2.2 Microfabrication of PCR chip

In order to ensure high performance devices, all microfabrication processes combining photolithography, etching and lift-off techniques required a controlled environment. This environment is mandatory to avoid air impurities to interfere with device performance, as the microfabricated structures dimensions are so small comparing to some dust grains present in the atmosphere. In INESC MN clean room, there are three areas with different classes shown in Figure 2-1. The class number translates the maximum number of dust particles larger than 1μm per cubic feet of air in each region. A clean room area of 250m^2, has two areas classified as, class 100 (white area) with sputtering, chemical vapour deposition (CVD) and ion beam deposition (IBD) systems, wet bench and characterization tools and class 10 (yellow area) with optical lithography system, spin coating systems and microscopes. Another adjoining area is nominated grey area, with 250m^2 and is classified as class 10000 where sputtering and CVD machines are located.

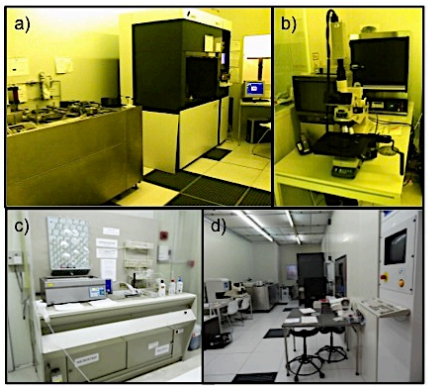

Figure 2-1: Clean room facilities: a) Class 10: Yellow area b) Yellow area: microscope c) Class 100: Wet bench d) Class 100: White area.

2.2.1 Thin film Deposition Techniques

At INESC MN there are three different techniques to perform the thin film deposition, IBD, sputtering and CVD, which were described in these subchapter.

2.2.1.1 Ion Beam Deposition Systems

The IBD systems use a highly energetic broad ion beam generated by the deposition gun that is then focused on a grounded metallic or dielectric target. In this system, the plasma is created in the deposition gun distant from the targets. Most IBD systems also use a secondary ion source, assist gun, which acts directly on the substrate, delivering energetic noble or reactive ions during the material deposition, consequently improving the quality of the deposited films. This assist gun can be also used to perform ion milling etching, the main dry etch method applied in this thesis, in which ions are accelerated at high energy to the surface, removing the material with a controlled etching rate. A deposition neutralizer is also required when insulating materials are deposited, avoiding the accumulation of ion charge on top of the insulating target. The Figure 2-2a) shows the geometry of a IBD tool. In this work, two IBD systems installed at INESC MN (Nordiko 3000 and Nordiko 3600, shown in Figure2-2b)) were used to deposit spin valve (SV) sensors, thin film and to perform highly uniform etch during the microfabrication process (37, 38).

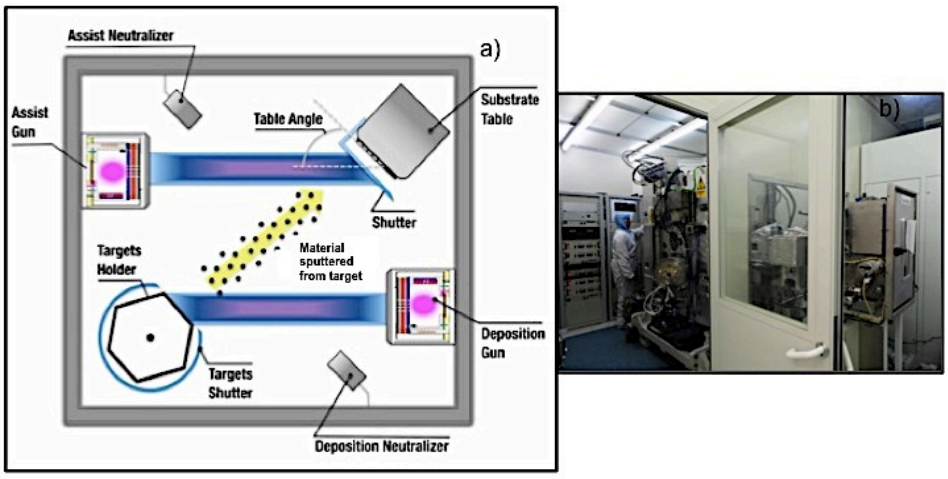

Figure 2-2: IBD System: a) Scheme of IBD operation mode b) Nordiko 3600 installed in INESC MN.

2.2.1.2 Sputtering Systems

Sputtering is a physical deposition method for depositing both thin metal and insulating films onto a substrate. This system consists in highly energetic ions bombardment towards solid target material, where atoms are ejected from it to a substrate table with a controlled deposition rate, due to transfer of momentum between these ions and the atoms of a target. The plasma is created in a vacuum chamber, which is controllably filled with an inert gas (Ar or Xe). The target is held at a negative bias voltage while the shielding surrounding is grounded. This negative voltage accelerates ions present in

the plasma towards the target, removing the material to deposit onto the sample. This process is called DC sputtering and it is valid only for conductive targets. For non-conductive materials, the target has to be connected to a RF power supply. The substrate may either be grounded or connected to the RF power supply. In last case, the ions are directly accelerated to the substrate and its material is removed. This process called sputter etch is used to remove material from the substrate or to control the roughness/structure of the material (37, 39). The sputtering machines installed at INESC MN used in this work were: Alcatel SCM450 shown in Figure 2-3a) (SiO_2 and Au deposition) and Ultra High Vacuum (UHVII) (Al_2O_3) deposition presented in Figure 2-3b).

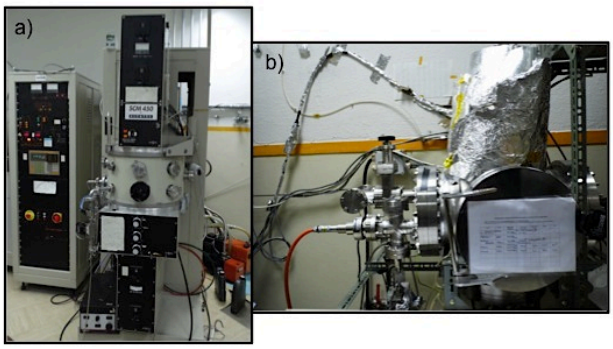

Figure 2-3: Sputtering Machines: a) Alcatel SCM450 b) UHVII.

2.2.1.3 Chemical Vapour Deposition

CVD produce high-purity, high-performance solid material. The CVD film growth occurs through the chemical reaction of the component chemicals, i.e. chemical precursor. The chemical precursors are transported to the vicinity of the substrate via the vapour phase, which react and/or decompose on the substrate surface. The film-forming chemical reactions typically utilize thermal energy from a heated substrate at 300ºC. The evaporated precursors are homogenously distributed by a showerhead at 350ºC. The most straightforward type of CVD involves chemical precursor compounds that are sufficiently stable gases and such processes are used for the deposition of insulators and interlayer dielectrics, like SiO_2 and SiN (39). Examples of the reactions involved are the thermal decomposition of silane, SiH_4 and ammonia, NH_3 for the deposition of:

Si- Nitride: $3SiH_4 + 4NH_3 \leftrightarrow Si_3N_4 + 12H_2$

Si-Dioxide: $SiH_4 + O_2 \leftrightarrow SiO_2 + 2H_2$

The Eletrotech Delta 201 (Figure 2-4) uses an automatic vacuum robot and an automatic loading cassette under vacuum. Film uniformity better than 6% over a 150mm diameter wafer and a film thickness from 1000Å to 1µm can be achieved.

Figure 2-4: CVD Machine: Electrotech.

2.2.2 Photolithography

Lithography comes from Greek, λιθοσ 'a stone' and γραφειυ 'to write'. Considered the most important technique used in graphic art, the lithography is based on the printing art from stone. Technically, the main goal of photolithography is to define a pattern on a substrate with a desired shape. A radiation source, a sample coated with a light-sensitive material and an image system that controls which part should be illuminated compose the lithography system. The photolithography process involves three major steps:

- **Coating:** Before any step, the sample should be exposed to a pre-treatment that consists on the deposition of an organic compound (Hexamethyldisilane, $C_6H_{18}Si_2$, (HDMS)), in vacuum under a temperature of 130°, in the Vapour Prime machine (Figure 2-5a). This pre-treatment is fundamental to promote photoresist (PR) adhesion. PRs are polymers that become soluble when exposed to a specific wavelength. The sample can be coated with two different types of PR: positive PR, in which exposed areas are dissolved in developer or negative PR, in which exposed areas are remained hardened. In this work, a positive PR (PFR 7790G 27cP, JSR Electronics) was used in all the process. The spin coating is made in a Silicon Valley Group (SVG) system in autonomous track devoted to the coating, track 2 (Figure 2-5b)). Rotation of 3200 rpm during 30 seconds is used to ensure the PR thickness equal to 1.5 μm. After, the sample is soft backed at 85º during 60 seconds to remove solvents and stress, to minimize the susceptibility to particle contamination and also to promote the adhesion of PR (18, 40).

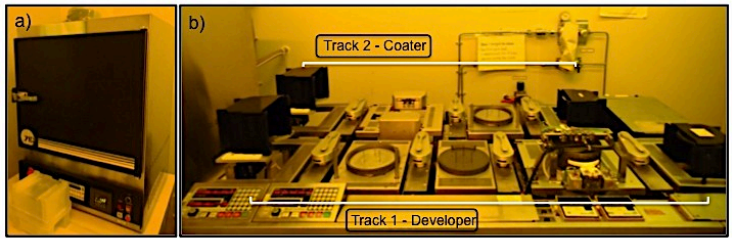

Figure 2-5: Yellow area clean room: a) Vapour Prime Machine b) SVG system used for coating and development PR, in track 2 and 1 respectively.

- **Exposure:** The first point of the lithography process is to define a mask, normally processed as a CAD-file and subsequently converted into a laser machine language. This mask provides the pattern that should be transferred to the sample by a 2.0 direct write laser (DWL) system, using a 440nm NeAr laser (Figure 2-6). This laser enables a maximum feature resolution of 0.8μm and the alignment precision is limited by the stage resolution of 0.1μm (18, 37, 38).

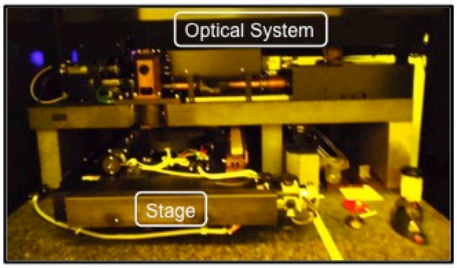

Figure 2-6: DWL 2.0 Lithography System.

- **Development:** Development of the exposed PR is made using the track 1 – station 2 of the SVG (Figure 2-5b)). Before development, the sample undergoes a soft bake at 110°C during 60 seconds to ensure that uncompleted PR reactions are stopped. A suitable developer (JSR Micro PTH70EG) is used to dissolve the exposed PR, during 60 seconds. The developer dissolves the regions that are exposed to the laser light, while the non exposed areas remain intact. After developing process, the sample is washed with deionized water (DI) and dried by high speed spinning. The final resist pattern can be transferred to the sample by an etching step that removes the parts completely uncovered by resist and protects the areas that are still covered by the same (18, 37, 38).

2.2.3 Etch

Etch process consists in the unprotected material removal from the substrate through ion bombardment or chemical reaction. After PR patterning by photolithography (Figure 2-7a), the sample is submitted to an etching step, and the unprotected material is removed (Figure 2-7b). Then, the PR is removed in a resist solution leaving only the patterned thin film layer (Figure 2-7c).

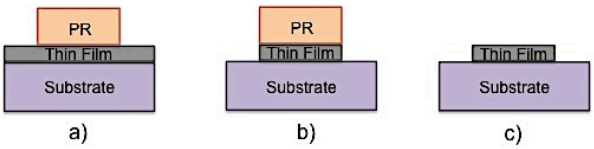

Figure 2-7: Etching Process: a) Patterning of the PR by photolithography b) Etching of the unprotected material c) Removal of the PR.

Two different etch mechanisms can be distinguished – physical and chemical etching. In physical etching, ions of inert gases are accelerated to the surface and its momentum transfer knocks off surface atoms. In chemical reaction, the surface material is chemically etched from the neutral or activated gas and forms soluble and volatile etch products at low pressures. Although much less

selective, dry processes show improved process control and repeatability and lower waste disposal, when compared with chemical wet etching. In this thesis, the ion milling was the preferred etch method used (39).

Ion Milling

During etching, Ar ions are accelerated at high energy into a thin film surface that is coated with a PR pattern. The resulting force from the impact of the atoms with the exposed surface promotes the unprotected material removal, and the thin film is patterned at a controlled etching rate. The assist guns of the IBD systems Nordiko 3600 and Nordiko 3000 are used to perform the ion milling etching. The ion incidence angle (i.e. angle between the ion beam and sample surface) can be set from 20º to 90º for the etching processes. In the SV microfabrication process, the assist gun is set an angle of 70°(Figure 2-8a). At 70°, a collimated beam of Ar ions bombards the sample almost perpendicularly and the redeposition of the etched material may occur. In the other cases, when the material redeposition has to be prevented, the etching angle of 40° should be used (Figure 2-9a). Using these two configurations the profile of the material protected by the PR is different as shown in Figure 2-8b) and 2-9b) (18, 38, 39).

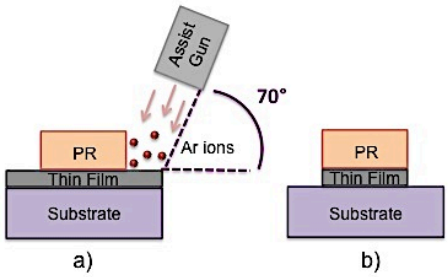

Figure 2-8: Ion Milling: a) An Ar plasma beam bombards the sample at an angle of 70° b) Removal of the unprotected thin film.

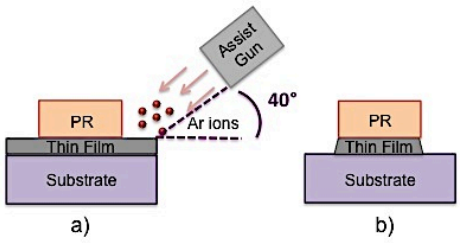

Figure 2-9: Ion Milling: a) An Ar plasma beam bombards the sample at an angle of 40° b) The unprotected thin film was removed.

2.2.4 Lift-Off

The lift-off process is an alternative technique to etching in order to pattern a thin film. The substrate is covered with a PR layer patterned by photolithography (Figure 2-10a). Next, the thin film is deposited on top of PR (Figure 2-10b). Finally, the PR and the material placed on top of it is removed, when the sample is submersed in a resist strip solution, Microstrip 3001 (Fujifilm), at 65°C, as shown

in Figure 2-10c). Some ultrasounds are applied during the process to accelerate the removal. The patterned thin film remains in the area previously non occupied by the PR.

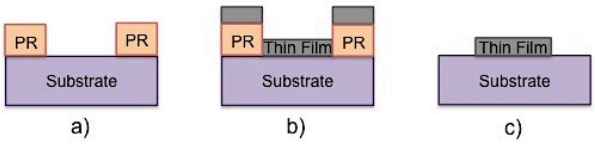

Figure 2-10: Lift-off Process: a) Patterning of the PR layer by photolithography b) Thin film layer deposition c) Removal of the PR and the material above it by a resist strip solution.

This technique is suitable for thin film patterning but it has a drawback like the rough edge features, rabbit ears (Al pieces that remains on the edge of the Al tracks), which should be optimized (18, 39). The lift-off process optimization, described in detail in subchapter 3.3.1, consists in the PR pre-development step before exposure. This pre-development step will harden the PR and will make the top surface less sensible to the laser. Therefore, with the pre-development step, the PR acquires an undercut profile instead of a vertical profile (Figure 2-11), avoiding the rabbit ears presence when the lift-off is complete.

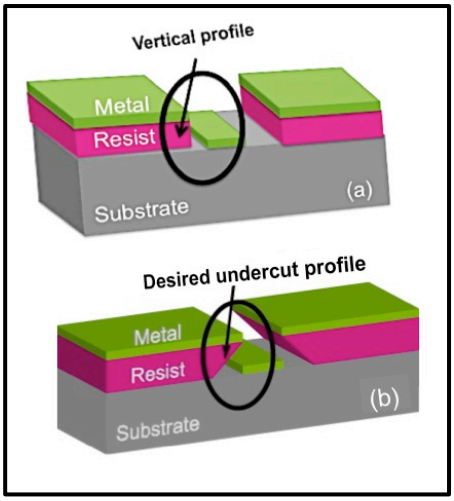

Figure 2-11: PR profile a) when a sample is not submitted to the pre-development step, the PR acquires a vertical profile b) when a sample is submitted to a pre-development step the desired undercut profile is achieved (adapted from (41)).

2.2.5 Microfabrication Run Sheet

In this subchapter, the microfabrication of a biochip integrating SV sensors and a current line is described in detail. Microfabrication of the biochip-based SV sensors was performed using a Run Sheet designed by Filipe Cardoso and Verónica Martins [18], in which mainly two processes were optimized. More details about the 14 steps that comprise the process are described in Run Sheet Biochip with Spin Valve Sensors in Appendix I.

Biochip Microfabrication: Runsheet Biochip with spin valve sensors

- **Step 1 - Substrate preparing:** This step consists in preparation of the substrate. For this process, 1x1inch^2 glass substrate was used. Proper cleaning procedures should be followed: Cleaning substrate in an alconox solution (a detergent) for grease removal in ultra-sound for 10 minutes. After, the substrate has to be rinsed with isopropyl alcohol (IPA) and DI. Finally, the sample must be blow-dried with a compressed air gun.

- **Step 2 – Spin Valve deposition:** This process can be performed by IBD systems that are available at INESC MN: Nordiko 3000 and Nordiko 3600 (each one with 6-target of different materials). In this project, Nordiko 3000 was used to deposit SV sensors. The SV structure was optimized in order to achieve a linear response. The sensor stack was deposited on a glass substrate and its structure was as follows: Ta 20Å/$Ni_{80}Fe_{20}$ 36Å/$Co_{81}Fe_{19}$ 23Å/Cu 25Å/$Co_{81}Fe_{19}$ 23Å/$Mn_{76}Ir_{24}$ 80Å /Ta 30Å/$Ti_{10}W_{90}$ (N)150Å.

- **Step 3 – First mask exposure in DWL (spin valve definition):** The glass substrate with sensor stack deposited in previous step was coated with PR, which was exposed and developed as described in subchapter 2.2.2. This step consists in the SV definition, which are disposed in 6 different areas, organized in 2 columns, each with 5 U-shaped SV sensors (2.5 x 80µm^2) oriented in opposite direction as shown in Figure 2-12.

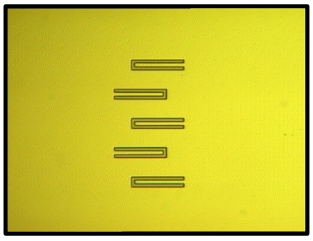

Figure 2-12: SV definition: sensors were disposed in 6 different areas, organized in 2 columns, each with 5 U-shaped SV sensors.

- **Step 4 - Spin valve etching:** It is the last step of SV sensor definition, which involves the material removal that is not covered by the PR. Ion milling performed in Nordiko 3600, using an angle of 70°, was the etching technique used to removing the material. An overetch step should be made ensuring that all SV stack thickness is etched. The total etching thickness was about 400Å (including 30Å overetch). The ion milling technique was depicted in subchapter 2.2.3.

- **Step 5 – Resist stripping:** This step performed in wet bench at clean room facilities comprises the PR mask removal. A specific protocol was made with following steps: Sample immersion into Microstrip 3001 solution at a temperature of 65°C. In order to accelerate and improve the PR removal, some ultrasounds can be applied during short period of time, about 10-15 minutes. The sample has to stay in solution until the PR removal is completed. After that, the sample was

rinsed with IPA and DI and blow-dried with a compressed air gun. In Figure 2-13 is presented the final aspect of SV defined.

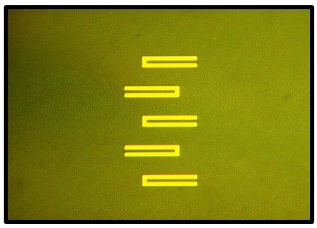

Figure 2-13: Aspect of SV defined after the etching process and resist stripping.

- **Step 6 - Second mask exposure in DWL (contact leads definition):** In this step, contact leads were defined in PR following the steps detailed in subchapter 2.2.2. It was one of processes optimized based on the original Run Sheet designed by Filipe Cardoso and Verónica Martins (18). Several PR profile tests were made and described in subchapter 3.3 in order to improve the lift- off process. PR profile optimizations consisted in change the energy of exposure (from 75% to 95%) and perform a pre-development step, during about 20-30 minutes, before exposure. The mask used to define the contact leads is shown in Figure 2-14.

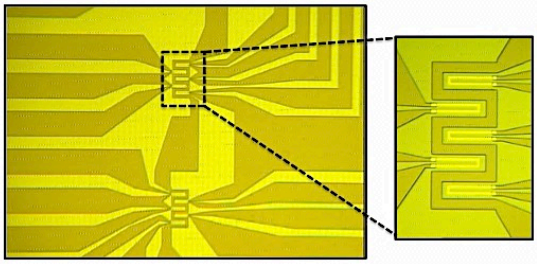

Figure 2-14: Contact leads definition.

- **Step 7 - Contact Leads deposition:** This step consists in deposition of Al layer. The thickness of Al layer was 3000Å and this layer will be used to make the contact lead between spin valve sensor and pads. The Al deposition was made in Nordiko 3600 using a deposition angle equal to 180° and the other conditions were described in Appendix I.

- **Step 8 - Al Lift-Off:** This step performed in the wet bench consists in lift-off of the Al layer. The protocol followed is the same used in step 5. With the optimizations performed during the lithography step, the lift-off total time can be minimized from days to hours, consequently minimizing the total time of biochip microfabrication process. In Figure 2-15 are presented the sample features after Al lift-off.

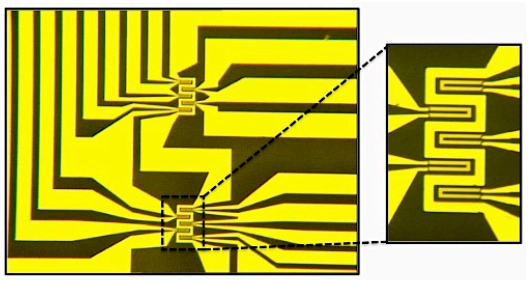

Figure 2-15: Aspect of current leads defined after lift-off.

- **Step 9 – Passivation layer deposition:** Passivation layer, SiN 3000Å, was deposited by CVD in Electrotech, described in section 2.2.1. Selection of passivation layer was the main optimization accomplished in this Run Sheet. All oxides that exist in INESC MN were submitted to different tests. Detailed characterization will be discussed in subchapter 3.4. All oxide tests were performed in order to find the passivation layer with optimal features, avoiding the instability and the corrosion. It was necessary to find the SiN deposition rate, using different deposition times and measuring samples with different thicknesses in the ellipsometer. A SiN 1000Å thickness was deposited and checked by ellipsometer and consequently the deposition time to 3000Å was achieved. The deposition rate was calculated in 40Å/sec.

- **Step 10 - Third mask exposure in DWL (Pads definition):** Third lithography was made to define the pads presented in Figure 2-16. In this step, because the following step is an etching step instead of lift-off, the same exposure conditions performed of step 3. In Figure 2-16 is presented the definition of pads.

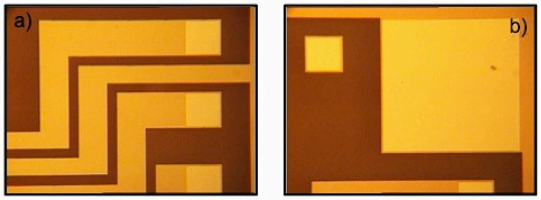

Figure 2-16: Pads definition. a) Two first pads (200 μm^2) will be used to address sensors whereas the third squared pad will be used to bias the U-shaped current line b) The biggest squared pad (750 μm^2) will be one out 4 common contacts to all sensors.

- **Step 11 – Pads etching:** Pads etching is the last step of pads definition. This was performed by ion milling using an angle equal to 70°, at Nordiko 3600, described in subchapter 2.2.3, in order to open pads allowing posteriorly the contact with sensors.

- **Step 12 – Resist stripping:** The sample was dipped on Microstrip 3001 at a temperature of 65° and the PR was stripped from the sample as described previously on step 5.

- **Step 13 - Fourth mask exposure in DWL (Au Pads definition):** Au pads (4.5x43μm^2) was patterned on top of 4 out of 5 SV in each area, defining the biological active area of the sensor as shown in Figure 2-17. The sensor without biologically active area operates as a reference sensor

whereas all 4 are used to the immobilization and hybridization of probes. The optimizations of lithography process depicted in step 6 were also applied in this case.

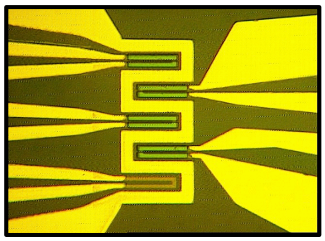

Figure 2-17: Au pads definition patterned on top of 4 SV in each area.

- **Step 14 – Au layer deposition:** This step was achieved by physical vapour deposition (PVD) in Alcatel SCM450 machine, described in subchapter 2.2.1. Before Au layer deposition, a thin film of 50Å Cr was deposited in order to improve the Au adhesion. After that, a 400Å Au layer was deposited in the patterned areas, defining the biological active area of sensors (Figure 2-18).

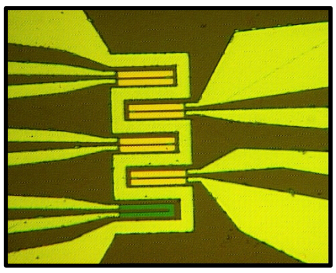

Figure 2-18: Sensors with biological active area defined and the reference sensor without biological active area.

- **Step 15 – Sample dicing:** The final sample had 4 dies (for 1x1 $inch^2$ sample). This step comprised the individualization of dies in order to encapsulate them in a printed circuit board (PCB) chip carrier and integrating in the platform to perform measurements. An automatic dicing system (DAD 321) was used to cut the sample dies.

- **Step 16 – Wire bonding:** This was the last step of biochip microfabrication process. Each die was mounted on a PCB chip carrier with 34 contacts. A wire bonding technique was used to connect the chip to the PCB chip carrier. This technique consists in ultrasonic vibrations to weld a thin aluminium wire to the metal contact on the chip. A protection of wirebondings is mandatory in order to prevent the corrosion of delicate contact areas. This protection step involved the application of soft silicon gel covering all wirebondings and a drying step for a 3 -4 hours at room temperature.

2.3 Characterization Techniques

For the purpose to ensure the successful working devices, the characterization of materials and devices has to be performed during and after the fabrication process. In this thesis, the topographic characterization of samples under process was made during the experimental work whereas the

electrical characterization was performed after fabrication the process. This is important to check its performance and applicability to specific goals.

2.3.1 Topographic Characterization

2.3.1.1 Ellipsometer

The ellipsometer (AutoEl) available at INESC MN clean room is used to determine the refractive index (n) and the thin transparent film thickness. This machine is presented in Figure 2-19a). A monochromatic and collimated beam irradiates a sample with a specific angle and wavelength. The transparent film, an oxide or nitride, must be deposited on top of an opaque substrate, such as Si, which provides total reflection. The difference between the states of polarization of the incident and reflected beams are determined in terms of angles, Δ and Ψ, and quantified by a numerical model to evaluate the refractive index and thickness of the film. In this thesis, the refractive index and thickness of two different films, SiN and SiO_2 were analysed (38, 40).

2.3.1.2 Profilometer

The profilometer (Dektak 3030 ST Veeco) showed in Figure 2-18b), performs sample topography measurement. The thin film thickness is determined by measuring the step height, usually at the edges of patterned structures. The measurement is based on a surface contact technique with a piezoresistive sensor, which is used to drag the sample surface for a defined range and detects any changes in topography. This equipment presents a lateral resolution about 20μm limited by tip dimensions, and a vertical resolution around 5Å, although due to environment noise a thickness higher than 300Å is required (38, 40).

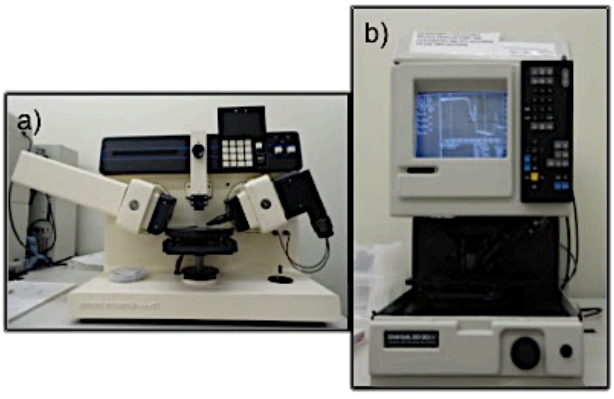

Figure 2-19: Characterization Tools: a) Ellipsometer AutoEl b) Profilometer Dektak.

2.3.2 Transport Characterization

2.3.2.1 Manual Transport Measurement Setup

In order to evaluate the electrical characterization of a MR sensor, in this case SV, its transport behaviour has to be analysed, as a function of an external magnetic field. This characterization can be performed using a manual transport measurement setup developed at INESC MN, presented in Figure 2-20a), and its scheme shown in Figure 2-20b). This setup is prepared to perform measurements on chip already integrated on a chip carrier or as processed samples, using 2 or 4 micro-positioner probes equipped with tungsten needles. SV measurement is usually performed using 2-probes that supply the MR sensor with a current (Keithley 220) while measuring the voltage at these terminals by a voltmeter (Keithlet 182). The magnetic field applied to the MR sensor, during the transfer curve measurement is created by two Helmholtz coils, which are connected in series and powered by a current source (Kepco Biporal operational power supply). All the setup components are automatically controlled by a computer through a General Purpose Interface Bus (GPIB) connection and software developed at INESC MN. To avoid electrostatic discharges when placing the probes in contact with the pads, two shunt switches are connected in parallel to the current source and voltmeter. A transfer curve of a spin valve used in a biochip is shown in Figure 2-21 with a resistance between 800Ω and 900Ω and a magnetoresistance of 7% (18, 38, 40).

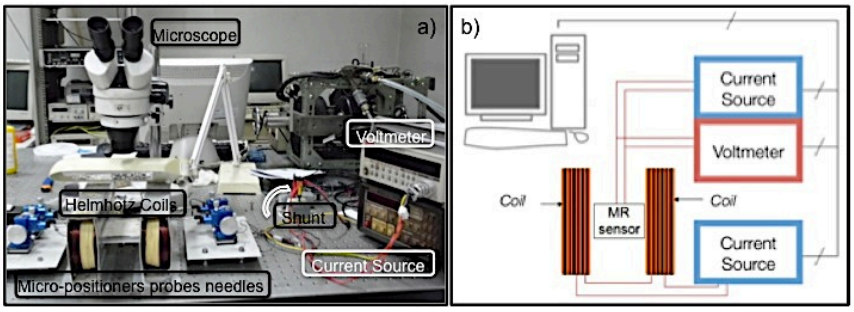

Figure 2-20: a) Manual transport measurement setup picture for electrical characterization of MR sensors b) Schematic of the manual measurement setup.

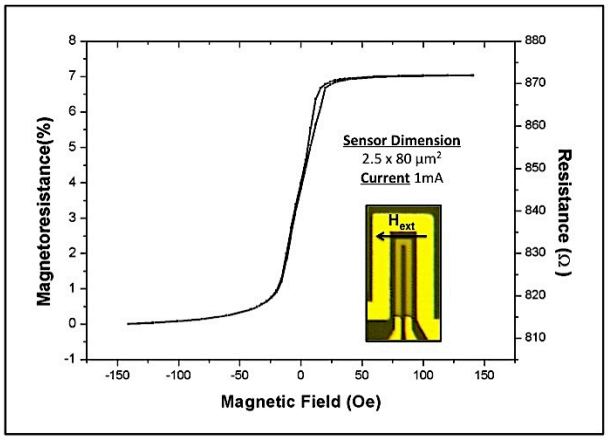

Figure 2-21: Typical transfer curve of a SV taken at a bias current of 1mA. The image shows the U-shaped 2.5x80μm^2 and a U-shaped current line surrounding the spin valve that is used for sample heating.

2.3.3 Magnetic Thermal Annealing

In this thesis, it was used the annealing setup available at INESC MN, Figure 2-22. In this system samples are placed in a metal holder, which is connected to the quartz rod inside the quartz tube. After, the metal holder is pulled into the furnace using the quartz rod, the system can be closed and pumped for making vacuum. First, the system has to be pumped with a mechanical pump, to achieve vacuum pressure below 10^{-3} Torr. After this, a turbo molecular pump is started, reaching pressures below 10^{-6} Torr. Then, the sample is heated until a set temperature, 220ºC with a slope of 5°C/min, and then this temperature is maintained during 10minutes. When the stabilization plateau is completed, the quartz rod is pushed to the interior of the permanent magnet (1T) and the samples are cooled down inside of it. In this process step, the pressure rises to ~ 10^{-5} Torr. When the cooling down step finishes, the system has to vent so that samples can be removed. The annealing of several samples at the same time is the advantage of this annealing setup. However, the magnetic field is only applied during the cooling down of samples, instead of during the entire thermal cycle, which in same cases can be a drawback (38).

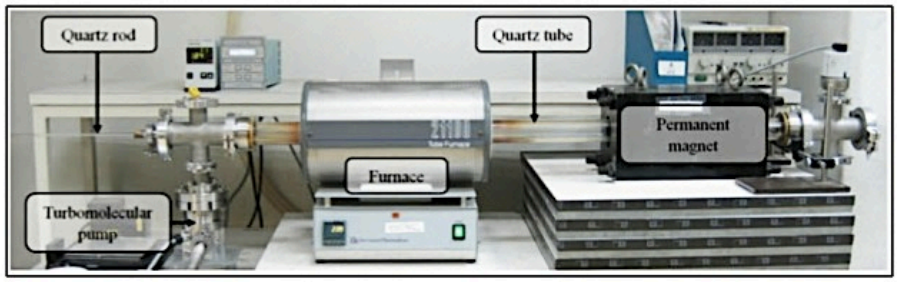

Figure 2-22: Magnetic thermal annealing: system where the magnetic field is only applied during cool down.

2.4 Magnetoresistive Portable Platform

The main propose of this project is the integration of PCR in a MR biochip inserted into a portable platform. The biochip is incorporated with a standard microfluidic platform that is used to specifically control the fluids flow (e.g. solution with target DNAs), which is put in contact with the chip to perform PCR on chip. Development of smaller, faster, more cost-effective and more powerful instrument, minimization of sample biological analysis time and volume and its independence of a laboratory are main advantages of this portable platform. From the user point of view, the platform operation mode and sample handling must be simplified. With these conditions, the user can perform the biological analysis near the most convenient place by just following some simple specific instructions. To accomplish all these specifications, an autonomous electronic platform capable of measuring and evaluating the biochip signal, controlling temperature and performing PCR was used.

2.4.1 Electronic Platform

The biochip platform used in this project, shown in Figure 2-23, includes all hardware components that are required to perform temperature control, real time signal processing and PCR on chip ensuring its portability (13). A typical biochip platform comprises the sensing chip (including transducing elements), magnetic particles as reporter systems, biological active interface with the biorecognition probes, electronic circuitry for system control, a transducer read-out and a microfluidic transportation system (13, 22). The platform is also provided with a battery, which guarantees power and portability to the system. The biochip connected to the PCB is integrated in an electronic circuitry, which performs the addressing, driving and reading-out of magnetic and electric signals provided to all sensors (13, 18, 25). Then, taking advantage of digital signal processing techniques, the acquired signals are processed in real time and transmitted to a digital analyser that enables the user to control and follow the experiment through a graphical user interface (13).

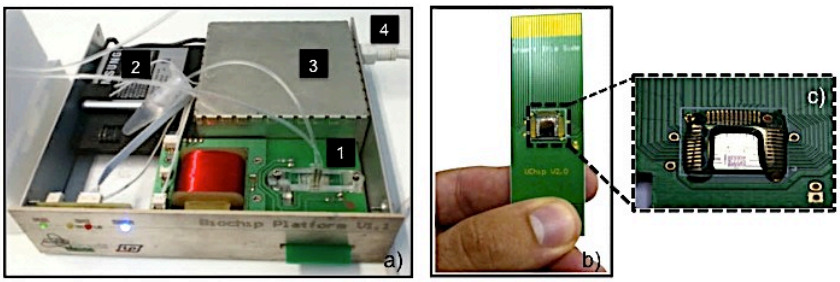

Figure 2-23: Topview of the portable platform for biological assays using a MR biochip: a) 1) Biochip encapsulated in a PCB chip carrier with microfluidic platform 2) Battery 3) Acquisition and control board (the PCBs are placed inside this box) 4) USB connector; b) and c) Biochip encapsulated in a PCB chip carrier.

2.4.2 Chip Design

The designed biochip comprises 6 different hybridization areas, each one with 5 SV sensors used for temperature and magnetic detection, and a current line for sample heating and magnetic focusing (Figure 2-24). In each area, the 5 sensors were disposed in one column, and one of these is a reference sensor (SV without biologically active area). All sensors have the same common contact, which corresponds to the top left and/or right biggest squared pads (750 μm^2). All the other squared pads with 200 μm^2 (except the third squared pads aligned left and/or right that are used to bias the U-shaped current line) are used to address each sensor. The current should pass between one of these squared pads and the common pad. The biochip with U-shaped SV sensor, which constitute the biochip core was deposited in a Nordiko 3000 onto a glass substrate with the following structure: Ta 20Å/$Ni_{80}Fe_{20}$ 36Å/$Co_{81}Fe_{19}$ 23Å/Cu 25Å/$Co_{81}Fe_{19}$ 23Å/$Mn_{76}Ir_{24}$ 80Å /Ta 30Å/$Ti_{10}W_{90}$(N) 150Å. The definition of a sensor area of 2.5x80 μm^2 by ion milling was processed and the contact leads of Al 3000Å were deposited by IBD and defined by lift-off. After, a passivation layer of SiN 3000Å was deposited by CVD over the whole chip and pads were defined by ion milling.

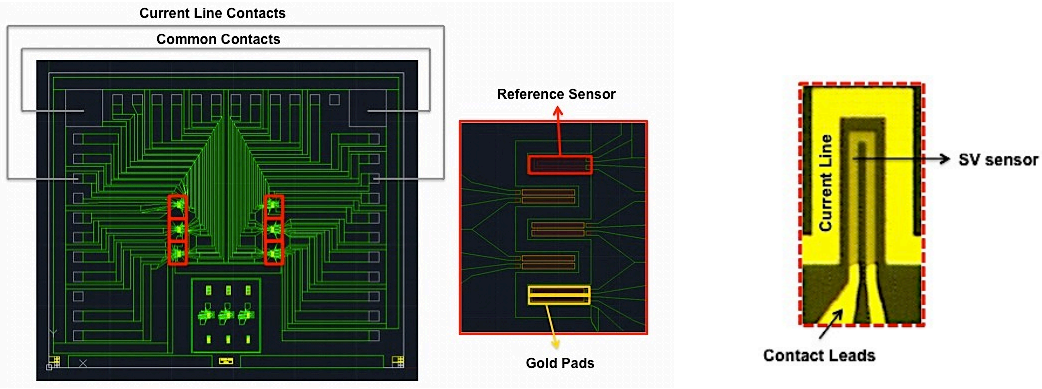

Figure 2-24: Chip design with 6 independent areas. Each area comprises 4 sensors and 1 reference sensor (SV without biological active area).

Finally, the gold pads of 4.5x43 μm^2 were deposited, in 4 out of 5 sensors and defined by lift-off. All sensors were optimized in order to achieve a linear response. The U-shaped current line surrounding the sensors was designed to enable the sample heating and subsequent the focusing of the particles onto the sensing area (18).

2.4.3 Microfluidic System

The biochip platform discussed in this subchapter is also provided with a microfluidic module that consists of two different polymers: polymethylsiloxane (PDMS) and polymethylmethacrylate (PMMA). PDMS was chosen to fabricate the U-shaped channel due to its biocompatibility, its price and fast casting techniques, and PMMA was used to fabricate the holder, enabling the miniaturization of microfluidic device (18). Thereby, the biochip is incorporated in the platform and the U-shaped microfluidic channel is aligned with the sensors column and sealed (Figure 2-25).

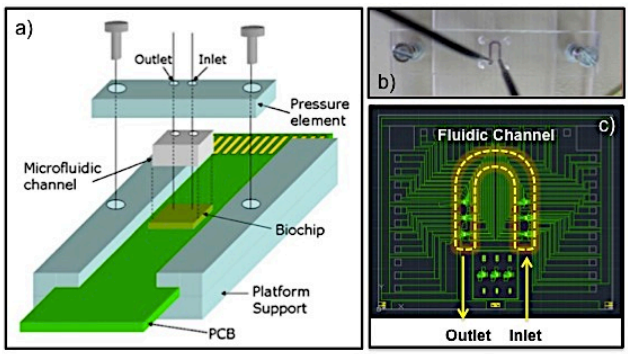

Figure 2-25: Microfluidic platform: a) Scheme of microfluidic platform that includes PCB aligned with the PDMS channel and PMMA holder b) PDMS element: U-shaped fluidic channel c) Chip representation with the U-shaped fluidic channel aligned and sealed with sensors inside the channel.

The sealing of the U-shaped channel to the chip is achieved with a pressure platform, which consists of a PCB holder and the pressure element where the PDMS channel fits in. Two springs, placed along two screws aligned with the holder, apply the pressure required over the PDMS always keeping the

sensors inside the channel. Compressing the springs (pushing up the pressure element) the PCB can be replaced without channel realignment. Finally, solutions can be put in contact with the chip (PCR mixture, buffer and particles solution) and its inlet and outlet can be regulated through a controlled method (22). Microfluidic PCR chips have been important to control the thermal cycle reproducibility in the biochip and to localize efficiently the target molecules in the sensing zone (42). The main advantages of this microfluidic system are the reproducibility of the measurements, sample evaporation reduction during analysis, its biocompatibility enabling gaseous exchanges between the environment and the interior of the channels and good thermal stability (22).

3. Configuration PCR Chip

3.1 Overview

Micro-electric-mechanical-system (MEMS) technology and microfabrication techniques have been reported to the fabrication of temperature control systems suitable for biomedical applications and to execution of chemical an biochemical reactions on a microchip (43). Several devices have been designed specifically to miniaturize and to integrate the polymerase chain reaction (PCR) technique, a crucial amplification method in the field of molecular biology (43, 44). Integrated PCR microchips have shown considerable potential for rapid DNA amplification. PCR system miniaturization offers some advantages such as, improvement of analysis processes and thermal cycling times, low power consumption, low cost, sensitivity, portability and disposability (43, 45).

3.2 Substrate Materials Background

Materials optimization for PCR chip microfabrication process is mandatory in order to ensure temperature uniformity, to improve temperature heating and cooling ramp times and biocompatibility required for the PCR. Microfabricated PCR chips and thermocyclers have generally been fabricated using the three most popular materials, silicon (Si), glass and polymers. Each substrate has different properties and therefore different advantages and disadvantages.

3.2.1 Si

Si has been incorporated in biochips microfabrication processes due to its easily micromachined and then precise and complex chip structures have been successfully achieved (8, 46). Si has an excellent thermal conductivity (157 mW/K) that ensures a temperature rapid increase (rapid PCR cycling) and a homogeneous local temperature distribution (43, 47). Due to its high thermal conductivity, the silicon requires thermal isolation resulting in structural complexity and its surface has to be covered with another material, such as silicon oxide or silicon nitride, since the untreated silicon surface can inhibit the PCR (31, 43, 46, 48).

3.2.2 Glass

Glass has been one the most widely used materials in lab-on-a-chip (LOC) devices since a vast array of well-established integrated circuit and microfabrication technologies are available. Glass can be an excellent choice for PCR devices microfabrication since it is impermeable for gases, presents a superior biocompatibility compared with Si, and its surface is readily treated by a variety of surface coating agents to reduce DNA and enzyme adsorption (43, 46, 48, 49). Moreover, microfabrication

process of glass microdevices generally is easy and at lower cost and a short response time and low power consumption are achieved (43, 50). Although, glass thermal conductivity is 1.1 mW/K (more than a hundred times lower than that of Si) and the thermal delay time of glass is longer than that of Si-based materials, the systems made of glass are well-thermally isolated (31, 43). Another advantage of glass substrates is its high dielectric strength (50).

3.2.3 PDMS

Other materials commonly used for PCR devices microfabrication are polymers, such as PDMS or PMMA. Polymers have some advantaged characteristics such as simple fabrication, inexpensiveness, and biocompatibility and can be easily integrated with other system (46). However, the thermal conductivity of PDMS is normally low leading to poor performance in short thermal cycling time (45). This is the main disadvantage of PDMS when it is used as material substrate. Therefore, the PDMS should be combined with either metal or Si in order to achieve the desired thermal properties (31).

Initially, in this project, a Si-based substrate was chosen for the biochip microfabrication process, presenting several advantages and good thermal characteristics. However, the high thermal conductivity of Si makes it difficult to maintain the zones available for fluid with uniform temperature due to its lateral heat conduction. This disadvantage induces a high dissipation of heat by Si substrate instead of promoting the heat transfer to the fluid ensuring a rapid PCR cycling. In order to overcome the main disadvantage of Si substrate, the glass was chosen as substrate material in the PCR chip microfabrication process. As the thermal conductivity of glass is lower than that of Si, glass was presented as a suitable material due to its electrical insulating properties and ability to establish uniform temperature within a confined area while limiting lateral heat conduction. Then, using a glass substrate the heat transfer to the PCR sample being amplified was ensured. In this project, the PDMS was also integrated in the PCR microdevice. Due to its cheap and fast casting techniques and biocompatibility, PDMS was used to fabricate the microfluidic channel. Moreover, in this case the low thermal conductivity of PDMS was not presented as a disadvantage for PCR microdevice, since it makes it possible to ensure the thermal uniformity of fluid inside the channel.

3.3 Photoresist Profile Optimization

The main goal of this subchapter consists in the description of the efforts done in order to characterize the lithography process performance. Some parameters have an important effect on final pattern quality. In particular, photoresist (PR) properties and performance are associated with several variables, such as pre-development and development conditions and exposure parameters (energy) that directly affect the PR evaluation. Therefore, this characterization was orientated to optimize the exposure, pre-development and development conditions, which discussion of results is presented in subchapter 3.3.1. The study of these conditions contributed to improve the PR profile and minimize

the period of time required for lift-off process and consequently the total time of microfabrication process.

3.3.1 Photoresist and Development Study

During the microfabrication process of biochip following the run-sheet designed by Filipe Cardoso and Verónica Martins (18) the edge roughness behaviour (presented in Figure 3.1) was observed at step 8 (Al lift-off).

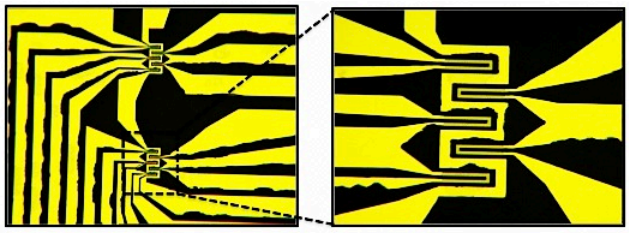

Figure 3-1: Edge roughness result when lift-off process was complete.

In order to evaluate the reasons for this behaviour, the study of PR profile was mandatory, which is described in detail in following subchapter. The lithography parameters characterization included the analysis and optimization of exposure energy and, pre-development and development in lithography steps that were processed before lift-off process, while all lithography steps made before etching were performed with normal and set conditions. Varying these specific parameters, a PR profile modification can be achieved, improving the lift-off process results. Using normal lithography parameters (no pre-development and 75% exposure energy) the PR usually acquires a profile identical to that represented in Figure 3-2a. However, this PR profile, favours the arising of rabbit ears (Figure 3-2c), which consists in Al pieces that remains on the edge of the Al tracks, when the lift-off process was complete. If these rabbit ears fall on the surface, an unwanted shape on the substrate can be performed. But, is these remains on the surface unwanted connections could be caused when different layer is deposited on top of the surface.

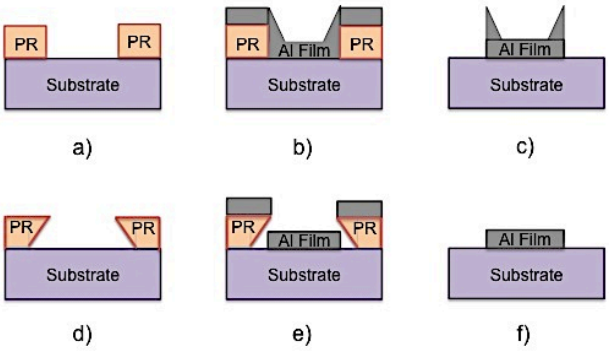

Figure 3-2: PR profile optimization: a) PR profile achieved when normal lithography parameters (no pre-development step and 75% exposure energy) was performed b) Al film deposition c) When the lift-off process was complete the rabbit ears presence was verified d) An PR undercut profile was achieved when lithography parameters were optimized e) Al film deposition c) No rabbit ears when the lift-off process was complete.

The extensive time required to complete the lift-off process using this PR profile can be considered other disadvantage. Then, in order to minimize the total time of lift-off process and to avoid the rabbit ears presence, a undercut profile should be achieved, as presented in Figure 3-2d), following the lithography parameters optimization (pre-development step and exposure energy) described in the specific Run Sheet Photoresist Profile Optimization in Appendix II.

3.3.1.1 Lithography Parameters Characterization

With the purpose of evaluating the effect of alterations on the lift-off performance, a simplified microfabrication process was accomplished, which is described in detail in the Run Sheet for Photoresist Profile Optimization in Appendix II. In this process it was used a ¼ of 6-inch silicon wafer with Al_2O_3 500Å deposited at Nordiko 3600.

Run Sheet for Photoresist Profile Optimization

- **Step 1 – Mask exposure in DWL (contact leads definition):** In this step it was patterned the second layer of the mask that consisted in contact leads definition, presented in Figure 3-3. This layer was used due to its complexity and smaller dimensions so that the efficiency of lift-off process could be evaluated.

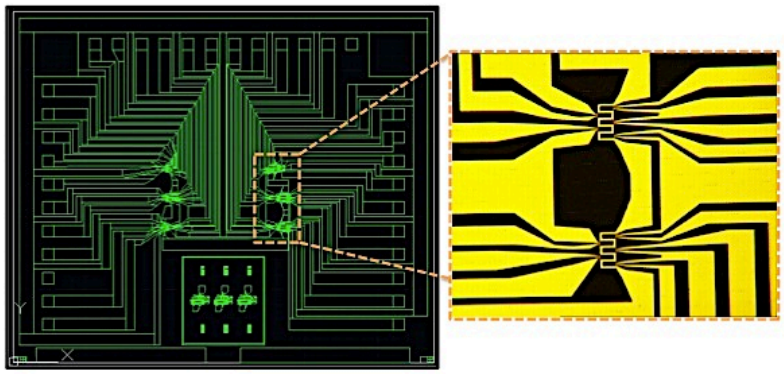

Figure 3-3: Second layer of mask patterned on samples used to lithography parameters characterization.

The optimization procedure of PR profile was initiated with the application of a thin and uniform PR layer, which is critical for the success of the lithographic process. The coating conditions described in subchapter 2.2.2 were maintained. The conditions of pre-development and exposure energy in each die were changed and evaluated using the following method:

- **First Sample:** No pre-development step and exposure energy variation between 75% and 100%.
- **Second Sample:** Pre-development during 30 seconds (before exposure) and exposure energy variation between 75% and 100%.
- **Third Sample:** Pre-development during 60 seconds (before exposure) and exposure energy variation between 75% and 100%.

Dies position in each sample is presented in Figure 3-4 with respective conditions of variables tested. Development time after exposure was adapted for each specific sample.

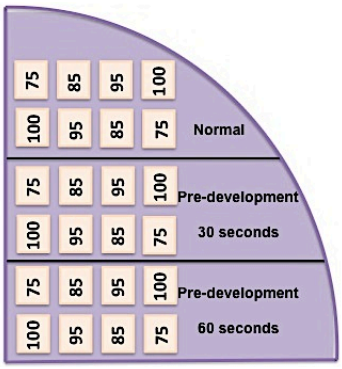

Figure 3-4: Dies position in each sample with respective energy variation. Normal: No pre-development and energy variation between 75% and 100%; Pre-development 30 seconds and energy variation 75% and 100%; Pre-development 60 seconds and energy variation 75% and 100%.

- **Step 2 – Contact Leads deposition:** This step involves the Al 3000Å layer deposition and it was processed in order to simulate the step 7 of original Run Sheet. The layer thickness deposited was checked in profilometer.

- **Step 3 – Al Lift-Off:** Lift-off was made with the same conditions of step 8 in the Run Sheet described in subchapter 2.2.5. This step was also crucial in the characterization and optimization of profile PR. The effectiveness and the time required to complete lift-off were analysed in detail for each die with different time of pre-development and exposure energy in order to define optimal conditions for future microfabrication steps.

The crucial result of this optimization was obtained when lift-off process was completed. The optimal result would be to achieve an effective lift-off in a short time, minimizing the process time from days to minutes. The lift-off of the sample submitted to pre-development during 30 seconds was completed after 100 minutes (80 minutes, total time in hot µ-strip at 65ºC and 20 minutes in ultrasounds). The Figure 3-5 shows the lift-off results of sample submitted to pre-development during 30 seconds and at different energy exposure

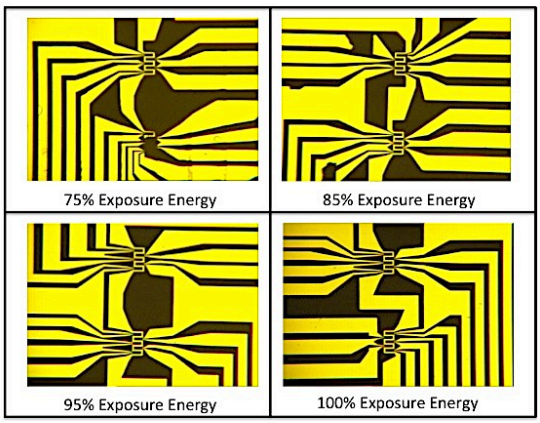

Figure 3-5: Lift-off results of sample submitted to pre-development during 30 seconds and at different energy exposure.

Dies exposed with 95% and 100% of energy presented the intended results, which are good definition of strips. However, using 75% and 85% of exposure energy, the results were inadequate since dies presented Al pilling in unwanted areas (Figure 3-5).

The results of the sample submitted to pre-development during 60 seconds were different from expected. Using 75% of exposure energy, it was impossible to obtain results due to the fact that two dies revealed over development under these conditions. In the two dies exposed with 85% and 95% energy, Al pilling was observed by optical inspection (Figure 3-6). When using 60 seconds pre-development only dies exposed to 100% energy presented a good definition of strips (Figure 3-6). Time required to conclude lift-off was the same used for the sample with pre-development during 30 seconds.

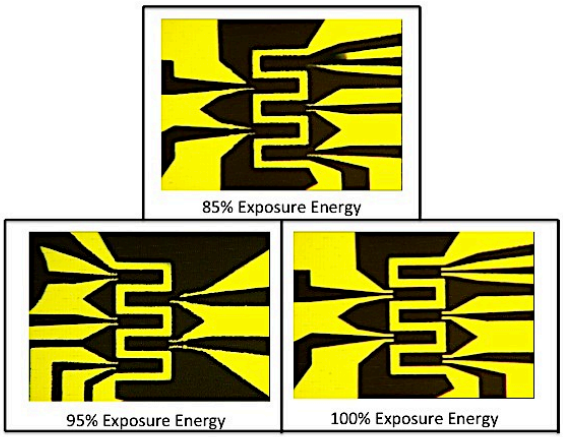

Figure 3-6: Lift-off results of sample submitted for pre-development during 60 seconds and at different energy exposure.

Normal sample non submitted to pre-development and exposed with energy variation between 75% and 100% showed completely different results. First, this sample was submitted to the same lift-off time used for samples with pre-development. However, in this case the lift-off of the sample was incomplete (Figure 3-7).

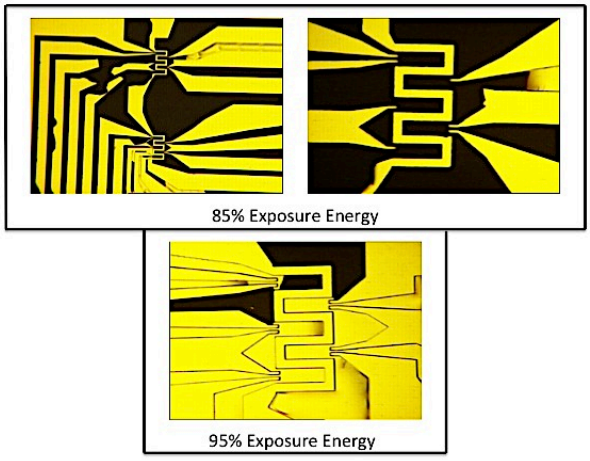

Figure 3-7: Lift-off results of sample non-submitted to pre-development but with different energy exposure. Dies exposed with 85% shows contact leads damaged before the process was complete. Incomplete lift-off process is observed in dies with 95% of exposure energy.

Moreover, dies exposed with 85% of exposure energy presented the contact leads damaged before lift-off was complete (Figure 3-7). Therefore, in order to accomplish the complete lift-off two more days in hot µ-strip at 65ºC alternating with ultrasounds was required.

The time required to finalize the lift-off was different between sample without pre-development and samples, which were exposed to pre-development (30 and 60 seconds). In order to compare directly the results obtained with the respective time required to accomplish the test goal the reader is referred to Table 3-1.

Table 3-1: Summary of PR profile optimization results comparing the results obtained for different samples with or without pre-development at different energy of exposure with time required to complete the process.

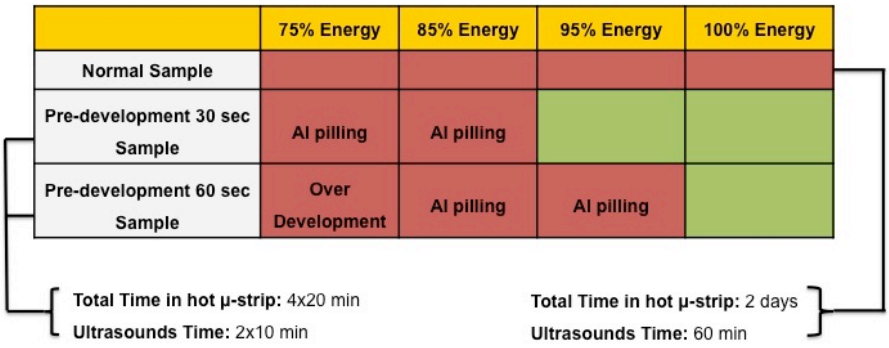

Regarding the information provided by Table 3-1 can be concluded that the optimal result for profile optimization consisted in the pre-development during 30 seconds in maximal, and 95% or 100% exposure energy. Although the sample submitted to the pre-development during 60 seconds and 100% exposure energy had presented suitable results, there was a considerable probability to occur overdevelopment.

3.4 Oxide Characterization: Passivation Layer Optimization

Oxide characterization and optimization comprises the evaluation of all oxides existing at INESC MN and oxide selection that presents optimal characteristics as passivation layers, in order to ensure a uniform insulation of biochip, which is fundamental for proper biological assay performance. These tests were proposed due to corrosion of Al_2O_3/SiO_2 passivation layer (used previously by Filipe Cardoso e Verónica Martins (18)) when a test with fluids was performed at the magnetoresistive (MR) biochip (Figure 3-8). The goal of this test consisted in signal acquisition of biochip sensors at the platform, when a 10µl droplet of phosphate buffer (PB) was dispensed on top of the biochip. For this acquisition, the sensors were submitted to a DC current of 1mA and a field AC of 13.5Oe. The decreasing of sensors signal was observable during acquisition. Therefore, assays were not finalized, due to corrosion of oxide that covered the biochip surface meaning total loss of sensors signal during the assay.

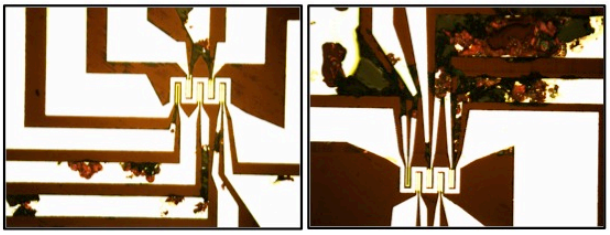

Figure 3-8: Corrosion of SiO_2/Al_2O_3 passivation layer after fluid test and consequently total lost of sensors signal.

In order to prevent the corrosion all existing oxides at INESC MN, SiO_2 (Alcatel), Al_2O_3 (UHVII), Al_2O_3 (Nordiko 3600) with different deposition angles, SiO_2 and SiN (Electrotech) were evaluated. Therefore, for these optimization tests three different samples were microfabricated, each half with a different oxide. The evaluation of several variables such as, oxide breakdown voltage, metal overlay, metal resistivity, scanning electron microscope (SEM) analysis and tests with fluids were performed for each oxide. The passivation layer characterization consisted in a simplified microfabrication process that involves three lithography steps described in detail at Run Sheet for Passivation Layer Optimization presented in Appendix III. During this thesis, a test die was also strategically designed by Filipe Cardoso, in order to perform all tests required. A subsequent advantage of this test die consists in its integration, with a specific distribution, in a 6-inch wafer for a microfabrication process, promoting the electrical inspection in different zones of the wafer during the process.

Run Sheet for Passivation Layer Optimization: Oxide Characterization

The mask used for the microfabrication process of test samples, was strategically designed in order to perform all tests required. The geometry designed was maintained similar to that used in biochip microfabrication process. In this process, three pieces of 1-inch Si wafer with Al_2O_3 500Å deposited at Nordiko 3600 on its top were used (Figure 3-9). Its configuration consisted of two metallic layers intercalated with a passivation layer. The passivation layer that presents the optimal insulation features was chosen for biochip microfabrication process.

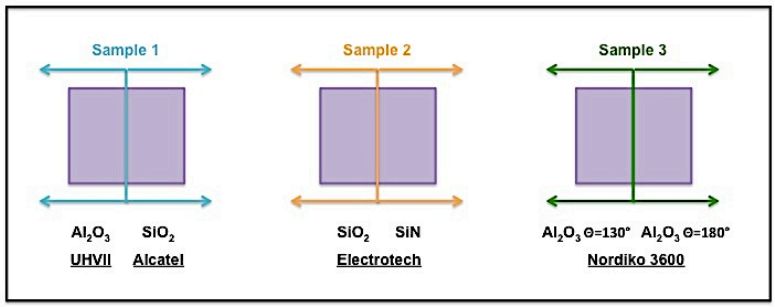

Figure 3-9: Schematic of oxide distribution in three pieces of 1-inch silicon wafer with Al_2O_3 500Å deposited at Nordiko 3600.

- **Step 1 – First mask exposure in DWL (first metallization layer definition):** This step consisted in defining the first metallization layer, presented in Figure 3-10. All lithography steps were made following its description in subchapter 2.2.2. The variables optimized in PR profile tests were applied in this step, which consisted in the pre-development during 30 seconds and 95% of exposure energy.

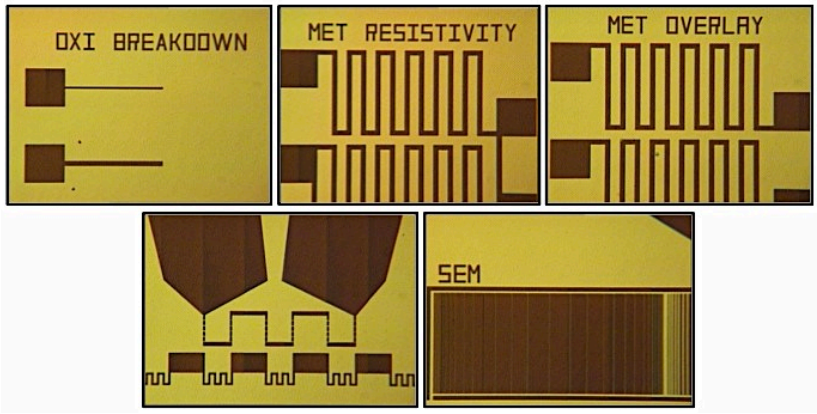

Figure 3-10: First metallization layer definition with all variables represented: oxide breakdown voltage, metal resistivity, metal overlay, fluid tests and SEM analysis.

- **Step 2 – First Metallization Layer Deposition:** Metallization layer was deposited in Nordiko 3600 and its thickness was Al 3000Å. The deposition conditions are described in Appendix III.

- **Step 3 – First Metallization Layer Lift-Off**: This step was performed in wet bench following the protocol described in subchapter 2.2.4. With the optimizations performed during the lithography step, lift-off was completed in 100 minutes. Some lift-off results are presented in Figure 3-11.

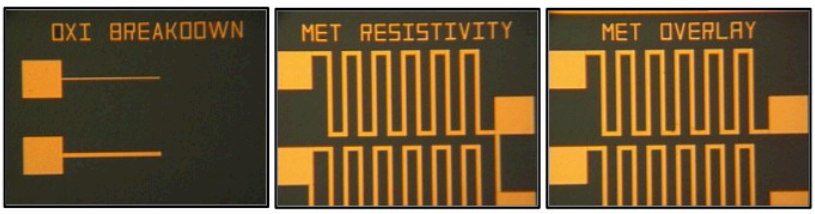

Figure 3-11: Illustrative pictures of first metallization layer lift-off.

Next steps were only performed for samples 1 and 3. For sample 2, these steps were achieved following Run Sheet for Passivation Layer Optimization presented in Appendix III, using the defined mask. In left side of the sample was deposited SiO_2 and on the right side, SiN by chemical vapour deposition (CVD) in Electrotech (Figure 3-9).

- **Step 4 – Second mask exposure in DWL (pads definition):** The third layer of the mask was used to pattern the pads. The lithography process followed the same conditions used in step 1.

- **Step 5 – Oxide Deposition:** In this step specific oxides in each sample were deposited. A layer of Al_2O_3 3000Å (UHVII) and another of SiO_2 3000Å (Alcatel) were deposited on the left and right side of sample 1, respectively. Using different deposition angles an Al_2O_3 3000Å layer (Nordiko

3600) was deposited on top of sample 3. On the left side the deposition angle was 130º and on right side the deposition angle was 180º. Other deposition conditions are described in detail in Appendix III.

- **Step 6 – Oxide Lift-Off**: Same conditions than step 3 were used for oxide lift-off.

- **Step 7 - Third mask exposure in DWL (second metallization layer definition):** This step consisted in the definition of second metallization layer in which it was used the fourth layer of the mask (Figure 3-12). All lithography steps were made with the same conditions than those presented in step 1.

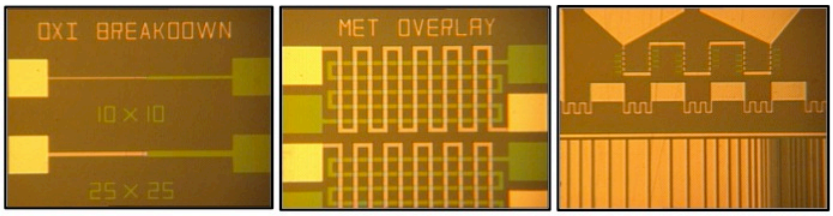

Figure 3-12: Second metallization layer definition in some parts of die.

- **Step 8 – Second Metallization Layer Deposition:** In this step it was deposited the second layer of Al 3000Å, in Nordiko 3600 using a deposition angle of 180º and other conditions decribed in Appendix III.

- **Step 3 – Second Metallization Layer Lift-off**: The test sample process was completed with this step, which consisted in Al second metallization layer lift-off (Figure 3-13). The final geometry of the test sample comprised two metallization layers intercalated with a passivation layer.

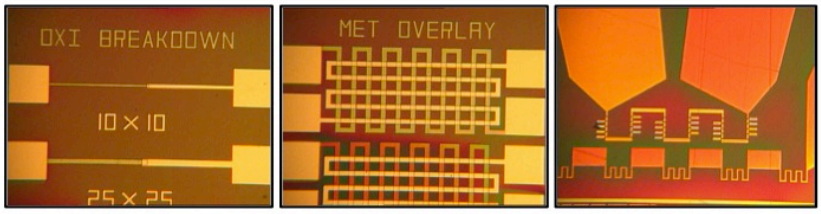

Figure 3-13: Last step of test sample microfabrication process: second metallization layer lift-off.

When the test sample microfabrication was completed all tests were performed in order to find the oxide with optimal features for passivation layer, the best insulation layer, totally avoiding the current flow between to two metallic layers. The manual transport measurement setup described in subchapter 2.3.2.1 was used to perform the oxide tests. In these tests an additional DC power supply source HPE3612A was used. In order to avoid electrostatic discharges when the electric probes are placed in pads, the shunt switches must be in short circuit.

3.4.1 Oxide Breakdown Voltage

The aim of oxide breakdown voltage test consisted in defining the oxide with the highest possible breakdown voltage, which consisted in voltage applied across the oxide layer that irreversibly destroys the electrical insulation. The procedure used to analyse this behaviour was based on the evaluation of the limit voltage supported by each oxide until achieving its disruption. A DC power supply source and electrical 2-probes were used for this measurement. It was mandatory to ensure that the DC power supply source was not in current controlled mode. The first step of this procedure consisted in putting the electrical probes on two pads as presented in Figure 3-14.

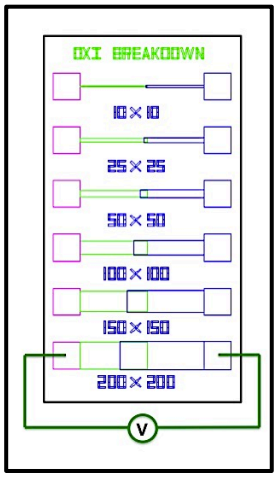

Figure 3-14: Scheme of measurement procedure of oxide breakdown voltage.

After that, it was observed if there was contact between two pads (short circuit) or not (open circuit). An open circuit was expected, which explains the insulation of two metallic layers. After checking open circuit a voltage in pads was applied, using a DC power supply source. The voltage was increased until reaching the breakdown voltage (when a short circuit appears on the display and by optical inspection, as presented in Figure 3-15). The short circuit reveals that the current flows between two metallic layers and disruption of oxide was achieved.

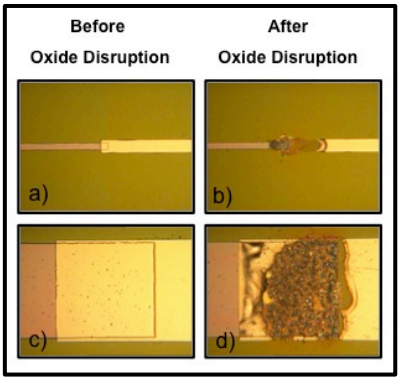

Figure 3-15: Optic results of oxide breakdown voltage test a) Contact area of 10x10 μm^2 before breakdown voltage c) Contact area of 200x200 μm^2 before breakdown voltage b) and d) Oxide disruption when breakdown voltage was achieved.

According to the results expressed in Figure 3-16 an intensive analysis can be performed.

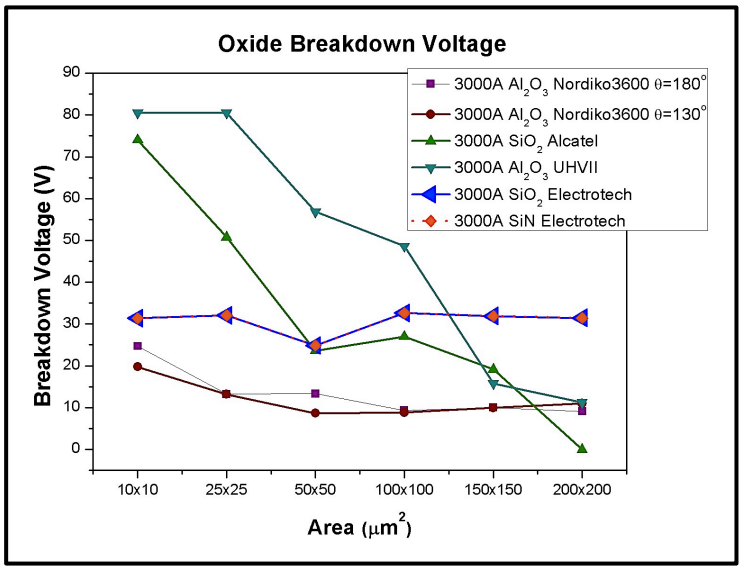

Figure 3-16: Results of oxide breakdown voltage test. Representation of breakdown voltage (V) in function the area (μm^2) to each passivation layer.

Oxides deposited by sputtering in Alcatel and UHVII presented the highest breakdown voltage although a value of about 30V for breakdown voltage would be adequate. However, these values of breakdown voltage are too high and are not constant with the area and therefore should be questioned. Al_2O_3 film deposited in Nordiko 3600 with different deposition angles demonstrated similar results and uniform behaviour, although values of breakdown voltage achieved were unsatisfactory, between 25V and 12V. Films deposited by CVD in Eletrotech revealed satisfactory breakdown voltage values between 30V and 35V. Moreover, higher values than 35V could be achieved for CVD films, but the oxide performance was only verified until 35V. With these results it was observed that the breakdown voltage decreases with area increase, excepting the two CVD films in which the breakdown voltage remained constant. An additional study Figure 3-17 was performed in order to evaluate and quantify the presence of short circuits in structures of each different area for all oxide films, before measurements. This was crucial data to select the optimal oxide according to the results of breakdown voltage test.

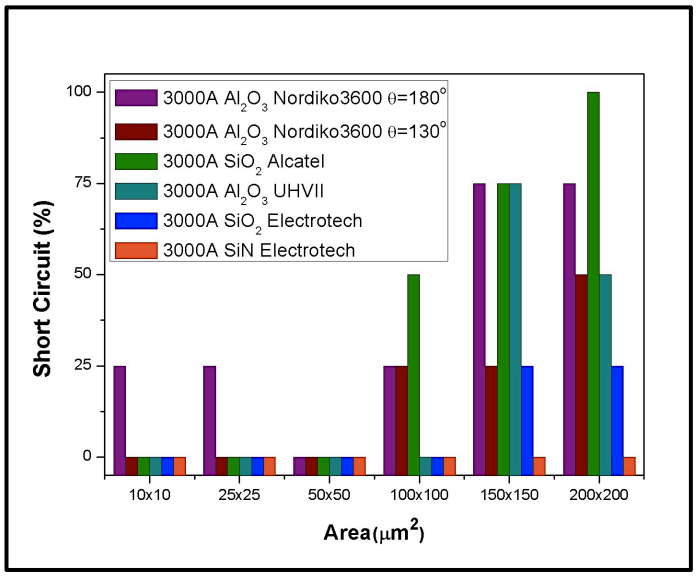

Figure 3-17: Evaluation of short circuit in structures of each different area for all oxide films, before measurements.

3.4.2 Metal Overlay

Aiming metal overlay and metal disruption voltage evaluation it was deposited a metallic layer on top of another metallic layer intercalated with an oxide layer. For this test a measuring setup presented in Figure 3-18 was used. This measurement setup consisted in allocating the electrical probes in serpentine shaped pads corresponding to each metallization layer. After that, it was mandatory to verify if there was a contact (short circuit) or not (open circuit) between the two metallic layers. An open circuit was expected meaning that no current flew through the passivation layer and the selected oxide had ideal isolating features. If an open circuit was achieved, then a voltage until 10V was applied in order to evaluate the operation mode of the serpentines. For this procedure a DC power supply source in voltage controlled mode was also used.

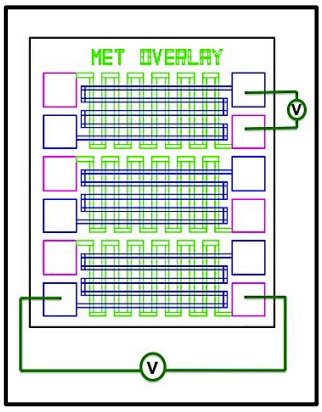

Figure 3-18: Scheme of measurement procedure of metal overlay.

Once a short circuit was observed the oxide achieved its disruption voltage and the contact area of two metallic layers appeared damaged. All serpentines were inspected and a statistical result was achieved.

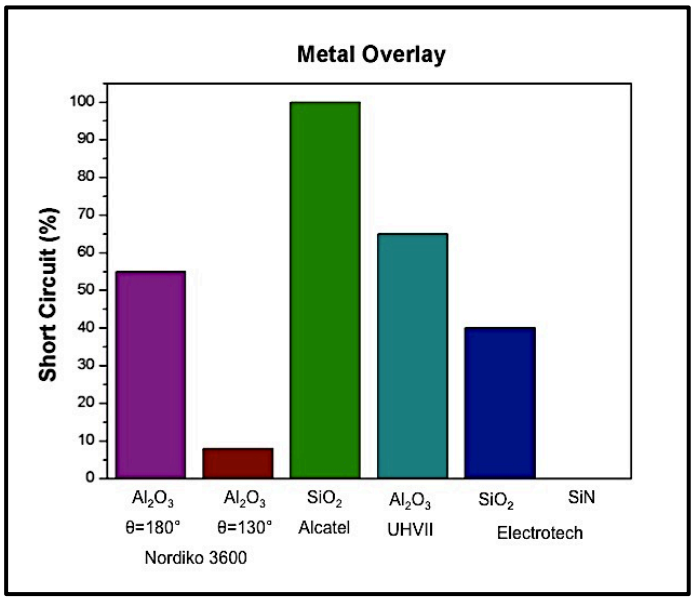

Figure 3-19: Results of metal overlay tests. Short circuit percentage is demonstrated for samples with different oxides deposited as passivation layer.

The results obtained in this geometry Figure 3-19 were coherent with results presented in Figure 3-18. SiO_2 (Alcatel), Al_2O_3 (UHV II) and Al_2O_3 (Nordiko 3600 θ=180º) revealed a higher percentage of short circuits, 100%, 62% and 55% respectively. This behaviour can be explained by the presence of rabbit ears (a result of Al lift-off), which are not totally covered by the passivation layer, since these oxides were deposited by sputtering, performing a anisotropic and non conform deposition. On the other hand, SiO_2 (Electrotech), Al_2O_3 (Nordiko 3600 θ=130º) and SiN (Electrotech) showed a lower percentage of short circuits, 42%, 8% and 0%. These results are typical of a conform deposition system of oxides. In these cases, even if the presence of rabbit ears was verified the passivation system is so conform that short circuit is impossible to occur. After an open circuit was verified 10V were injected to evaluate the serpentines behaviour. With this voltage, the different oxides were not disrupted.

3.4.3 Metal Resistivity

The resistivity is denominated as a factor of measure of the material resistive nature and quantifies how strongly a given material opposes the flow of electric current. Moreover, the resistivity is directly proportional to resistance, and regarding Ohm's Law for the same applied voltage, when the resistance decreases, the current increases. Therefore, a low resistivity indicates that a material readily allows the movement of electric charge. An increase of the electric charge movement means that the material has a low resistivity. So, for metal resistivity inspection, four electrical probes connected to DC power supply source were used. The procedure used to execute the metal resistivity

measurement is illustrated in Figure 3.20. This measurement consisted in putting the electrical probes on specific pads (probes that conduct current are placed in exterior pads and probes that measure the voltage in interior pads). After that, a 1mA current could be injected on the exterior pads and the voltage value measured and registered on the interior pads. In order to calculate the resistance value the Ohm's Law was used:

$$\boldsymbol{R} = \frac{\boldsymbol{V}}{\boldsymbol{I}}\ [\boldsymbol{\Omega}] \tag{3-1}$$

where, R is the resistance, V the voltage and I the current. After calculating the resistance value, the resistivity can be determined using this equation:

$$\boldsymbol{\rho} = \boldsymbol{R}\frac{\boldsymbol{t}\times\boldsymbol{w}}{\boldsymbol{L}}\ [\boldsymbol{\Omega}.\boldsymbol{m}] \tag{3-2}$$

where ρ is the resistivity, R is the resistance, t is the thickness of layer, w the layer width and L the length.

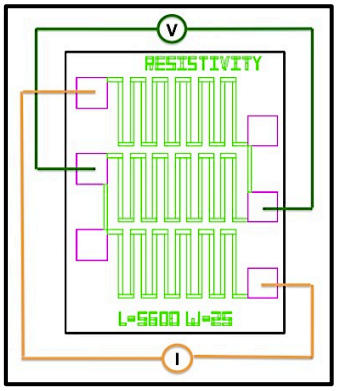

Figure 3-20: Scheme of measurement procedure of metal resistivity using electrical 4-probes, in which 2 probes conduct current while other 2 probes measure the voltage in interior pads.

In this case, the thickness of the Al layer was 3000Å, with 5600μm length and 25μm width as represented in Figure 3-20. In Figure 3-21 the metal resistivity, after finalization of samples microfabrication process can be evaluated. In the case of sample covered with SiO_2 and SiN (Electrotech) the first metallization layer is exposed at 300ºC during 1 minute and 14 seconds, during the oxide deposition, and the Al grain structure can be modified. This step can explain the lower resistivity of the metal verified in these two samples. However, these values of lower resistivity do not have a negative influence on biochip performance. Moreover, if these samples had been submitted to higher temperatures during a longer period of time, the resistance could be decreased to more satisfactory values. Comparing with the other two samples it can be verified that the process of SiO_2 (Alcatel) and Al_2O_3 (UHVII) deposition (sputtering) was performed at higher temperatures than Al_2O_3 deposition performed by IBD at Nordiko 3600. In samples covered by Al_2O_3 with different angles in Nordiko 3600, the highest resistivity was formed.

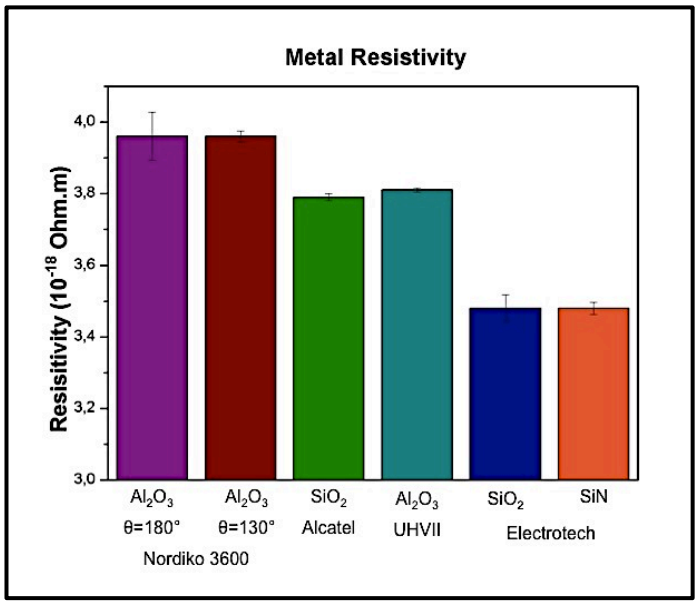

Figure 3-21: Metal resistivity measurements results.

3.4.4 Scanning Electron Microscope

The RAITH 150 system at INESC MN is available to perform scanning electron microscope (SEM) inspection. This system is installed at the white area of INESC MN clean room (Figure 3-22). SEM consists in electron microscope technique that produces images of a sample by scanning with a focused beam of electrons. The interaction of electrons bombarded and electrons in the sample generates several signals that can be detected and that contain information about sample surface topography and composition. The electron beam is generally scanned in a raster scan pattern, and the beam position is combined with the detected signal to produce an image. Samples are placed directly and stress free onto a sample holder, designed for long term stability.

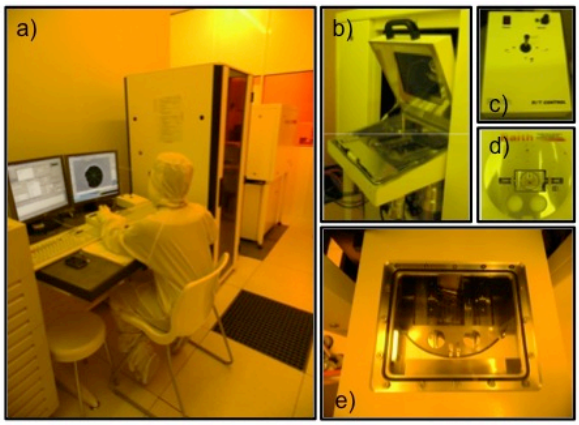

Figure 3-22: SEM imaging a) The RAITH 150 system comprises two computers responsible for the lithography pattern generation (Software P – Left PC) and SEM mode operation (Column PC – Right PC) b) Opened loadlock showing the platform where the sample holders are placed. c) Unit to control Rotation-Tilt holder d) Rotation-Tilt Module controlled by joystick e) Closed loadlock with the universal sample holder inside.

All test samples covered by different passivation layers were submitted to SEM inspection in order to evaluate its topography, film roughness, films growth mode and rabbit ears presence. The rabbit ears consist in extra Al pieces, with a specific height, that remained after lift-off on the edge of the Al tracks. This feature could be a disadvantage, when the passivation layer was deposited since the oxide could not cover the rabbit ears and permit a short circuit with the seam metal overlay. For this inspection, some tracks with different spacing between them were designed and a horizontal cut was performed (Figure 3-23). This manual cut required extreme precision because tracks had to be included and the die was required to have 8mm maximal height. In order to improve SEM imaging, samples should be covered with Cu 50 Å deposited in Nordiko 3000 that enhances the image contrast. The SEM scanning was accomplished with support of technical expertise of Diana Leitão.

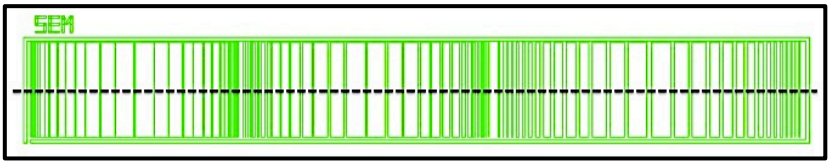

Figure 3-23: Streaks with different spacing designed to perform SEM inspection and respective horizontal cut.

In Figure 3-24 the results obtained for samples with oxides deposited in Nordiko 3600 with different deposition angles were evaluated. Two images for the sample covered with Al_2O_3 deposited with an angle equal to 180º and two images of the sample with Al_2O_3 deposited with an angle equal to 130º are shown on the left and right, respectively (Figure 3-24).

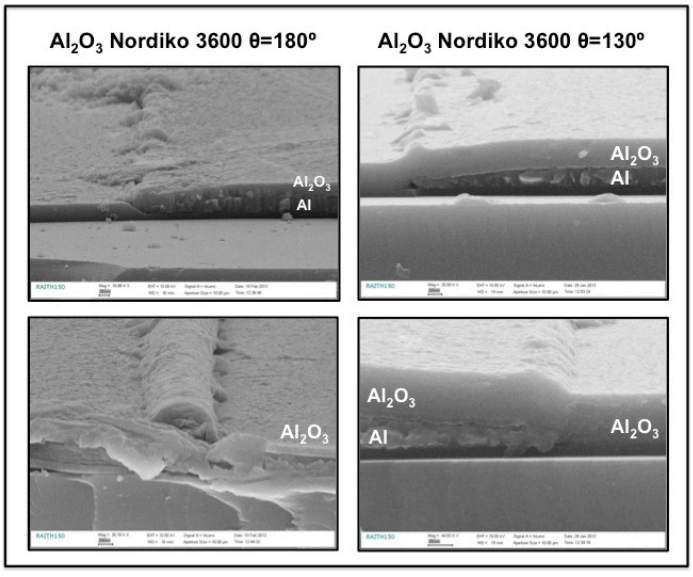

Figure 3-24: SEM inspection of sample with oxides deposited by IBD in Nordiko 3600. In left side, are presented two pictures of Al_2O_3 film deposited at 180º and on the right side, two pictures of film Al_2O_3 film deposited at 130º.

The overlaying layers presented in three images correspond to an Al layer deposited below of an Al_2O_3 layer. In these images, it can be verified that the topography of sample is identical when the oxide is deposited above the Al film or when it is deposited above de Si substrate. This behaviour can be explained, since the same deposition system (IBD) and machine (Nordiko 3600) was used for the

Al_2O_3 and Al films deposition. Evaluating the images on the right side, it can be also verified that a conform deposition was performed, minimizing the probability of short circuit occurs. Using the images available for the sample covered with Al_2O_3 deposited at 180º, was difficult to observe the intended features, since the cut almost not include the tracks required to analyse the sample topography. However, it can be observable that this oxide has a different growth mode comparing to the other oxides, presented in Figure 3-25 (SiO_2 (Alcatel) and Al_2O_3 (UHVII)), in which the deposition was also anisotropic. Moreover, by comparing the images obtained for the same Al_2O_3 film, although deposited with different angles, it was possible to conclude that the film deposited at 130º presents a more conform deposition and minimizes the short circuit occurrence when the fluid tests were performed.

In Figure 3-25 the results obtained for samples with oxides deposited by sputtering are evaluated. Two images obtained for the sample with SiO_2 (Alcatel) and two images of sample with Al_2O_3 (UHVII) deposited as passivation layer are shown on the left and right of Figure 3-25, respectively. The two overlaying layers presented in all images correspond to a layer of Al deposited below of an oxide layer, SiO_2 or Al_2O_3 depending on the case.

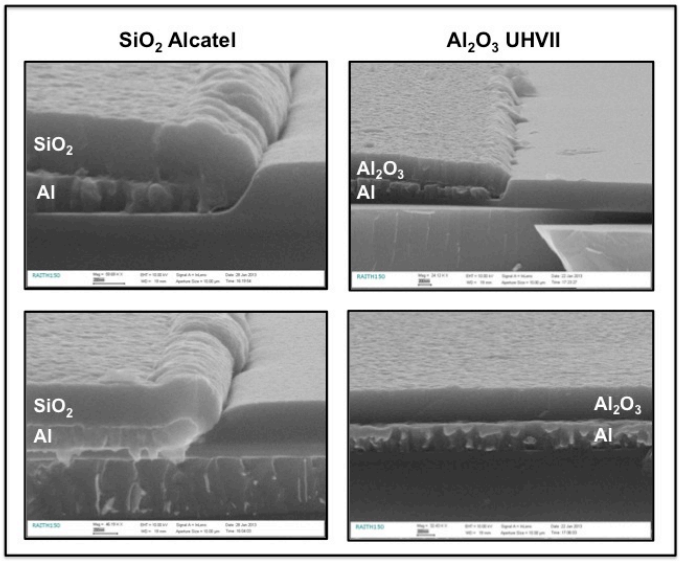

Figure 3-25: SEM inspection of sample with oxides deposited by sputtering in Alcatel and UHVII. In left side, are presented two pictures of SiO_2 film and on the right side, two pictures of Al_2O_3 film.

In these images, the topography of samples, which is different for the same oxide in the two different situations, can be evaluated. When the oxide is deposited above the Al film, its surface presents an accentuated roughness comparing to the oxide deposited above the Si substrate. Evaluating these images it can also be referred the growth mode of the two films deposited by sputtering. For this case, two oxide layers seem to have an individual growth mode, enhancing the probability of vacuum holes existence, which is presented in the two first images of SiO_2 and Al_2O_3. This deposition profile is non

intended, since enhances short circuit occurrence when the fluid tests are performed. In the second image of Al_2O_3 (UHVII) were observed the normal features of Al film grains.

In Figure 3-26 presents images obtained by SEM inspection of samples in which the passivation layer was deposited by CVD in Electrotech. In corresponding images to the SiO_2 film it is possible to observe two different layers on the right side of the image and just one layer on the left side. On the right side, the inferior layer corresponds to Al while the superior layer to SiO_2. On the left side is only presented a SiO_2 layer.

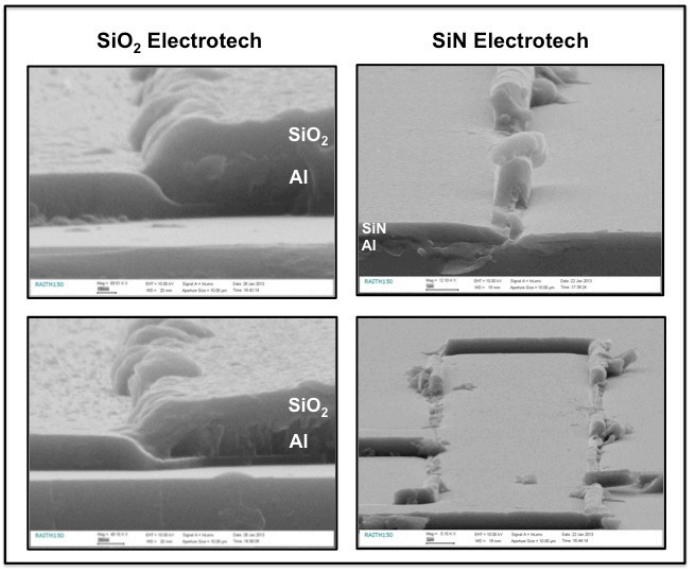

Figure 3-26: SEM inspection of sample with oxides deposited by CVD in Electrotech. On the left side are presented two pictures of SiO_2 film, on the right side, two pictures of SiN film.

SiO_2 images show a conform deposition of material in which the rabbit ears presented are totally covered by the oxide film. In SiN images, it is verified an important result. In the first image of SiN, on the left side an Al layer below of a SiN layer is presented, and on the right side only a SiN layer. The important result observed is exactly the high rabbit ear totally covered by passivation layer. This could be a serious problem if the rabbit ear was not uniformly covered. However, this conform cover explains the fact of the non existence of any short circuit in previous tests in this sample. Moreover, the topography of sample surface, which is presented in the second image of SiN should be minimized, decreasing the thickness of layer but ensuring that the short circuit behaviour continues absente.

3.4.5 Fluid Tests

Fluid test consists in the evaluation of oxide behaviour in contact with a buffer solution, verifying if occurs or not the corrosion of passivation and contacts layers. For this, one sample of each different process was exposed to ultraviolet light/ozone plasma for 15 min inside an UVO cleaner machine

from (Jelight, USA) while the correspondent other sample were not exposed. The UVO cleaner, a cleaning method, consists in photosensitized oxidation in which the organic contaminant molecules and traces of PR polymer are completely removed by the absorption of short wavelength UV radiation. The UVO cleaner was performed in order to completely remove traces of PR polymer and other organic contaminants and to provide a sample surface more hydrophilic, increasing the number of –OH groups on the surface. For the fluidic tests, a DC power supply source in current controlled mode was used, and two electrical probes placed on external pads as presented in Figure 3-27. First step of fluid test consisted in verifying the presence of short circuit or open circuit. If a short circuit was checked then 6V were injected (corresponding to 150 mA) in the pads. After that, 5μl or 10μl of phosphate buffer (PB), 0.1 M, pH 7.4, 0.02% (v/v) tween20 (depending of surface hydrophilicity) were dispensed on top of current line and current variation was registered during the process time. It was important that the fluid droplet would not enter in contact with the pads, where the electrical 2-probes were placed. If the oxide was not disrupted after 1hour and 30minutes with a PB droplet on top then a stronger saline solution, phosphate buffer saline (PBS), 0.1M and pH 7.2 was dispensed in the same quantity, 5μl or 10μl, during 1hour if possible. Once the current value was equal to zero (no current flow) disruption of oxide and consequent corrosion of the Al track occurred. The oxide presenting disruption after the longest time was selected as the best passivation layer, following the requisites of this test. These tests were crucial to perform PCR on chip successfully and to avoid the biochip corrosion.

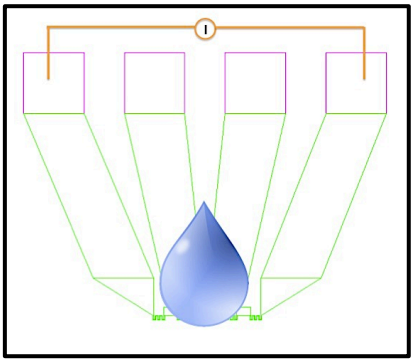

Figure 3-27: Scheme of measurement procedure of fluid tests. The droplet corresponds to PB or PBS solution in a volume of 5μl or 10μl.

Figure 3-28 illustrates surface characteristics of the samples covered with different oxides after fluid test. These illustrative pictures characterize the corrosion of different contacts during the fluid test until this disruption was achieved. All samples presented the current line interruption. However, the passivation layer corrosion was less accentuated in the sample covered with Al_2O_3 deposited in Nordiko 3600 with an angle of deposition equal to 130º.

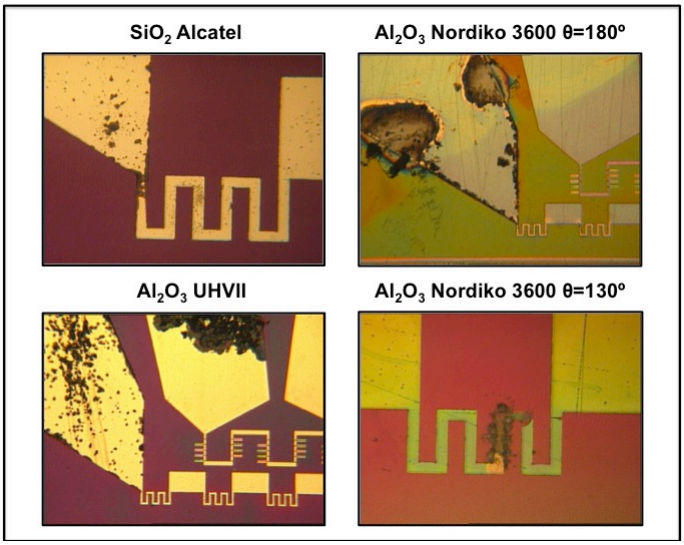

Figure 3-28: Surface characteristics of samples surface covered with different oxides after fluid test.

Moreover, the expected results (Figure 3-29) were only obtained with sample covered with SiN by CVD, which have not presented any surface corrosion and were only observed the current line interruption when the oxide disruption was achieved.

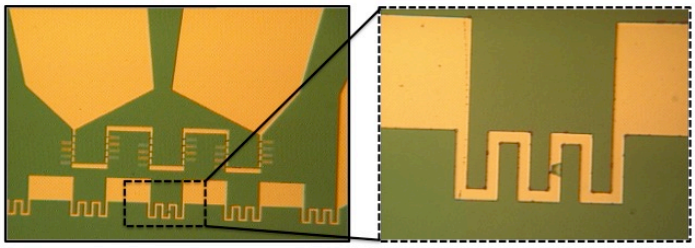

Figure 3-29: Pictures of surface of sample covered with SiN by CDV in Electrotech after fluid tests. The surface seems totally clean, without passivation layer corrosion and with only the current line interruption.

In Figure 3-30 a summary of the results are presented. For samples with Al_2O_3 deposited in Nordiko 3600 with different angles, the obtained results correspond to the expected results. In samples with Al_2O_3 deposited with an angle equal to 130º were presented satisfactory results due to the conform deposition around the sample provided by the deposition angle. In the other hand, in samples in which the oxide deposition was anisotropic, can be observed that the short circuit and oxide disruption occured before the time provided. For samples with oxide deposited by sputtering, the result for SiO_2 sample was expected due to vacuum hole formed during its deposition. However, the unexpected result obtained for Al_2O_3 can be explained by lower short circuit percentage obtained comparing to SiO_2. Samples with oxide deposited by CVD in Electrotech presented the suitable results. The results obtained to SiO_2 were not expected although its performance could be extremely improved using the UVO cleaner process, which improves the layer hydrophilic properties. Regarding the results to fluid tests without UVO cleaner, only the samples covered with Al_2O_3 (Nordiko 3600 θ=130º), Al_2O_3 (UHVII) and SiN demonstrated the expected results after 90 minutes in contact with PB. However, in contact with PBS, the three oxides achieved its disruption after 15 minutes.

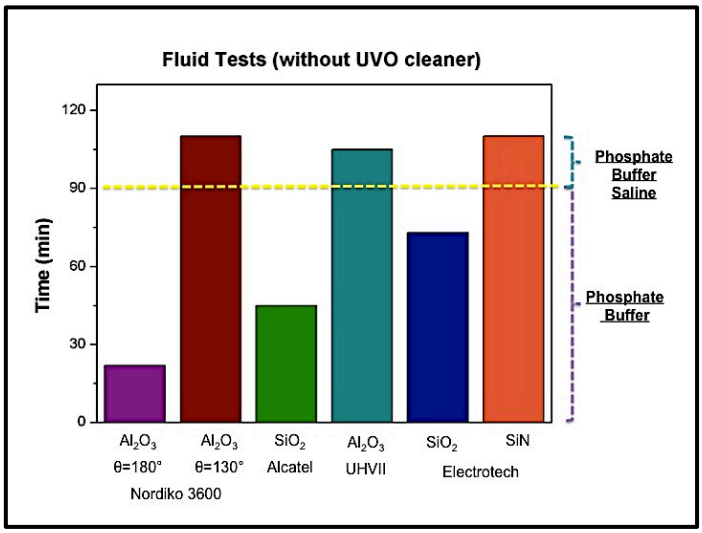

Figure 3-30: Fluid tests results for all samples that were not submitted to UVO cleaner. Samples performance in contact with PB during 90 minutes and with PBS during 15 minutes.

After this test, all samples were submitted to 15minutes in UVO cleaner to remove all organic contaminant molecules and traces of PR polymer and the results obtained were different.

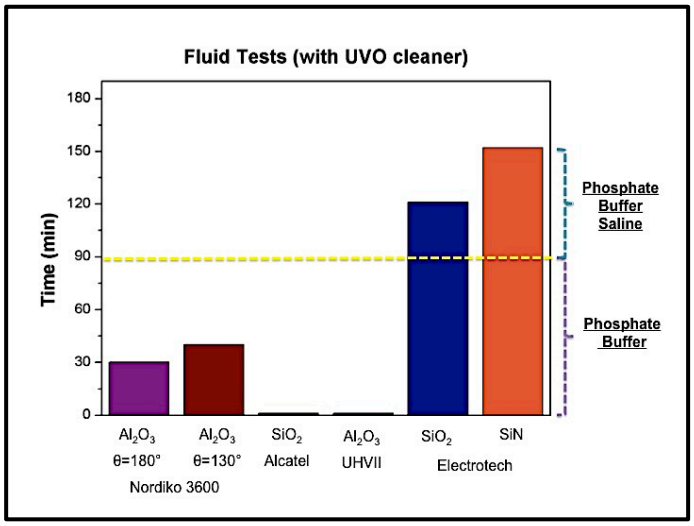

Figure 3-31: Fluid tests results for all samples submitted to UVO cleaner during 15 minutes. Samples performance in contact with PB during 90 minutes and with PBS during 60 minutes.

The results obtained in Figure 3-31 seemed appropriate. Fluid tests were not performed in samples covered with SiO_2 (Alcatel) and Al_2O_3 (UHVII) that were submitted to UVO cleaner, since the UVO cleaner process increased the surface hydrophilicity and the droplet of PB was spread for all over the surface, entering in contact with pads. For samples covered with Al_2O_3 in Nordiko 3600, the results were different according with two deposition angles. For the sample covered with an angle equal to 180º, the result was improved comparing to that obtained without UVO cleaner. However, the sample covered with an angle equal to 130º presented a non intended result. In this case, would be expected similar results for the sample with an angle deposition equal to 130º and for samples covered with

oxide deposited by CVD, since that oxide deposition is conform for all surface, avoiding the oxide disruption and short circuit occurrence. Samples covered with oxides deposited by CVD showed the best results. For both samples, SiO_2 and SiN were not disrupted during the 90 minutes in contact with PB. Then, a droplet of PBS was dispensed on the current line and the SiO_2 was disrupted after 30 minutes and the SiN after 60 minutes, accomplishing the goal of fluid test successfully. This result was crucial to allow PCR on chip performance.

3.5 Discussion

Regarding the study of different substrate materials and its features, a suitable substrate was selected. The substrate selection was made taking into account two fundamental features, good thermal conductivity and low heat dissipation. So, the glass was selected as the best substrate, since presents a suitable thermal conductivity and the ability to establish uniform temperature zones within a confined area while limiting heat dissipation.

The goal of PR profile optimization tests was successfully accomplished by improving the lift-off process time and its efficiency and reproducibility. The optimal exposure conditions for future microfabrication process were chosen after PR profile characterization in order to guarantee an efficient lift-off process in a short period of time, about of 2 hours. As expected, the lift-off for the sample non-submitted to predevelopment was complete only after 2 days, in hot µ-strip at 65ºC alternating with ultrasounds. Samples tested with pre-development step presented a lift-off faster than sample non submitted to pre-development. For these samples, the time required to complete lift-off was about 80 minutes in hot µ-strip at 65ºC and 20 minutes in ultrasounds. Although the time required to complete this process was the same for both samples, the effectiveness and success of lift-off was dissimilar. Sample submitted to pre-development during 60 seconds presented overdevelopment when exposed with 75% energy, and to 85% and 95% and Al pilling in unwanted areas was verified. Only dies exposed to 100% energy showed the intended result. However, the overdevelopment could be avoided decreasing the pre-development time. Therefore, the sample submitted to pre-development during 30 seconds not presented over development, although a high energy was necessary to insure a successfully lift-off. Dies exposed with 75% and 85% revealed some Al pilling while dies exposed with 95% and 100% presented the best intended results. Aiming minimization of Al pilling, the pre-development time could be changed to 20 seconds. Thereby, the optimal result obtained with these tests was achieved with pre-development during 30 seconds and 95% of exposure energy, ensuring the improvement of lift-off process and minimization of process time and consequently total time of biochip microfabrication process.

Some tests were performed, in order to select the passivation layer with optimal characteristics to perform PCR on chip. Such tests included, oxide breakdown voltage, metal overlay, metal resistivity, SEM inspection, and fluid tests. Regarding, these tests, some interesting results were observed. For example, an observable difference obtained between results for samples covered with an oxide deposited anisotropically (SiO_2 (Alcatel), Al_2O_3 (UHVII) and Al_2O_3 (Nordiko 3600 θ=180º)) and the

other samples (Al_2O_3 (Nordiko 3600 θ=130º) and SiO_2 and SiN (Electrotech)) with an isotropic deposition. These differences were based on the percentage of short circuit, SEM imaging and the performance of passivation layer when exposed to saline solutions. After an exhaustive analysis of all obtained results, the SiN was chosen as the oxide with optimal features as passivation layer, regarding several details. The SiN presented a minor percentage of short circuits and the metal resistivity value of this sample is suitable to perform the thermal control. Using SEM it was possible to verify a totally conform deposition of this oxide, avoiding any possibility of short circuit occurrence. Finally, it was only possible to accomplish the fluid test in the desired time with the required surface characteristics when the sample was covered with SiN. Therefore, SiN was the oxide selected as the optimal passivation layer, incorporated in step 9 of biochip microfabrication process, allowing the PCR on chip performance.

4. Temperature Sensors Characterization

4.1 Overview

After the biochip microfabrication process, the biochip was wire bonded to a printed circuit board (PCB) that was used as a chip carrier. An important aspect of this PCB chip carrier is its low cost comparing to convectional ceramic chip carrier, since the biochip should be disposable. The PCB was easily inserted into an edge connector placed in the sensing and processing module (SPM) main board. Its size and shape were fully customized and adjusted to optimize the interface with a fluid system. This SPM provides signals required to perform the magnetic and electric drive of biochip sensors and multiplexing of the sensors signals, to control fluids, and to acquire a conditioned signal, in order to achieve digital signal processing in a digital signal processor (DSP). Some requirements of the portable platform, described in subchapter 2.4, were taken into account such as, performing of real-time signal processing, using standard technologies on the communications interfaces in order to minimize the development time and to increase biocompatibility and the transmitted data must be encrypted. A graphical user interface (GUI), implemented on a personal computer, is also used to fully control the measurement process. Using a GUI, it is possible to automatically measure the transfer curves of all biochip sensors. The user only needs to select which sensors will be measured for a specific selected biochip type and to set the sensor bias current and the other measurement parameters. Finally, the user can perform a deeper analysis of the measured data, which are stored in extensible markup language (XML) or comma separated value (CVS) file format (22, 25). In this thesis, the magnetoresistive (MR) sensors calibration as temperature sensors and the measurement of thermal and electrical parameters were performed after the biochip was wire bonded to the PCB. A rigorous and accurate calibration of temperature sensors was mandatory, in order to accomplish the optimal reaction temperatures which are key to successful DNA amplification. Moreover, exposure times of the sample to each temperature, temperature uniformity, thermal/fluid control of heat transfer rates and DNA sample velocities are considered critical issues in PCR technology. The temperature uniformity can be accomplished by maintaining the temperature at a constant level in the heating elements. During this thesis, Pulse Width Modulation Control (PWM) controller was used. The Proportional Integral Derivative Controller (PID) algorithm will be developed for future tests.

4.2 Temperature Sensors Calibration

In this project, MR sensors were calibrated as temperature sensors, which were used to detect temperature distributions while integrated current lines were used as local heating elements, instead

of heating elements with different temperature zones as reported in previous studies (51-54).

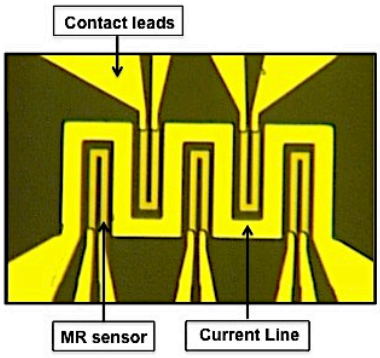

Figure 4-1: Representation of MR sensors surrounded by current line. MR sensors were used to detect the temperature and current line was used as the heating element.

The combination of the MR sensor and the current line has demonstrated high heating and cooling ramps and a precise temperature control. The heating procedure consisted on applying a specific current value in the current line. This consequently produces a resistance variation of MR sensors. In order to ensure that the resistance variation was not influenced by any magnetic contribution, a field DC of 50Oe was applied, assuring the MR sensors saturation. The resistance variation can be transduced in a temperature variation. Then, applying different current values in the current line will translate into different temperature variations, specifically 95ºC, 58ºC to 68Cº and 72ºC to 74ºC. The correlation between the resistance value R of a resistor and temperature difference can be described by following simplified equation (31).

$$\boldsymbol{R = R_0\,(1 + \alpha \Delta T)} \tag{4-1}$$

where R_0 is the resistor initial value at room temperature, α is the material temperature coefficient of resistance (TCR) and ΔT is the temperature variation.

Equation 4-1 was used to calculate the temperature variation, which results will be discussed in subchapter 4.3. Moreover, the factor α (TCR) is given by ratio of resistance variation (ΔR) to temperature variation (ΔT) during a set period of time.

$$\alpha = \frac{\Delta \boldsymbol{R}}{\Delta \boldsymbol{T}} = \frac{\boldsymbol{Rmax - Rmin}}{\boldsymbol{Tmax - Tmin}} \tag{4-2}$$

where ΔR is resistance variation and ΔT is temperature variation. In theory, the TCR value was estimated in 1Ω/°C. The TCR value obtained for the characterized sensors will be calculated and discussed in subchapter 4.3. For these measurements, some parameters were defined, such as a current DC value of 1mA, which was used to bias the sensor, a field DC of 50Oe ensuring the sensor saturation and a total measurement time that was equal to 35seconds. This saturation was crucial in order to assure that any observed variation was due to the temperature and it was not influenced by

any magnetic contribution. In the temperature sensors calibration, three deionised water (DI) samples at different temperatures, 100ºC, 8ºC and 22ºC (room temperature (RT)) were used. The calibration of sensors consisted in heating up and cooling down two DI water samples at specific temperatures and in the evaluation of the resistance variation for each temperature. In order to ensure that the specific temperatures of different DI water samples were achieved, a thermopar was used. Moreover, a heating plate was used to heat up the DI water sample at 100ºC and for 8ºC an eppendorf with DI water was cooled down in the fridge. The procedure used to calibrate the sensors consisted in two main steps. The first step comprised the biochip introduction in the platform and the dispensing of a 10µl droplet of DI water at RT on its top. The second step was the removal and substitution of this droplet by a 10µl droplet of DI water at 100ºC. For DI water sample at 8ºC, the same method was used. The process of sensor calibration was repeated several times in order to obtain a statistic value, and the resistance variation was annotated and analysed in detail.

When the sensor calibration procedure for DI water sample at 100ºC was completed, the data collected were analysed in function of the voltage for a constant current value. In this case, it was verified an instable maximal voltage value for a temperature equal to 100ºC. Therefore, the voltage average value obtained at RT, 22ºC that is represented by green colour in Figure 4-2, was the real value used. These results were used to determine the TCR value, which will be analysed in subchapter 4.3.

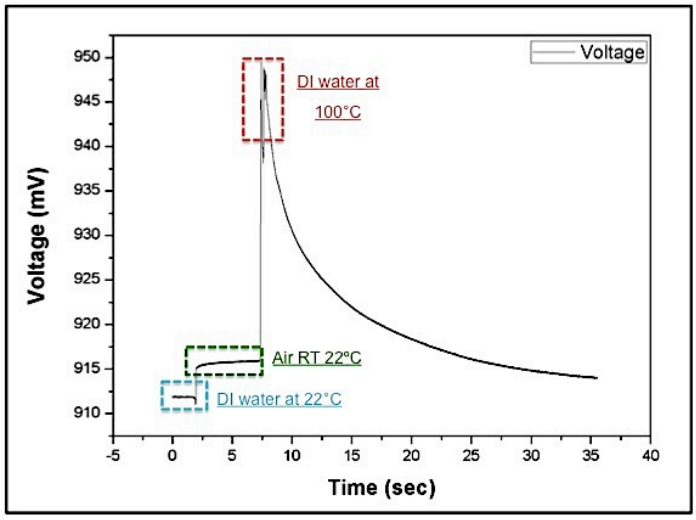

Figure 4-2: Calibration sensor. The sensors were biased with a current DC 1mA and the voltage variation was measured in function of a set time. A field DC of 50Oe was also applied to ensure the sensor saturation. Blue square: Sensor voltage when a DI water droplet of 10µl at RT was dispensed on biochip top; Green square: Sensor voltage at RT, when the droplet DI water was removed; Red square: Sensor voltage with a 10µl droplet DI water at 100ºC on top of the biochip.

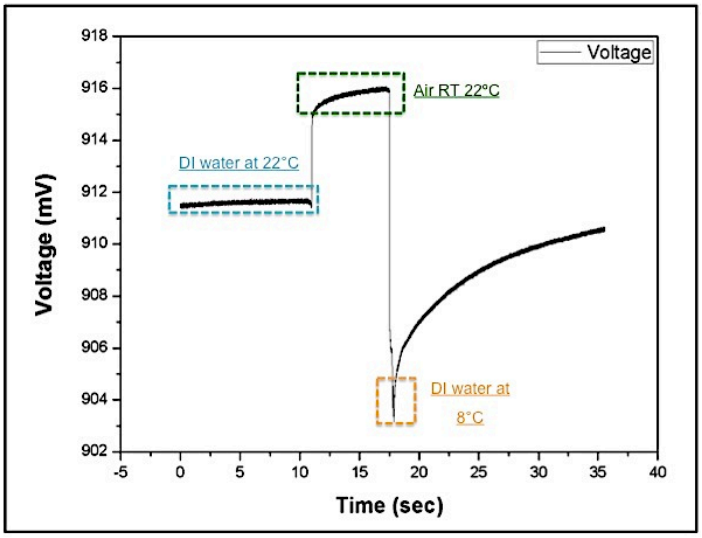

Figure 4-3: Sensor calibration. The sensors were biased with a current DC 1mA and the voltage variation was measured in function of a set time. . A field DC of 50Oe was also applied to ensure the sensor saturation Blue square: Sensor voltage when a 10µl droplet DI water at RT was dispensed on biochip top; Green square: Sensor voltage at RT, when the droplet DI water was removed; Orange square: Sensor voltage with a 10µl droplet DI water at 8ºC on top of the biochip.

As described previously, the same method was used for a 10µl droplet of DI water that was cooled down at 8ºC. When this DI water droplet was dispensed on top of biochip, the sensor voltage was registered. The Figure 4-3 describes the voltage variation when two 10µl droplets of DI water, at RT and at 8ºC were placed on biochip top during a set time of data acquisition. The average value of minimal voltage registered at 8ºC was taken into account to the TCR value estimation. In order to estimate the TCR value, the voltage variation for these crucial temperatures will be analysed and discussed in subchapter 4.3.

4.2.1 Thermal Parameters

The thermal behaviour of any system is described by the differential heat balance equation, which is presented by the following equation (31):

$$\boldsymbol{H\frac{dT}{dt}+G\Delta T=\ \Delta P} \tag{4-3}$$

where H is the thermal capacitance, G is the thermal conductance, ΔT is the temperature change, t is time and ΔP represents the dissipated power change within the system. The time thermal constant of the system, τ is given by the ratio of thermal capacitance (H) to thermal conductance (G). Solving the Equation 4-3, which gives ΔT as a function of time, the Equation 4-4 was obtained. Then, considering a non linear fitting, based on the Equation 4-4, the thermal parameters can be estimated in detail.

$$\frac{\Delta \boldsymbol{P}}{\boldsymbol{G}} \left(\mathbf{1} - \boldsymbol{e}^{-\boldsymbol{t}/\boldsymbol{\tau}}\right) = \Delta \boldsymbol{T}$$

(4.4)

where G is the thermal conductance, ΔP is the dissipated power change within the system, t is time and τ represents thermal time constant of the system. The results of thermal parameters characterization will be evaluated and discussed in subchapter 4.3.

4.2.1.1 Thermal Conductance Parameter

The thermal conductance is the property of a material to conduct heat, which occurs at a higher rate across materials of high thermal conductivity than across materials of low thermal conductivity. Materials with a high thermal conductivity are widely used in heat dissipation applications while materials with a low thermal conductivity are used as thermal insulation. This material property is temperature dependent and can be measured using several strategies, following the Equation 4-4.

In the first strategy, a 10µl droplet of a saline solution, phosphate buffer (PB), was dispensed on top of biochip, and different current values (from 10mA until 60mA) were applied in current line (Figure 4-1) using five different percentages of duty cycle, specifically 0% until to 100%. Duty cycle concept represents the percentage of time in which a system is operational and it will be discussed in detail in subchapter 4.2.2.1. Current value equal to 60mA was the maximum value used, since a higher current value could damage the current line until its disruption. After TCR estimation it was possible to quantify the temperature variation detected by the MR sensors, for each current value applied during the respective duty cycle.

Moreover, the instantaneous electric power, which represents the rate of energy converted from the electrical energy of the moving charged to heat, was also calculated by using the product between applied voltage and electric current on a resistor in a DC circuit. The electrical power equation is presented in Equation 4-5.

$$\boldsymbol{P} = \boldsymbol{V} \times \boldsymbol{I} \; [\boldsymbol{W}]$$

(4.5)

where P is the instantaneous power, V is the potential difference across the component and I is the current applied. However, a convenient expression for the power dissipated in a resistor can be obtained using the Ohm's Law. Moreover, knowing that the current line resistance was 44Ω and the current value applied in current line, the power dissipated can be calculated using the following equation:

$$\boldsymbol{P} = \boldsymbol{I}^{\mathbf{2}} \times \boldsymbol{R} \; [\boldsymbol{W}]$$

(4.6)

where P is the power dissipated, I is the current applied and R is the resistance of the component. Through this relation it was possible to determine the power and current value required to achieve the specific temperature. Considering the Equation 4-4, it was possible to evaluate that when time tends to infinity, the thermal conductance is given by the ratio of system power to temperature variation.

Then, a linear fit of power was performed using a specific tool of fitting available in OriginPro 8, a data analysis and graphic software application. The obtained results for this linear fitting were crucial to estimate the thermal conductance parameter and will be presented in subchapter 4.3.1.

4.2.1.2 Thermal Capacitance Parameter

The thermal capacitance parameter is defined as the physical measurement that shows the amount of heat required to change the temperature of an object. As referred in the previous chapter, the technique used to estimate the thermal capacitance was based on applying a maximal current value of 60mA in the current line, in which different percentages of duty cycle (0% - 100%) were applied during a maximal pulse duration imposed by the system that was equal to 8.8ms. The sampling frequency was 3000Hz and the total time of data acquisition was 6s. After data acquisition, the respective treatment was processed. The data handling consisted in performing a non linear fit, following the Equation 4-4, in exponential segment of the curve that was obtained for the different conditions. The collected data were expressed in temperature variation in function of the acquisition time. In order to perform a non linear fit curve, a data analysis and graphic software application, OriginPro 8, was used. Using this tool designed to fitting, it was possible to create a new function, by introducing the equation, parameters, and variables in study. With the acquired equation, the estimation of thermal capacitance and corresponding thermal conductance was obtained. The results achieved will be discussed in detail in subchapter 4.3.

4.2.1.3 Thermal Time Constant

Thermal time constant is a feature of the thermal system, used when a system have a uniform rate of heating and cooling. After the thermal conductance and capacitance estimation, the system thermal time constant was calculated, which is represented by the ratio of thermal capacitance to thermal conductance and by the following equation (31):

$$\boldsymbol{\tau} = \frac{\boldsymbol{H}}{\boldsymbol{G}} \left[\frac{\boldsymbol{mJ}/℃}{\boldsymbol{mW}/℃}\right][\boldsymbol{s}] \tag{4-7}$$

where H is the thermal capacitance and G is the thermal conductance. Thermal time constant value will be presented in subchapter 4-3 and compared with other studies in subchapter 4.4.

4.2.2 Temperature Control

In this thesis, the temperature sensors calibration and PCR on chip tests were performed by programming the digital processor to generate current pulses modulated in width. The main function of PWM controller is to allow the control of power supplied to electrical devices and its operation mode is based on duty cycle concept. Other control strategy will be integrated in future tests of PCR on chip. This control strategy consists in a PID controller, a generic control loop feedback mechanism

widely used in industrial control systems. The PID algorithm involves three separate constant parameters, the proportional, the integral and derivative value, denoted P, I and D, respectively.

4.2.2.1 Pulse Width Modulation Control

The PWM technique has shown a theoretical and practical development over the years. Nowadays PWM has been widely used in several applications such as electronic and electrical systems, including control systems, signal processing, power control systems and telecommunications (55, 56). PWM theorem represents a signal as a series of pulses with constant amplitude and variable widths (55). Some reasons can be noted for the wide applicability of PWM such as, simple operation mode and large signals processing with high efficiency and low sensitivity to noise (56). Specifically, the PWM software can be used when a frequency not too high is required, for example for running a heater. PWM can be also functional for digital control, since its on/off nature can easily set the needed duty cycle. This duty cycle concept is the basis of the operating mode of this controller, which is expressed in percentage and is described as the proportion of time in which the system is on mode for a regular interval or period of time. A low duty cycle corresponds to low power, since there is practically no current and the power is off for most of the time, as can be observed in Figure 4-4.

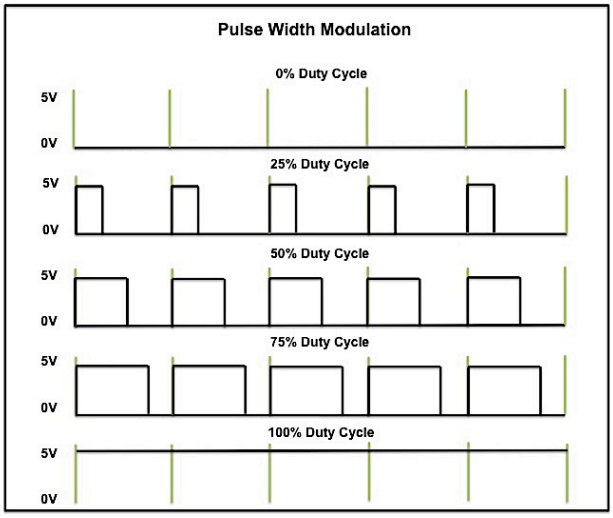

Figure 4-4: Pulse Width Modulation Controller. 0% Duty Cycle: Power was off during of period the time; 25% Duty Cycle: Power was on-mode during 25% of period the time; 50% Duty Cycle: Power was on-mode during 50% of period the time; 75% Duty Cycle: Power was on-mode during 75% of period the time; 100% Duty Cycle: Power was always on-mode during of period the time.

When a duty cycle of 100% is applied then the system is in fully active mode (57). In this thesis, the PWM was used to control the amount of power delivered and to heat the DNA sample, which is governed by the specific duty cycle percentage. Programming language software, MATLAB, was used to program the PWM algorithm. This PWM algorithm played a crucial role in the thermal parameters estimation, thermal conductance and thermal capacitance, and the PCR cycles

performance. In the first case, it was applied different current values, between 10mA and 60mA, and percentages of duty cycle from 0% to 100% in order to accomplish the thermal study. In the second case, it was essential studying the optimal current value needed and respective percentage of duty cycle aiming to obtain three different temperatures to an optimal PCR thermal control. Hence, this controller was the key for the experiments of DNA amplification. However in these experiments, it was required a constant current induction and application of different percentages of the duty cycle, consequently consuming more power than other control system. Therefore, an alternative control system, computer control PID controller, will be integrated to obtain a more rigorous thermal control with less power consumption.

4.2.2.2 Proportional Integral Derivative Controller

The PID controller has been the most commonly used control algorithm for a wide range of applications and has gone through many changes in technology. Some PID applications can be considered such as the process control, temperature regulation, magnetic and optic memories, the flow rate regulation and instrumentation (56). This controller is a key component for process control and presents a simplified version for temperature control. PID function consists in the estimation of an error value given as the difference between a desired set point and a measured variable (57). PID algorithm involves three separate constant parameters, which are the proportional, the integral and the derivative values, denoted P, I and D, respectively. These values can be interpreted by following form:

- Proportional: Output value is proportional to the control error value.
- Integral: Sum of the instantaneous error over time and gives the accumulated offset that should have been corrected previously. Makes sure the process output agrees with the set point in steady state.
- Derivative: Improves system stability and reaction to set point changes.

The proportional, integral and derivative terms are summed to calculate the output of the PID controller. Defining $u(t)$ as the controller ouput, the final form of PID algorithm is given by the following equation:

$$\boldsymbol{u(t) = K_p\, e(t) + K_i \int_0^t e(\tau)\, d\tau + K_d \frac{d}{dt}\, e(t)} \tag{4.8}$$

where K_p is the proportional gain, K_i is the integral gain, K_d is the derivative gain, e is the error, t is the time or instantaneous time and τ is the variable of integration. Each variable used in Equation 4-8 can be described in detail. The error is defined as the difference between the set point value (desired temperature) and the process output. A proportional controller (K_p) has the effect of reducing the rise time and steady state error but never eliminate it. An integral control (K_i) has the effect of eliminating the steady state error for a constant or step input. A derivative control (K_d) is responsible for increasing the stability of the system, reducing the overshoot. In this thesis, the PID controller was not used but it will be implemented in future assays of PCR on chip. The PID implementation will consist

in 3 crucial steps. First step consists in resistance data acquisition and its conversion in temperature variation through the Equation 4-1, using the TCR factor value previously calculated. The second step involves the error estimation, which is given by the difference between temperature target and temperature measured. The last step comprises the output variable calculation, in this case, power variation, which is given by the proportional gain times error value. This algorithm will be crucial in advanced PCR experiments since the power consumption can be minimized, and the transition step between different temperatures can be faster and sharper comparing to PWM controller, if applying a specific current value when was only required.

4.3 Results

The MR sensors calibration as temperature sensors was a crucial step in order to perform the specific cycles of PCR, as well as to calculate the thermal parameters. The main goal of this chapter consisted in the sensor calibration, TCR value estimation, evaluation of the maximal temperature variation that could be achieved, the maximal current value required and thermal parameters characterization.

In order to estimate the TCR, sensors were calibrated following the procedure described in subchapter 4.2. Using the Figures 4-2 and 4-3, which were obtained for these calibrations, the required values to calculate the TCR were noted. The voltage values presented in these graphs can be easily converted on resistance values, knowing that a constant current value equal to 1mA was used to bias the sensors. A field DC of 50Oe was also applied in order to assure the sensors saturation and to eliminate any magnetic contribution.

The required values to estimate TCR factor correspond to maximal and minimal average value of the resistance obtained for maximal and minimal temperature (Figure 4-5). In the first measurement, the maximal average value of resistance corresponding to temperature equal to 100ºC should have been used. However, this value was not considered rigorous for this calibration. Then, the resistance average value, 916Ω ± 0.0002Ω, corresponding to RT, 22ºC (represented by green colour in Figure 4-5a) was obtained. On the other hand, the resistance average value, 902Ω ± 0.0004Ω, correspondent to minimal temperature, 8ºC (presented by orange colour in Figure 4-5b) was obtained. Therefore, knowing that the TCR factor is given by the ratio of resistance variation to temperature variation (Equation 4-2), it was estimated around 1.053Ω/ºC ± 0.08 Ω/ºC.

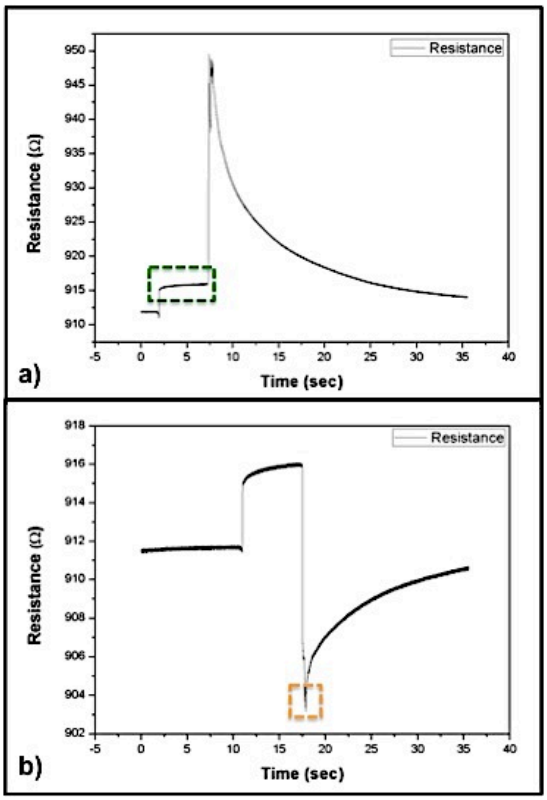

Figure 4-5: Sensors calibration: a) DI Water at 100ºC: Green square presents the maximal average value of resistance corresponding to temperature equal to 22ºC b) DI water at 8ºC: Orange square presents the minimal average value of resistance corresponding to temperature equal 8ºC.

Using a PWM controller, several heating curves were performed in order to study the increase of temperature variation with the rise of the current value and the duty cycle percentage. For this study, 10μl of PB, 0.1 M, pH 7.4, 0.02% (v/v) tween20 solution was injected into the microfluidic channel placed on top of the biochip. Moreover, current values between 10mA and 60mA were applied in the current line, and different percentages of duty cycle, between 0% and 100%, were used in different times of data acquisition. Hence, it was obtained a heating curve for each current value with different percentages of duty cycle applied. Other parameters such as, field DC of 50Oe ensuring the sensor saturation, pulse duration of 1ms, a total time of data acquisition of 35 seconds were also applied in this procedure. The Figure 4-6 shows the increasing of resistance variation for a constant current value, when the duty cycle percentage was also increased from 0% to 100% (percentage of time in which the system was in a active operation mode).

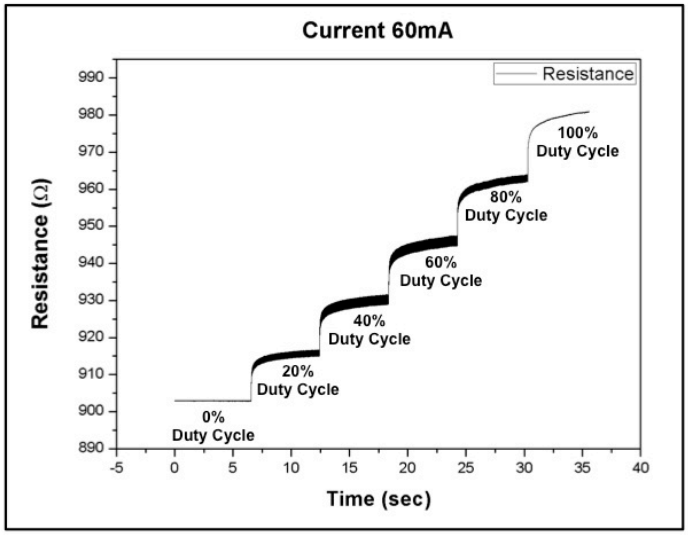

Figure 4-6: Heating curve for maximal current value equal to 60mA. Each step corresponds to different percentages of duty cycle.

Using the Equation 4-1 and the TCR value previously calculated, it was possible to convert the resistance values into temperature variation values. By applying a current of 60mA in the current line and varying the percentage of duty cycle, made possible to obtain the results expressed in Figure 4.7.

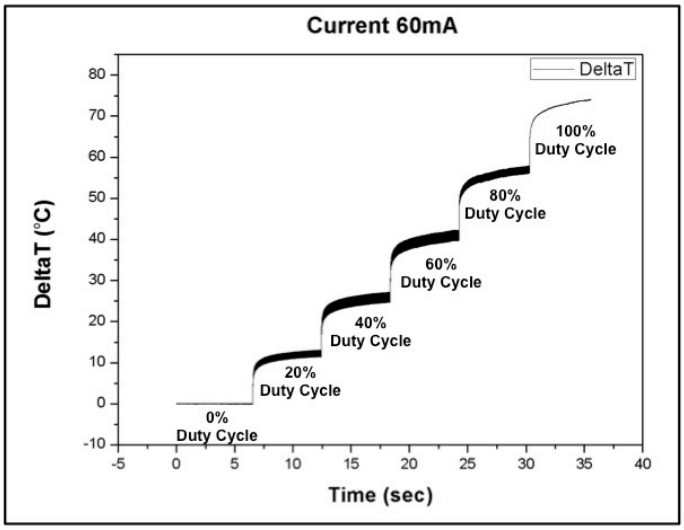

Figure 4-7: Temperature variation when a current of 60mA was inducted in the current line with respective different percentages of duty cycle.

In this graph, it is possible to evaluate the temperature variation when the percentage of duty cycle increases. Using 20%, 40%, 60%, 80% and 100% duty cycle was obtained a ΔT corresponding to 11ºC, 25ºC, 40ºC, 55ºC and 73ºC, respectively. Therefore, and knowing that these measurements were performed at RT of 22ºC, using a current of 60mA and the maximal percentage of duty cycle

(system always in active operation mode), the maximal temperature required for PCR cycle (95ºC) was achieved.

4.3.1 Thermal Conductance Parameter

The thermal conductance parameter was obtained using two different strategies but following the same Equation 4-4. In this subchapter, it will be presented the first approach, while in following subchapter the second approach will be discussed with the thermal capacitance. In the first approach, different current values were presented in function of temperature variation and different percentages of duty cycle, as presented in Figure 4.8.

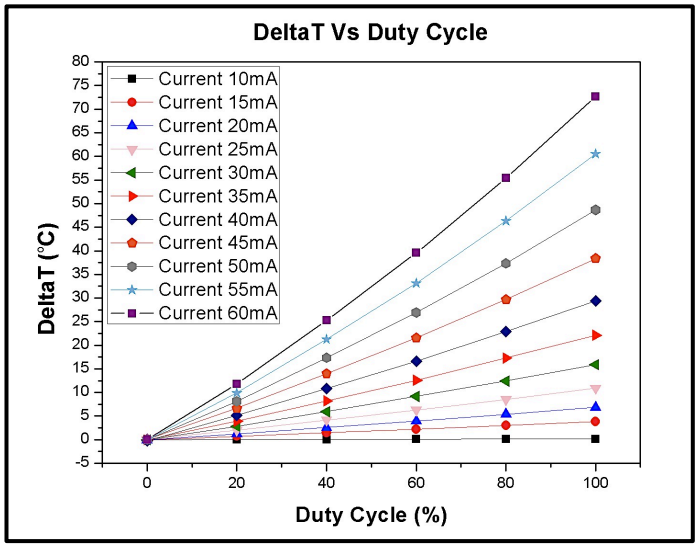

Figure 4-8: Temperature variation in function of different percentage of duty cycle for different current values applied in current line.

Figure 4-8 allowed the evaluation of the temperature variation, by increasing of current value and percentage of duty cycle applied. It was observed that the temperature variation increases linearly with percentage of duty cycle. The most satisfactory case was obtained when a current value of 60mA was applied in current line, in which a ΔT of 73ºC was accomplished ideally. After that, as described in detail previously and using the Equation 4-6, a graph that relates the power required to achieve a specific temperature variation was obtained (Figure 4-9). Regarding to the information available in Figure 4-9, it is possible to quantify the system power necessary to achieve a specific temperature. In order to obtain this graphic, it was necessary to calculate the power for all different current values with the corresponding percentage of duty cycle. Moreover, it can be observed by graphic analysis that when applied a current value of 60mA at 100% of duty cycle (power on during total acquisition time), a higher temperature variation was obtained because a higher power amount was applied as expected.

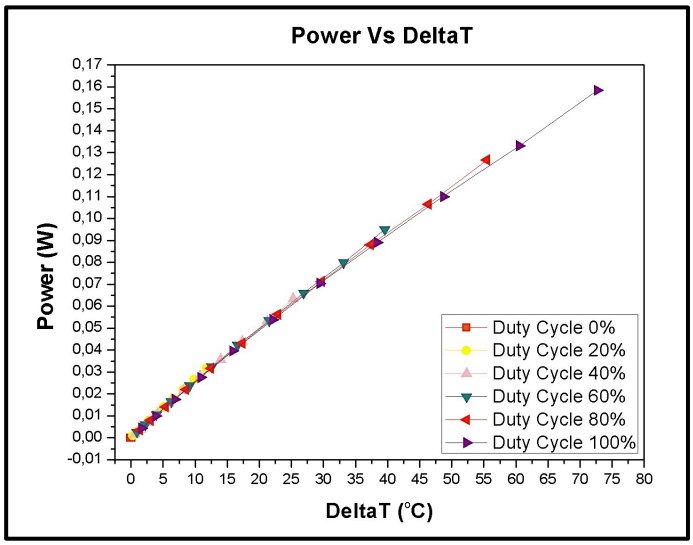

Figure 4-9: Representation of power and percentage of duty cycle applied to different current values required in order to obtain a specific temperature variation.

With the aim of estimating the value of thermal conductance, the Figure 4-10 was obtained. This graph only shows the collected data when the system was always in active operation mode (100% duty cycle for different current values). Hence, this graph demonstrates the relation between power and temperature variation when different current values are applied during a duty cycle equal to 100%. As described in subchapter 4.2.1.1, the thermal conductance parameter is given by the ratio of system power to temperature variation. Then, using a specific tool for fitting, a linear fit of power was performed, being the thermal conductance estimated as its slope in Figure 4-10. In this thesis, the thermal conductance parameter was estimated around 2.2mW/ºC.

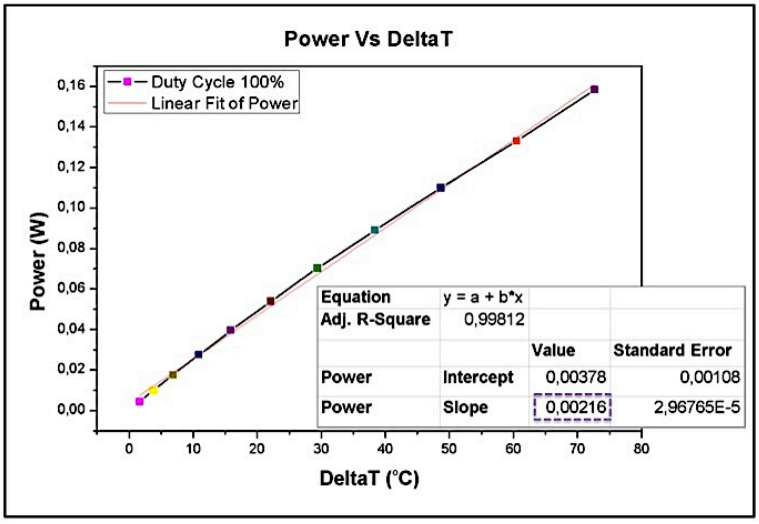

Figure 4-10: Representation of a linear fit of power when different current values were applied during the total acquisition time (100% duty cycle). Thermal conductance value estimation was around 2.2mW/ºC.

4.3.2 Thermal Capacitance Parameter

The study of thermal capacitance parameter consisted in creating a new function, based on Equation 4-4, with the respective parameters in order to perform a non linear fit curve. It was used a sampling frequency of 3000Hz in order to obtain the maximum sample number of study in exponential segment of different curves. A pulse with 8.8ms maximal duration was also applied. The Equation 4-9 was created to perform a non linear fit curve.

$$y = (1 - e^{((-x \times G/H)}) \frac{\Delta P}{G} \tag{4.9}$$

in which y and x variables correspond to temperature variation and acquisition time, respectively. G and H represent the thermal conductance and capacitance parameters that were estimated. ΔP corresponds to the power variation, the fixed parameter. The values of thermal capacitance and conductance (2.2mW/ºC) parameters were not fixed while the power variation was fixed in values corresponding to percentage of duty cycle (in this case 0.026W, 0.053W, 0.079W and 0.107W for 20%, 40%, 60% and 80% of duty cycle). The Figure 4-11 represents the thermal parameters estimation when a current of 60mA was applied in the current line during the 40% duty cycle.

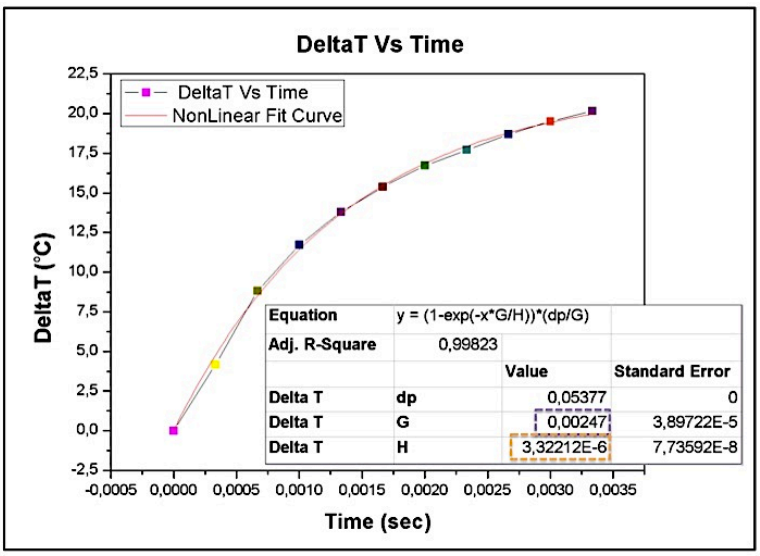

Figure 4-11: Thermal parameters estimation, H equal to 3.3μJ/ºC and G equal to 2.5mW/ºC. Non linear fit curve in which a current value of 60mA, duty cycle of 40%, total acquisition time of 6ms and pulse duration of 8.8ms were used.

Regarding the information of the Figure 4-11 it is possible to evaluate the two thermal parameters. The thermal conductance, previously calculated by the first approach (2.2mW/ºC), was estimated at a similar value 2.5mW/ºC. The thermal capacitance value was estimated around 3.3μJ/ºC.

4.3.3 Thermal Time Constant

Thermal time constant was calculated by direct ratio of thermal capacitance value to thermal conductance value. Therefore, after the thermal parameters estimation it was possible to calculate the thermal time constant, which was evaluated in 1.151ms. Table 4-1 resumes the thermal and electrical parameters for PCR system in order to perform PCR cycles.

Table 4-1: Electrical and thermal parameters of the PCR system. All values were measured at an ambient temperature of 22ºC.

Electrical and Thermal Parameters	
Sensor Resistance	916Ω
Current Line Resistance	44Ω
Sensor TCR	1.053Ω/°C
Thermal Conductance	2.2 mW/°C
Thermal Capacitance	3.3µJ/°C
Thermal Time Constant	1.151ms

4.4 Discussion

The main aim of this subchapter consisted in the calibration of MR sensors as temperature sensors. In order to accomplish this specific goal a calibration procedure, presented in subchapter 4.2 was required. Using this procedure was possible to calculate the TCR factor, estimated around 1.053Ω/ºC, which was crucial to interpret the resistance variation as temperature variation. The TCR factor value corresponded to the expected value, 1Ω/ºC approximately. It was also possible to simulate the heating curves by applying current values between 10mA and 60mA in current line and varying the percentage of duty cycle in order to achieve the optimal temperatures required for PCR cycles performing. These measurements were based on PWM controller focused on duty cycle concept, which was presented in subchapter 4.2.2.1. In this chapter, the thermal parameters, thermal conductance, thermal capacitance and thermal time constant were also studied. The thermal conductance was calculated by two different approaches. However, the estimated values for this parameter were similar for both approaches, which was calculated around 2.2mW/ºC. Using a nonlinear fitting in the exponential segment, the thermal capacitance was studied around 3.3µJ/ºC. Consequently, the thermal time constant was calculated with a value around of 1.151ms.

The results obtained to the thermal parameters estimation can be evaluated by comparing with the work of Neuzil and its co-workers (31). The Neuzil work consisted in the design, fabrication and test of a real time micro PCR system, which involved a microscope glass cover slip placed on top of a micromachined silicon chip integrated with a heater and a temperature sensor. A single mL of a DNA sample was placed on the glass and encapsulated with mineral oil, forming a virtual reaction chamber. Both works consisted in different PCR systems, substrate materials, heating elements as well as the amount of sample containing DNA. However, the thermal parameters can be compared. In this thesis, the thermal parameters estimation presented lower values than that obtained by Neuzil work. The results obtained in Neuzil work were specifically a thermal conductance of 4.4mW/ºC,

thermal capacitance of 6.6mJ/ºC and consequently a thermal time constant of 1.74s. The differences between thermal conductance values seem reasonable, since the different substrate material was used. In our PCR on chip a substrate glass was used and in the Neuzil work was used a Si substrate. As expected, in this thesis, the low thermal conductance of glass is more suitable, providing thermal insulation instead of heat dissipation that is verified in materials, as Si, with a high thermal conductivity. Moreover, the thermal capacitance parameter was also estimated in different values. A significant difference was registered, since for our work was achieved a thermal capacitance of 3. 3μJ/ºC and in the Neuzil work a thermal capacitance of 6.6mJ/ºC. In this case, the value obtained for our PCR system was also more appropriate, because a lower DNA sample volume, about 10μL was used instead of 1mL volume. This value can be explained, since the thermal capacitance shows the amount of heat required to change the temperature of an object. After thermal parameters analysis separately, it can be verified that the thermal time constant was also very different consequently.

Using all these simulations completed with this meticulous method, it was possible to accomplish temperature variations required to perform PCR cycles, playing with different current values and percentages of duty cycle. For the first experiments it was used a PWM controller, and a PID algorithm will be implemented to accurate temperature control in future experiments. Moreover, additional studies and efforts should be made in order to ensure the uniformity of fluid temperature and the minimization of temperature variations.

5. Polymerase Chain Reaction

5.1 Overview

Since its appearance, polymerase chain reaction (PCR) became a major tool in genetic studies and a very promising approach in exponentially amplification of single DNA molecules through thermal control at three different temperatures (30). The principal aim of PCR consists in generating many billions of DNA molecules from selection of an adequate and specific DNA template (7). The manufacturing of miniaturized and integrated analytical systems has been based on microelectronics industry technologies for integrated circuits production. Nowadays, miniaturization of PCR chip devices has revealed many key benefits in comparison with conventional PCR instruments, such as portability large dynamic range, higher thermal cycling speed, simple operation, high throughput and sensitivity and low reagents/sample consumption. The ability to integrate all steps of an analytical procedure into a single device is an additional advantage of this technology (10, 58). In this chapter, the differences between three specific PCR methods specifically conventional, real time PCR (rt-PCR) and PCR on chip method will be presented. The differences will be evaluated taking into account the system complexity, thermal uniformity and PCR time and specificity.

5.2 PCR Procedure

Several methods of performing the PCR reaction, such as conventional, rt-PCR and PCR on chip will be referred in this subchapter. Although these methods have different features as system complexity, heating and cooling rate, thermal uniformity and PCR reaction time and specificity, all of these were based on the same established principle. A typical PCR cycle, as schematically shown in Figure 5-1, consists in three steps, which are performed at three different optimal temperatures. The first step, referred as denaturation consists in heating up the sample at 95ºC for denaturation of double stranded DNA (dsDNA) into an single stranded DNA (ssDNA). After the temperature is lowered to the annealing temperature, 58ºC to 68ºC, the ssDNA reacts with primers. When the primers are attached, an enzyme called DNA polymerase reacts with the DNA-primer complex and by adding nucleotides to the ssDNA, enzymatic extension of the primers occurs. This last step is performed at temperature equal to 72ºC, as this temperature is best suited for DNA extension, thus preventing annealing. Finally, the temperature is raised to the 95ºC again to denaturize all dsDNA followed by the next cycle of annealing and extension. After every successful cycle the amount of target DNA sequence is doubled (30). For exponential increase of target DNA sequence amount, 20-40 cycles were typically needed. However, the amplification time can vary from couple of hours for conventional PCR machines (30) to several minutes for lab-on-a-chip (LOC) devices (8, 32, 47, 59).

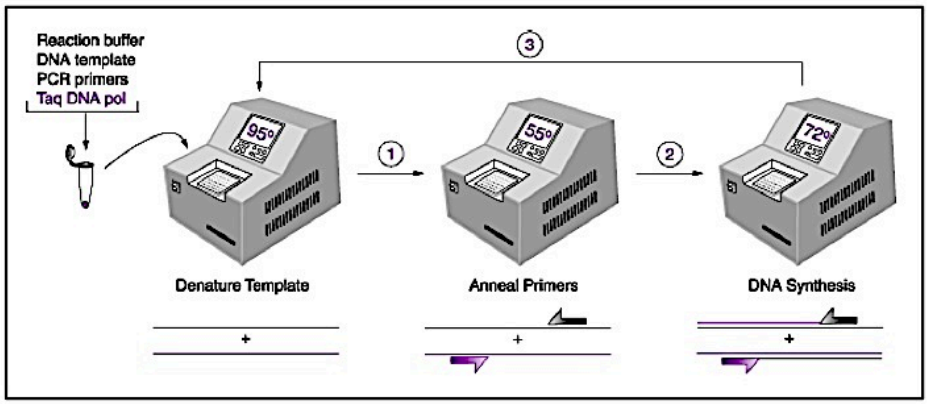

Figure 5-1: PCR reaction scheme: Each PCR cycle requires three optimal temperature to complete one round of DNA amplification. The PCR solution prepared that contains all PCR components is set to react at the thermocycler. At first, a temperature of 95ºC is necessary to perform the dsDNA denaturation. The temperature is decreased to around 55ºC allowing the primers hybridization with the ssDNA template DNA. At last, the temperature is increased to 72ºC to start the enzymatic extension and DNA synthesis.

In this thesis, a particular cell free DNA fragment of 115bp, from ALU repeated sequence, was targeted for amplification. The template used for amplification reaction consisted in the genomic DNA extracted from cultured Human Embryonic Kidney (HEK) 293T cells. ALU115bp is simulative of the total cell free DNA released from cell death, and is the most abundant repeated sequence in the human genome (more than 10% of the human genome content). For ALU115 fragment generation, a primer set for the amplicon was synthesized and purchased from StabVida, Portugal. The forward primer was designed to include a complementary region at the sense strand of dsDNA template, while the reverse primer at the anti-sense strand of dsDNA template. The Table 1 presents the primers set used.

Table 5-1: Primers set used for amplification reaction

ALU115	Primer Name	Sequence	Specifications
1	TD1F	5'-CCTGAGGTCAGGAGTTCGAG-3'	Forward Primer
2	TD1R	5'-CCCGAGTAGCTGGGATTACA-3'	Reverse Primer

Besides that, a PCR solution was prepared following a protocol used in previous work (60). The PCR reaction mixture included basic components, which are the template DNA molecule that contains the sequence to be amplified, 20ng genomic DNA (ALU115 fragment); two oligonucleotide primers (forward and reverse) that are complementary to the 3' ends of each of the strand of a double-stranded DNA template; a buffer solution, which provides a suitable chemical environment for DNA polymerase optimum activity and stability; a intercalation dye, SyBR Green, which is bonded to the DNA sequence so the fluorescence signal resulting from the interaction between the dye and the increasing amount DNA can be optically detected. Finally divalent cations (Mg^{2+}) are responsible for activation and increasing of DNA polymerase activity. Moreover, the SyBR Green mixture used for this protocol contains, the thermo stable DNA polymerase, which mediates the amplification process and the desoxynucleotide triphosphates (dNTPs) that consists in the building-block from which the

DNA polymerase synthesizes a new DNA strand. The PCR reaction procedure followed the typically three steps at different temperatures and only two techniques were used for its performing, specifically rt-PCR and PCR on chip.

5.2.1 Conventional PCR

Conventional PCR was referred as the PCR performed in conventional PCR machines, in this case Thermo Hybaid Px2. These apparatus are based on a temperature-controller metal block holding tubes containing the PCR mixture. Using this strategy, the entire amplification process occurs in a single closed tube inside of a thermocycler device following a specific program used to ensure the defined temperature steps for the whole reaction. The instrument complexity usually limits the speed of thermal cycling. Using a conventional machine, the processing time of PCR can reach 2 hours for a standard protocol of 30 thermal cycles, in which cycle times correspond to 10 min at 95ºC (enzyme activation), 1min at 95ºC (denaturation step), 50seg at 65ºC (annealing step) and 50seg at 72ºC (extension step). In these systems, a large fraction of that time is needed to heat and cool down the mixture since the large metal block has to reach the cycle equilibrium temperature and then transfer heat to the mixture through the microfuge tubes. Therefore, the cycle time is defined taking into account the thermal capacitance of metal block and the heat transfer trough the plastic microfuge tubes. However, a disadvantage of these conventional systems is related with the difficulty to ensure the thermal uniformity for the entire metal block that can influence the PCR specificity and thermal control (30). In this thesis, the conventional system was only used to perform an initial step, 10 min at 95ºC, to activate the enzyme in order to save time in PCR on chip technique.

5.2.2 Real Time PCR

The rt-PCR has become the gold standard method for accurate quantification and characterization of nucleic acids, in discovery and routine applications ranging from pathogen detection to mutation discovery and verification of expression profiles generated on microarrays. The LightCycler® was used to perform rt-PCR, which shows several advantages comparing to conventional PCR. This equipment allows the amplification monitoring of PCR products simultaneously in real-time. The PCR solution and a negative control sample, with 20µl volume each one, were prepared as described in previous section 5.2 and divided in two small capillary tubes in which a rigorous and accurate pipetting was required. The capillaries and air-mediated heating and cooling are two advantages of this equipment. Although, the glass capillaries were very delicate these can provide and ensure a high thermal uniformity, and present a heat transfer similar to channel used for PCR on chip. Then, many instructions were programmed in real-time thermocycler, which were, 25 cycles of 10sec at 95ºC (denaturation step), 4 sec at 65ºC (annealing step) and 4 sec at 72ºC (extension step). The initial step, 10 min at 95ºC was performed in a conventional thermocycler, as the PCR on chip, in order to evaluate if the PCR result was influenced by this external step. Moreover, a quantification mode was chosen and a heating rate of 20ºC/sec was verified. Using this method, it was also possible to

evaluate the existence of additional non intended PCR products by melting curve analysis. The rt-PCR was always performed as standard reliable result in order to compare the results obtained with PCR on chip.

5.2.3 PCR On Chip

PCR on chip concept was based in performing the PCR reaction in a biochip. A variety of previous studies have revealed two basic approaches in the PCR system conception, a stationary system with an incorporated thermal control device and PCR chips with dynamic fluid flow systems with three zones at different temperatures. In the stationary format of PCR system, the PCR solution is kept stationary and the PCR temperature cycling is performed on the chamber. During the past two, the miniaturization of such PCR devices has been of growing interest. This format of PCR chips can be classified as single chamber stationary PCR chip and multi chamber stationary system (8).

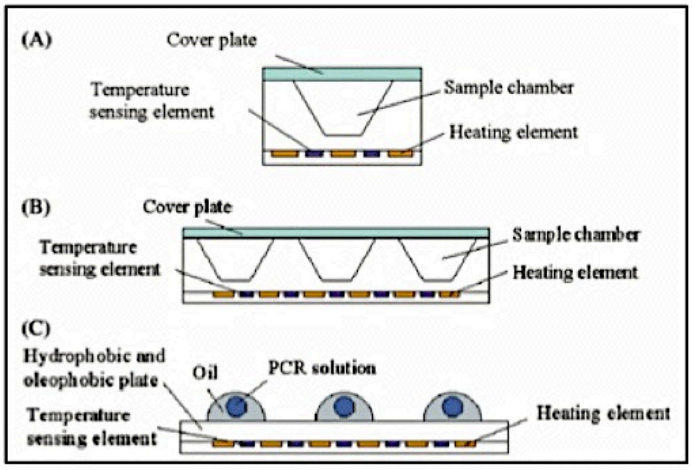

Figure 5-2: Stationary chamber-based PCR chip a) Single chamber PCR chip b) Multi chamber PCR chip c) Virtual reaction machine PCR (adapted from (8)) .

Northrup and its co-workers, in 1993, developed the first PCR chip stationary system (61). The single chamber stationary PCR chip offers beneficial properties such as a precise thermal and fluidic control preventing the crosstalk between chambers (Figure 5-2a). However, this system cannot realize high throughput. Then, in order to circumvent this drawback, multi-chamber stationary PCR have been developed (Figure 5-2b). Chamber-based PCR chips are usually constructed as closed systems, allowing an optimal and homogenous temperature between chambers. Guttenberg *et al.* proposed a different approach to handle a small sample using a hydrophobic/oleophobic surface, providing virtual fluid confinement (62). Further, Neuzil and its co-workers optimized the virtual reaction chamber (VRC) concept, applied for first time on the PCR chip in 2005 (Figure 5-2c). Neuzil work consisted in placing a disposable microscope glass cover slip on top of a micromachined silicon chip integrated with a heater and temperature sensor. A small DNA sample was placed on the glass and encapsulated with mineral oil, forming a VRC, eliminating cross-contamination between samples (31,

32). In fluid flow systems, a pumping method implementation is required, in order to promote the sample movement through a microfluidic channel, between different zones at constant temperatures over time. Different configurations, such as serpentine or spiral, can be achieved to the microfluidic channel (Figure 5-3) (8, 30, 33).

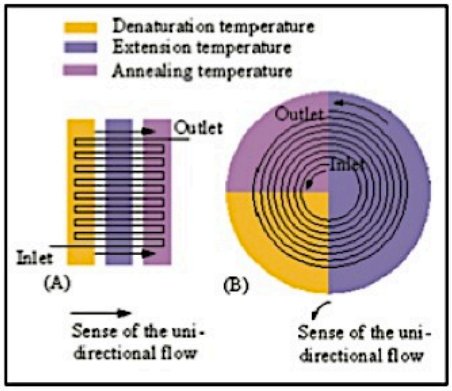

Figure 5-3: Continuous flow PCR a) The serpentine channel continuous-flow PCR b) The spiral channel continuous-flow PCR. The sample is introduced at the inlet and pumped unidirectionally towards the outlet (adapted from (8)).

In 1998, Koop *et al.* reported a continuous flow PCR chip using a serpentine channel passing through three thermostable copper blocks (Figure 5-3b) (33). Hashimoto and its co-workers proposed a hybrid chip incorporating the continuous-flow PCR and hybridization assays to perform analysis of single base mutation in genomic DNA. Hashimoto work was important due to the integration of the continuous-flow PCR with pre-PCR or post-PCR. (30). Li *et al.* developed a continuous-flow PCR chips with a serpentine channel of varying width for 'regional velocity control' (49). The continuous-flow PCR chip approach shows attractive features, such as, the nucleic acids analysis process can be performed in a dynamic format of an integrated PCR chip and the transition times between different temperatures depend only on the flow rate of the sample and the time required to reach a thermal equilibrium. However, continuous-flow PCR chips also present some drawbacks, for instance, gas bubbles formation influencing the PCR and the flow rate regulation of PCR solution between different temperature zones is difficult (8).

Since the optimal reaction temperatures and exposure times of the sample to each temperature are key to successful DNA amplification, thermal/fluid control of heat transfer, uniform temperature distributions, and sample velocities within the microfluidic channel and of the DNA sample are critical issues in PCR technology. Hence, the sample heating and cooling strategy is vital for high product yields and PCR specificity. Therefore, our proposal consists in PCR performing in a magnetoresistive (MR) biochip integrated in a platform, which controls all electronic system, temperature control and data acquisition in real time.

The main goal of PCR on chip consists in the DNA amplification from a very small amount of PCR mixture. This is the crucial difference from other methods, conventional PCR and rt-PCR. However, in an initial phase of PCR on chip experiments, a sample of 20µl mixture PCR was also used in order to

evaluate and compare the results obtained with reliable rt-PCR results simultaneously studied. In this strategy, a current line was used as heating element. By applying a current value of 60mA and varying the percentage of duty cycle it was possible to achieve the optimal three temperatures, as studied in chapter 4. Using this configuration, the fluid placed on top of current line can achieve a good uniformity temperature with a small temperature variation of 1/2ºC. Moreover, several PCR cycle times were experimented to achieve the optimal conditions to performing a specific PCR on chip. The PCR cycle time tested were similar to that obtained from rt-PCR specifically, an initial step dedicated to enzyme activation, 10 min at 95ºC, which was processed outside the platform in a conventional thermocycler, followed by 25 cycles of 13sec at 95ºC (denaturation step), 8 sec at 65ºC – 68ºC (annealing step) and 5 sec at 72ºC – 74ºC (extension step). In PCR on chip, an additional step of 30 sec at 95ºC in first PCR cycle was performed in order to ensure that the highest temperature, 95ºC was totally achieved.

5.3 PCR on chip – DNA Amplification

Recently, the research and development of LOC diagnosis and monitoring platforms has integrated a powerful technique for DNA amplification, PCR on chip. Biochips miniaturization has enabled to achieve several benefits such as analysis time minimization, reagent consumption reduction and minimization of risk of sample contamination and often enhance of assays performance, which have been critical for real time genotyping and diagnosis (63).

5.3.1 Instrumentation: PCR on chip Apparatus

With propose of performing the PCR reaction in a biochip it was necessary to ensure a rigorous temperature and PCR mixture flow control. The apparatus used, shown in Figure 5-4, consisted of a portable platform, a micro pump (HNP Mikrosysteme GmbH) and a personal computer interconnected in order to ensure the fluid and temperature control, to perform the PCR and to measure and evaluate the biochip signal obtained using a graphical interface. Hence, the platform and micropump was connected by USB to a personal computer.

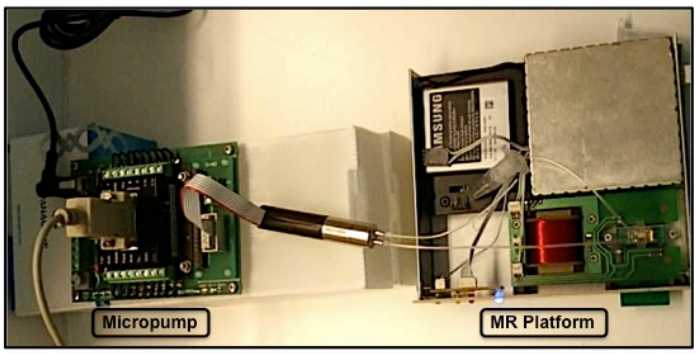

Figure 5-4: PCR on chip apparatus: Micropump and platform connected to personal computer. The PCR solution was pumped inside the microfluidic channel using a continuous flow with a flow rate of 0.05ml/min. A current value of 60mA was applyied in a current line and varying the percentage of duty cycle, the three optimal temperatures to PCR reaction were achieved. Then, the PCR solution of 10µl was recuperated and the amplified products were analysed in a gel electrophoresis.

Using this apparatus, the amplification process was repeated 20 times until reaching 10µl of sample PCR mixture were amplified. Although, 20µl of PCR mixture were prepared, only half of sample was amplified and evaluated relating to rt-PCR in same conditions. It was necessary a large amount of sample, since the analysis method of PCR products, namely gel electrophoresis requires a considerable volume of DNA amplification. After PCR solution preparation, this was submitted to 95ºC during 10 minutes in a conventional thermocycler in order to activate the enzyme. This step was made outside the platform aiming to minimize the process total time and to avoid the enzyme activation step in each volume of 0.5ul until amplify the 10µl total PCR solution.

Then, micropump parameters were studied and optimized taking into account the microchannel area and the PCR sample volume. These parameters included a continuous flow with a flow rate of 0.05ml/min to inject the PCR mixture into the microfluidic channel on top of the biochip, in contact with the heating element, and a dosage of 0.5µl to each volume that would be amplified. So, after the external enzyme activation, the PCR solution was cooled at room temperature (RT) and a rinsing step of channel with deionised (DI) water was made in order to avoid the air bubbles inside the channel, which can influence the normal flow of PCR solution, and consequently its lost. After that, the PCR solution was inserted into channel connected to the microfluidic channel inlet and a set flow rate was activated to inject the sample into the microfluidic channel, ensuring its contact with the heating elements.

Many instructions have to be regulated in order to obtain the temperature control necessary for the PCR. First, a 1mA current DC was applied to bias the sensor and a DC field of -50Oe to ensure that the measurements were made in the saturation zone of transfer curve of all sensors. A sampling frequency of 844Hz and a pulse with 0.1ms duration were also used. Following, a current value of 60mA was applied in the current line and the duty cycle percentage was tailored in order to control and to ensure the temperature variation required for entire PCR reaction accomplishment. In this case, the PCR cycle time consisted of an additional step of 30sec at 95ºC in first cycle (to ensure that

95ºC was accurate achieved), followed by 25 cycles for each 0.5µl of PCR mixture, 13sec at 95ºC (denaturation step), 8sec at 65ºC (annealing step) and 5sec at 72ºC (extension step). Then, three different percentage of duty cycle were used such as, 97%, 68% and 74% in order to achieve the three different temperatures, 95ºC, 68ºC and 72ºC respectively. After the amplification of total volume of PCR solution, this solution was analysed using an electrophoresis method, discussed in detail subchapter 5.4, and the results were evaluated in comparing with rt-PCR results simultaneously performed.

5.4 Results

In this work, the results of rt-PCR and PCR on chip were analysed and evaluated taking in account the real time cycle and temperatures achieved. For this, the data collected by the graphical interface of the platform and rt-PCR software were simultaneously analysed. Moreover, the agarose gel (2%) electrophoresis was used to confirm the results of PCR on chip and rt-PCR detection after the amplification products collection. This technique was combined with a fluorescent dye, the GelRed™ used for staining nucleic acids. In order to achieve an easy quantification and size determination, 5µl HyperLadder II Bioline marker (dispensed in first gel pad) was used to identify the DNA fragments molecular weigh. The HyperLadder II Bioline produces a pattern of 15 spaced bands, ranging from 50bp to 2kb. As each band contains an exact amount of dsDNA it was possible to achieve accurate quantification of sample bands. Then, the 10µl negative control, 10µl rt-PCR products and 10µl PCR on chip products were dispensed into the second, third and forth gel pads respectively. Besides that, the electrophoresis chamber was connected to a power source, Electrophoresis Power Supply 301, and applying a 400mA electric current and 80V voltage, the DNA molecules could move through the agarose gel. The larger molecules move slowly through the gel while the smaller molecules move faster. The different size molecules form distinct bands on the gel. At last, the results were visualized with a UV camera VWR Genosmart.

5.4.1 Real Time PCR

The rt-PCR revealed a crucial role in these experiments. The results of rt-PCR have been optimized and its real time analyses have shown an important advantage. The rt-PCR was always performed a few minutes before PCR on chip, in order to evaluate if any component of solution or condition (temperature or cycle time) could inhibit the amplification DNA. Figure 5-5 presents a typical rt-PCR thermocycling os 25 cycles for 10 sec at 95ºC, 4 sec at 65ºC and 4 sec at 72ºC. The initial step, 10 min at 95ºC was achieved in a conventional thermocycler. The last step consisted in 30 sec at 65ºC and after that the heating up until 95ºC at 0.1ºC/sec. This step was essential to perform the melting curves analysis. In this technique, a negative control sample consisting in the same components, except the genomic DNA, was also tested.

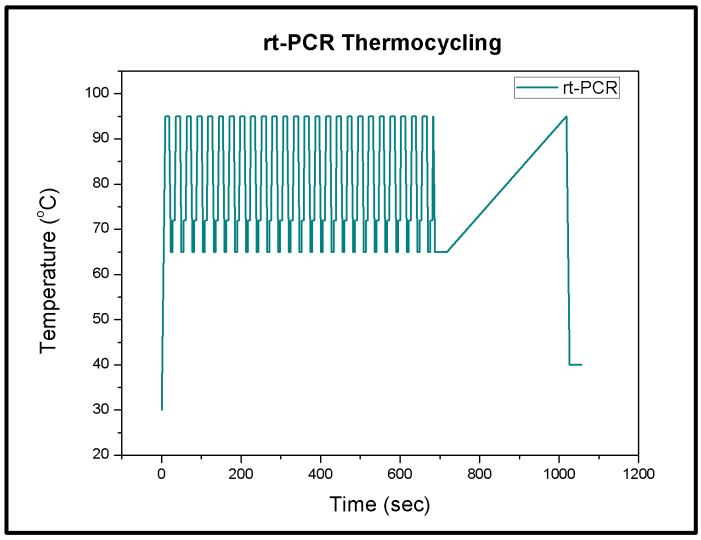

Figure 5-5: rt-PCR results: 25 cycles of 10 sec at 95ºC (denaturation step), 4 sec at 65ºC (annealing step) and 4 sec at 72ºC (extension step). The typical initial step to enzyme activation, 10min at 95ºC was performed in a conventional thermocycler.

In the Figure 5-6 are presented the amplification curves of rt-PCR products. The rt-PCR solution (blue line) presents the desired result, an exponential growth at 7 cycles. By analysing this curve can be possible to predict a fragment with a corresponding size of 115bp in the agarosis gel. The negative control sample (violet line) shows a non intended result. Taking into account that the negative control sample contains all components of rt-PCR solution, except genomic DNA, the amplification would not be expected. However, in this case, an irrelevant amplification was observed after 21 cycles. With this result, can be expected a poorly defined 115bp fragment in the agarosis gel. This result can be understood as a contamination, since the ALU115 is the most abundant repeated sequence in the human genome.

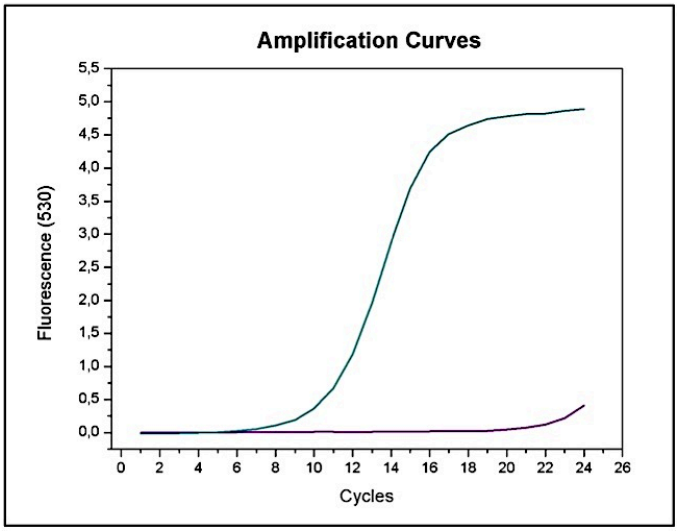

Figure 5-6: Amplification curves of rt-PCr results. rt-PCR amplification curve is represented by blue line and negative control sample result is presented by violet line

5.4.2 PCR on chip

In order to compare the results with a standard rt-PCR results in the same conditions a 10µl sample was used. Figure 5-7 shows the best obtained result after experimenting on several different cycle times. In this Figure, it was possible to verify that an identical thermocycle was obtained. An extra time was added in the first cycle, about 30 sec, in order to ensure that the highest temperature was completely achieved. The times per cycle were a quite different such as, 13 sec at 95ºC, 8 sec at 65ºC and 5 sec at 72ºC. The explanation for the use of these conditions can be explained by Figure 5-8 analysis.

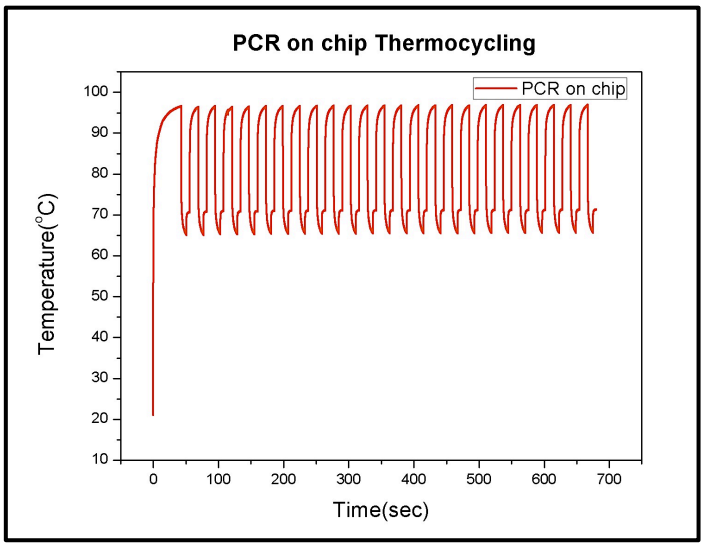

Figure 5-7: PCR on chip results: 25 cycles of 13 sec at 95ºC (denaturation step), 8 sec at 65ºC (annealing step) and 5 sec at 72ºC (extension step). The typical initial step to enzyme activation, 10min at 95ºC was performed in a conventional thermocycler. An extra time was added in first cycle, about 30 sec, in order to ensure that the intended temperature was completely achieved.

Figure 5-8 shows an overlap between the two different amplification techniques being used. With this overlap it was possible to evaluate that the cycle times were not totally equal. This can be explained by the fact that the data acquired and collected from rt-PCR software, only reveal the transition points between different temperatures and a sharp heating and cooling was obtained. However, the two curves were overlapped when using different times in each cycle, 10sec, 4 sec and 4 sec to rt-PCR and 13sec, 8sec and 5 sec, to PCR on chip. Thus, it can be verified that the times programmed in rt-PCR software were only accomplished after the temperature was achieved. In reality, a complete rt-PCR cycle corresponds to 13sec, 8 sec and 5 sec.

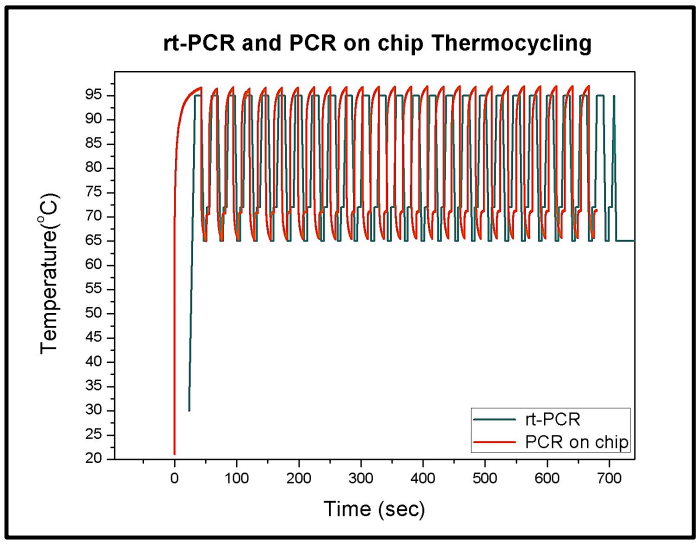

Figure 5-8: rt-PCR and PCR on chip results overlapping.

The behaviour presented in Figure 5-8 can be evaluated in detail in Figure 5-9, which presents the three first cycles. It was possible to observe detailed heating and cooling ramps and the transition and the residence times of the fluid in each temperature zone, specifically, the denaturation, the annealing and the extension step. These three steps of PCR cycle were represented by three illustrative animations. The thermocycle of rt-PCR was represented by the blue line and the PCR on chip thermocycle was represented by the orange line. Several efforts were made in order to achieve and ensure a rigorous control of the specific times and temperatures, by setting the current to a constant value with varying the percentage of duty cycle. Moreover, an accurate similarity between the thermocycles of two different PCR techniques could be highlighted. Although, the temperatures have not been achieved exactly, a temperature approximated was verified with a little maximal temperature variation of 2ºC.

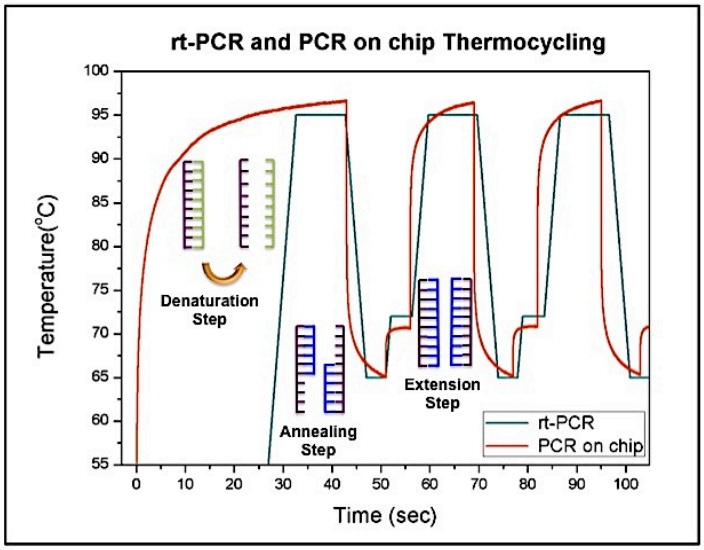

Figure 5-9: Analysis of the three first PCR cycles in detail. Representation of three crucial steps to PCR performing, 13 sec at 95ºC (denaturation step), 4 sec at 65ºC (annealing step) and 4 sec at 72ºC (extension step). The different temperatures were similarly achieved at the identical cycle times.

Agarose gel (2%) was used to analyse the results of rt-PCR and PCR on chip products. For this specific analysis a 10µl volume of each sample, specifically a negative control sample, rt-PCR mixture and PCR on chip solution, were dispensed in a defined gel pad. Although, the PCR mixture had already incorporated a small amount of SyBR Green, a fluorescent dye, which was bonded to the DNA sequence providing a fluorescence signal, the GelRed™ was also used for staining nucleic acids and improving the optically detection.

The Figure 5-10 presented the best result obtained for DNA amplification, which was visualized using a UV camera VWR Genosmart. In A gel pad was represented the HyperLadder II Bioline marker used to quantify the sample bands and identify the DNA fragments molecular weigh. The B, C and D gel pads correspond to the negative control sample, rt-PCR products sample and PCR on chip products sample respectively. In the negative control sample should not present amplification in any cycle or time. However, it was verified a fragment with 115bp, which can be understood as a contamination, taking into account that the sequence (ALU115 fragment) exists in a large quantity in the human genome. Nevertheless, the band intensity of the negative control was considered insignificant when comparing to the band appearing on rt-PCR products sample. The result obtained in C gel pad, was the intended result, a fragment with 115bp. This would also be the result also expected for the PCR on chip sample. Though, instead of a fragment with 115bp, it was verified a fragment positioned in the gel with a corresponding size of about 75bp. Although, the PCR on chip results demonstrate a non specific DNA amplification, this can be considered a crucial and promising result for PCR on chip research.

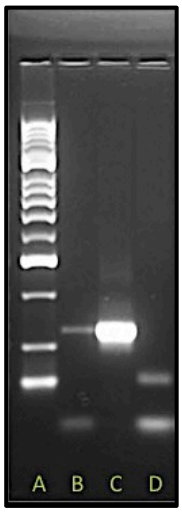

Figure 5-10: Analysis of PCR products in an agorose (2%) gel electrophoresis: A – HypperLadder II Bioline (ranging from 50bp to 2000bp); B – Negative control sample; C – rt-PCr products sample; D – PCR on chip products sample.

5.5 Discussion

PCR on chip is a promising DNA amplification technique, which will be intensively studied due to its specificity, fast speed and thermal uniformity. The thermal cycle results obtained for the two different PCR techniques were really identical, as it was shown in Figure 5-8. The thermal control achieved for PCR on chip, controlled by Pulse Width Modulation (PWM), was very rigorous and crucial for PCR on chip performing. However, some differences can also be referred, such as, the difference of time in which each temperature remained in a plateau step, the temperature rate in which a specific temperature was achieved and the temperature specificity. These aspects were taken into account to improve the future experiments and one solution can be presented. A rapid thermocycle (faster temperature rates) could be achieved implementing a PID algorithm, which can provide a rigorous temperature control, in which the transition and residence times of the fluid in each temperature zone would be accurately achieved. Using this strategy, a increasing of the speed of the reaction could be performed as well as the specificity (the correct part of the DNA multiplied) and the efficiency (the yield of the PCR cycle) of the reaction could be favored by fast and accurate temperature changes. The PID algorithm controller would be used to minimize the transition time between different temperatures by injection of different current values depending on temperature requirement.

The rt-PCR results presented in the agarose gel electrophoresis corresponded to the expected result, a fragment with 115 bp, and represented a reliable result to compare the PCR on chip products. The PCR on chip products were not specific, but it was considered an essential progress in PCR on chip work. In order to understand the obtained PCR on chip results, many possibilities can be mentioned. A non specific binding of primers to the DNA fragment can be established if an inhomogeneous temperature of sample, inside the microchannel, was verified. Another possibility is related with the fact that only 0.5µl of PCR mixture was amplified in each time until 10µl were achieved and the timeout of remaining sample could promote the primer-primer binding, creating primer dimers. Due to significantly increased surface to volume ratio and together with the surface properties the fragments can be tied on the biochip surface when the DNA sample amplified was collected.

Therefore, several modifications and improvements can be suggested in order to obtain a specific DNA amplification. Using an enzyme with a lower activation time, from 10 min to 1 min, the entire amplification process can be accomplished inside the MR platform, avoiding the possibility of primers dimers formation. The rigorous thermal control provided by PID algorithm implementation would be crucial to ensure that the three specific temperatures would be achieved, specially the annealing temperature that should not be undershoot in order to prevent false annealing primers and consequently decreasing the specificity of the PCR. The implementation of a continuous current line could improve and enhance the uniformity of temperature for total PCR sample. And the last solution consists in the modification of microdevices surface with chemical alteration processes. The surface passivation could be achieved by blocking the surface with passivation agents such as bovine serum albumin (BSA) to reduce the undesired adsorption of enzyme and DNA to channel wall and surface.

6. Conclusions

6.1 Thesis Contributions and Future Work

This thesis was based on the integration of PCR in a MR biochip, which has currently been integrated with other devices in order to obtain a fully integrated LOC device. Several requirements for this device have been reported such as, sensitivity, rapidity, low cost, portability and ease to use. One of the most important contributions of this work was the optimization and development of the PCR system. Several parameters including substrate materials selection, PR profile and development study and passivation layer optimization were crucial to obtain a MR biochip with accurate sensitivity and improved performance when biological assays were performed. Since, the PCR system (the biochip bonded to the PCB carrier) is disposable, the danger of sample to sample cross contamination will be completely eliminated. The microfluidic channel incorporation carried some benefits, such as the reproducibility and the rapidness of the system. The portability was also achieved by the integration of the MR biochip in a portable electronic platform, which performs the control and acquisition of the MR sensors signals. These signals are sent to a computer via USB and user-friendly software is available for its analysis.

Moreover, the calibration of MR sensors as temperature sensors was crucial to study of the thermal parameters, such as thermal conductance, thermal capacitance and time constant thermal, and to perform the PCR thermal cycling required. Using these temperature sensors and a thermal control controlled by a PWM, which is based on applying a specific current value and a percentage of duty cycle, a rigorous thermo cycling control was accomplished. The current value and percentage of duty cycle were selected taking into account the temperature variation required for an entire PCR reaction cycle. A typical PCR cycle that consists in three steps, heating up at 95ºC, cooling down at 65ºC and heating up at 72ºC was achieved by applying a 60mA current value and three different percentage of duty cycle, 97%, 68% and 74%, respectively. The thermal properties of the system are also dominated by the sample volume, which will be reduced making the PCR even more economical. Using an rt-PCR as evaluation point, several experiments were made in order to amplify a specific DNA fragment (ALU115 fragment). The best result demonstrated that the DNA amplification from integration of PCR in MR biochip can be accomplished and a rigorous thermal control was already implemented.

Therefore, during this thesis an important step was achieved on the integration of PCR in a MR biochip, however some improvements have to be considered in order to obtain a thermal uniformity and a PCR product with an accurate specificity. For instance, an enzyme with a lower activation time, 1 min instead of 10 min, could allow the entire amplification process inside the platform, eliminating the activation step in the convectional thermocycler and, consequently avoiding the possibility of primers dimers formation.

Furthermore, the rigorous thermal control provided by PID algorithm implementation would be crucial to ensure that the three specific temperatures would be achieved, during the desired time, specially the annealing temperature that should not be undershoot in order to prevent false annealing primers and consequently decreasing the specificity of the PCR.

Other suggestion would consist in the implementation of a continuous current line in order to improve and enhance the uniformity of temperature for total PCR sample.

And the last solution involves the modification of microdevices surface with chemical alteration processes. The surface passivation could be achieved by blocking the surface with passivation agents such as bovine serum albumin (BSA) to reduce the undesired adsorption of enzyme and DNA to channel wall and surface.

Several applications have emerged in the MR DNA biochip world. The PCR on chip developed in this thesis could be used to amplify the target sample being integrated in the detection and monitoring of cancer biomarkers in blood. The PCR on chip technique would be crucial in the target sample (e.g. genomic DNA) amplification step, minimizing the small amount of DNA sample, ensuring the rapidity of the total process as well as the portability of the platform, ensuring the DNA amplification and detection and monitoring of biomarkers inside the platform. After DNA sample amplification, this target sample labelled magnetically would be hybridized with probe molecules immobilized over MR sensor. Finally, an external magnetic field is applied to magnetize the labels and therefore creating a fringe field detected by a MR sensor. The principal advantage of this platform consists in the magnetic sensors integration, allowing the PCR performing, due to its calibration as temperature sensors and the detection of magnetic field produced by DNA hybridization.

References

[1] P. Yager, G. J. Domingo and J. Gerdes, "Point-of-care diagnostics for global health," *Annual review of biomedical engineering* **10**(107-144 (2008)

[2] D. C. Hay Burgess, J. Wasserman and C. A. Dahl, "Global health diagnostics," *Nature* **444**(1-2 (2006)

[3] C. D. Chin, V. Linder and S. K. Sia, "Lab-on-a-chip devices for global health: past studies and future opportunities," *Lab on a chip* **7**(1), 41-57 (2007)

[4] M. Urdea, L. A. Penny, S. S. Olmsted, M. Y. Giovanni, P. Kaspar, A. Shepherd, P. Wilson, C. A. Dahl, S. Buchbaum, G. Moeller and D. C. Hay Burgess, "Requirements for high impact diagnostics in the developing world," *Nature* 73-79 (2006)

[5] W. G. Lee, Y. G. Kim, B. G. Chung, U. Demirci and A. Khademhosseini, "Nano/Microfluidics for diagnosis of infectious diseases in developing countries," *Advanced drug delivery reviews* **62**(4-5), 449-457 (2010)

[6] "World Health Statistics," World Health Organization, Geneva, Switzerland (2012).

[7] M. G. Roper, C. J. Easley and J. P. Landers, "Advances in polymerase chain reaction on microfluidic chips," *Analytical chemistry* **77**(12), 3887-3893 (2005)

[8] C. Zhang and D. Xing, "Miniaturized PCR chips for nucleic acid amplification and analysis: latest advances and future trends," *Nucleic acids research* 35(13), 4223-4237 (2007)

[9] X. Qiu, M. G. Mauk, D. Chen, C. Liu and H. H. Bau, "A large volume, portable, real-time PCR reactor," *Lab on a chip* **10**(22), 3170-3177 (2010)

[10] P. J. Obeid, T. K. Christopoulos, H. J. Crabtree and C. J. Backhouse, "Microfabricated device for DNA and RNA amplification by continuous-flow polymerase chain reaction and reverse transcription-polymerase chain reaction with cycle number selection," *Analytical chemistry* **75**(2), 288-295 (2003)

[11] C. A. Heid, J. Stevens, K. J. Livak and P. M. Williams, "Real time quantitative PCR," *Genome research* **6**(10), 986-994 (1996)

[12] D. Lee, P. J. Chen and G. B. Lee, "The evolution of real-time PCR machines to real-time PCR chips," *Biosensors & bioelectronics* **25**(7), 1820-1824 (2010)

[13] J. Germano, V. C. Martins, F. A. Cardoso, T. M. Almeida, L. Sousa, P. P. Freitas and M. S. Piedade, "A portable and autonomous magnetic detection platform for biosensing," *Sensors* **9**(6), 4119-4137 (2009)

[14] B. M. de Boer, J. A. Kahlman, T. P. Jansen, H. Duric and J. Veen, "An integrated and sensitive detection platform for magneto-resistive biosensors," *Biosensors & bioelectronics* **22**(9-10), 2366-2370 (2007)

[15] D. L. Graham, H. A. Ferreira and P. P. Freitas, "Magnetoresistive-based biosensors and biochips," *Trends in biotechnology* **22**(9), 455-462 (2004)

[16] M. N. Baibich, J. M. Broto, A. Fert, F. Nguyen Van Dau, F. Petroff, P. Etienne, G. Creuzet, A. Friederich and J. Chazelas, "Giant magnetoresistance of (001)Fe/(001)Cr magnetic superlattices," *Physical review letters* **61**(21), 2472-2475 (1988)

[17] D. R. Baselt, G. U. Lee, M. Natesan, S. W. Metzger, P. E. Sheehan and R. J. Colton, "A biosensor based on magnetoresistance technology," *Biosensors & bioelectronics* **13**(7-8), 731-739 (1998)

[18] F. A. Cardoso, "Design, optimization and integration of magnetoresistive biochips," Instituto Superior Técnico (2010).

[19] P. P. Freitas, F. A. Cardoso, V. C. Martins, S. A. Martins, J. Loureiro, J. Amaral, R. C. Chaves, S. Cardoso, L. P. Fonseca, A. M. Sebastiao, M. Pannetier-Lecoeur and C. Fermon, "Spintronic platforms for biomedical applications," *Lab on a chip* **12**(3), 546-557 (2012)

[20] H. A. Ferreira, F. A. Cardoso, R. Ferreira, S. Cardoso and P. P. Freitas, "Magnetoresistive DNA chips based on ac field focusing of magnetic labels," *Journal of Applied Physics* **99**(08P105 (2006)

[21] H. A. Ferreira, N. Feliciano, D. L. Graham, L. A. Clarke, M. D. Amaral and P. P. Freitas, "Rapid DNA hybridization based on ac field focusing of magnetically labelled target DNA," *Applied Physics Letters* **87**(013901 (2005)
[22] V. C. Martins, J. Germano, F. A. Cardoso, J. Loureiro, S. Cardoso, L. Sousa, M. Piedade, L. P. Fonseca and P. P. Freitas, "Challenges and trends in the development of a magnetoresistive biochip portable platform," *Journal of Magnetism and Magnetic Materials* **322**(1655-1663 (2010)
[23] R. L. Millen, T. Kawaguchi, M. C. Granger, M. D. Porter and M. Tondra, "Giant magnetoresistive sensors and superparamagnetic nanoparticles: a chip-scale detection strategy for immunosorbent assays," *Analytical chemistry* **77**(20), 6581-6587 (2005)
[24] G. Li, V. Joshi, R. L. White, S. X. Wang, J. T. Kemp, C. Webb, R. W. Davis and S. Sun, "Detection of single micron–sized magnetic bead and magnetic nanoparticles using spin valve sensors for biological applications," *Journal of Applied Physics* **93**(7557-7755 (2003)
[25] M. Piedade, L. A. Sousa, T. M. de Almeida, J. Germano, B. D. da Costa, J. M. Lemos, P. P. Freitas, H. A. Ferreira and F. A. Cardoso, "A new hand-held microsystem architecture for biological analysis," *Ieee T Circuits-I* **53**(11), 2384-2395 (2006)
[26] G. Li, S. Sun, R. J. Wilson, R. L. White, N. Pourmand and S. X. Wang, "Spin valve sensors for ultrasensitive detection of superparamagnetic nanoparticles for biological applications," *Sensors and actuators. A, Physical* **126**(1), 98-106 (2006)
[27] A. P. Turner, "Tech.Sight. Biochemistry. Biosensors--sense and sensitivity," *Science* 290(5495), 1315-1317 (2000)
[28] V. C. Martins, F. A. Cardoso, J. Germano, S. Cardoso, L. Sousa, M. Piedade, P. P. Freitas and L. P. Fonseca, "Femtomolar limit of detection with a magnetoresistive biochip," *Biosensors & bioelectronics* **24**(8), 2690-2695 (2009)
[29] D. S. Lee and C. S. Chen, "Development of a temperature sensor array chip and a chip-based real-time PCR machine for DNA amplification efficiency-based quantification," *Biosensors & bioelectronics* **23**(7), 971-979 (2008)
[30] M. Hashimoto, P. C. Chen, M. W. Mitchell, D. E. Nikitopoulos, S. A. Soper and M. C. Murphy, "Rapid PCR in a continuous flow device," *Lab on a chip* **4**(6), 638-645 (2004)
[31] P. Neuzil, J. Pipper and T. M. Hsieh, "Disposable real-time microPCR device: lab-on-a-chip at a low cost," *Molecular bioSystems* **2**(6-7), 292-298 (2006)
[32] P. Neuzil, C. Zhang, J. Pipper, S. Oh and L. Zhuo, "Ultra fast miniaturized real-time PCR: 40 cycles in less than six minutes," *Nucleic acids research* **34**(11), e77 (2006)
[33] M. U. Koop, A. J. Mello and A. Manz, "Chemical amplification: Continuous-flow PCR on a Chip," *Science* **280**(1046-1048 (1998)
[34] P. Neuzil, L. Novak, J. Pipper, S. Lee, L. F. Ng and C. Zhang, "Rapid detection of viral RNA by a pocket-size real-time PCR system," *Lab on a chip* **10**(19), 2632-2634 (2010)
[35] N. C. Cady, S. Stelick, M. V. Kunnavakkam and C. A. Batt, "Real-time PCR detection of Listeria monocytogenes using an integrated microfluidics platform," *Sensor Actuat B-Chem* **107**(1), 332-341 (2005)
[36] S. H. Lee, S. W. Kim, J. Y. Kang and C. H. Ahn, "A polymer lab-on-a-chip for reverse transcription (RT)-PCR based point-of-care clinical diagnostics," *Lab on a chip* **8**(2121-2127 (2010)
[37] R. A. Ferreira, "Ion Beam Deposited Magnetic Spin Tunnel Junctions targeting HDD Read Heads, Non-volatile Memories and Magnetic Field Sensor Applications," Instituto Superior Técnico (2008).
[38] R. Macedo, "Spintronic Nano Devices: Nanofabrication of sub-50nm Magnetic Tunnel Junctions and Self-Powered Hybrid Sensors," Instituto Superior Técnico (2011).
[39] D. Burgler and P. Grunberg, *Nanoelectronics and Information Technology*, Weinheim, Germany (2005).
[40] L. M. Gameiro, "Magnetoresistive nanosensors with high spatial resolution for detecting ultra low magnetic fields," Instituto Superior Técnico (2012).

[41] V. Passi, A. Lecestre, C. Krzeminski, G. Larrieu, E. Dubois and J. P. Raskin, "A single layer hydrogen silsesquioxane (HSQ) based lift-off process for germanium and platinum," *Microelectron Eng* 87(10), 1872-1878 (2010)
[42] J. Heo and S. Z. Hua, "An overview of recent strategies in pathogen sensing," *Sensors* **9**(6), 4483-4502 (2009)
[43] T. M. Hsieh, C. H. Luo, G. B. Lee, C. S. Liao and F. C. Huang, "A Micromachined Low-power-consumption Portable PCR system," *Journal of Medical and Biological Engineering* **26**(43-49 (2005)
[44] C. Y. Lee, G. B. Lee, J. L. Lin, F. C. Huang and C. S. Liao, "Integrated microfluidic systems for cell lysis, mixing/pumping and DNA amplification," *J Micromech Microeng* **15**(6), 1215-1223 (2005)
[45] Z. Q. Zou, X. Chen, Q. H. Jin, M. S. Yang and J. L. Zhao, "A novel miniaturized PCR multi-reactor array fabricated using flip-chip bonding techniques," *J Micromech Microeng* **15**(8), 1476-1481 (2005)
[46] Z. Q. Niu, W. T. Chen, Y. S. Shao, X. Y. Jia and W. P. Zhang, "DNA amplification on a PDMS-glass hybrid microchip," *J Micromech Microeng* **16**(425-433 (2005)
[47] I. Schneegass, R. Brautigam and J. M. Kohler, "Miniaturized flow-through PCR with different template types in a silicon chip thermocycler," *Lab on a chip* **1**(1), 42-49 (2001)
[48] Y. K. Cho, J. Kim, Y. Lee, Y. A. Kim, K. Namkoong, H. Lim, K. W. Oh, S. Kim, J. Han, C. Park, Y. E. Pak, C. S. Ki, J. R. Choi, H. K. Myeong and C. Ko, "Clinical evaluation of micro-scale chip-based PCR system for rapid detection of hepatitis B virus," *Biosensors & bioelectronics* **21**(11), 2161-2169 (2006)
[49] S. Li, D. Y. Fozdar, M. F. Ali, H. Li, D. Shao, D. M. Vykoukal, J. Vykoukal, P. N. Floriano, M. Olsen, J. T. McDevitt, P. R. Gascoyne and S. Chen, "A Continuous-Flow Polymerase Chain Reaction Microchip With Regional Velocity Control," *Journal of microelectromechanical systems : a joint IEEE and ASME publication on microstructures, microactuators, microsensors, and microsystems* **15**(1), 223-236 (2006)
[50] C. N. Liu, N. M. Toriello and R. A. Mathies, "Multichannel PCR-CE microdevice for genetic analysis," *Analytical chemistry* **78**(15), 5474-5479 (2006)
[51] K. Sun, A. Yamaguchi, Y. Ishida, S. Matsuo and H. Misawa, "A heater-integrated transparent microchannel chip for continuous-flow PCR," *Sensor Actuat B-Chem* **84**(2-3), 283-289 (2002)
[52] J. A. Kim, J. Y. Lee, S. Seong, S. H. Cha, S. H. Lee, J. J. Kim and T. H. Park, "Fabrication and characterization of a PDMS–glass hybrid continuous-flow PCR chip," *Biochemical Engineering Journal* **29**(91-97 (2006)
[53] Q. T. Zhang, W. H. Wang, H. S. Zhang and Y. L. Wang, "Temperature analysis of continuous-flow micro-PCR based on FEA," *Sensor Actuat B-Chem* 82(1), 75-81 (2002)
[54] A. G. Sciancalepore, E. Mele, V. Arcadio, F. Reddavide, F. Grieco, G. Spano, P. Lucas, G. Mita and D. Pisignano, "Microdroplet-based multiplex PCR on chip to detect foodborne bacteria producing biogenic amines," *Food Microbiology* **35**(10e14 (2013)
[55] J. Huang, K. Padmanabhan and O. M. Collins, "The Sampling Theorem With Constant Amplitude Variable Width Pulses," *Ieee T Circuits-I* **58**(6), 1178-1190 (2011)
[56] C. H. Hsieh and J. H. Chou, "Design of optimal PID controllers for PWM feedback systems with bilinear plants," *Ieee T Contr Syst T* **15**(6), 1075-1079 (2007)
[57] W. S. Levine, *The Control Hankbook*, Boca Raton, Florida (2011).
[58] Q. Xiang, B. Xu and D. Li, "Miniature real time PCR on chip with multi-channel fiber optical fluorescence detection module," *Biomedical microdevices* 9(4), 443-449 (2007)
[59] F. Ahmad and S. A. Hashsham, "Miniaturized nucleic acid amplification systems for rapid and point-of-care diagnostics: a review," *Analytica chimica acta* **733**(1-15 (2012)
[60] T. Dias, "Magnetoresistive chip-based platform for the evaluation of cfDNA integrity as a potential biomarker in cancer diagnosis," Instituto Superior Técnico (2011).
[61] M. A. Northrup, B. Benett, D. Hadley, P. Landre, S. Lehew, J. Richards and P. Stratton, "A miniature analytical instrument for nucleic acids based on micromachined silicon reaction chambers," *Analytical chemistry* 70(5), 918-922 (1998)

[62] Z. Guttenberg, H. Muller, H. Habermuller, A. Geisbauer, J. Pipper, J. Felbel, M. Kielpinski, J. Scriba and A. Wixforth, "Planar chip device for PCR and hybridization with surface acoustic wave pump," *Lab on a chip* 5(3), 308-317 (2005)
[63] D. S. Lee, S. H. Park, H. S. Yang, K. H. Chung, T. H. Yoon, S. J. Kim, K. Kim and Y. T. Kim, "Bulk-micromachined submicroliter-volume PCR chip with very rapid thermal response and low power consumption," *Lab on a chip* 4(4), 401-407 (2004)

Appendix I

Run Sheet Biochip with Spin Valve Sensors

RUN: #1 **Filipe Cardoso/ Mariana Antunes**

Process Start: 12/11/2012 **Process Finish:** 29/11/2012

SV976 **MR=** 7.8% **Hf=** 14 Oe

Ta 20Å/$Ni_{80}Fe_{20}$ 36Å/$Co_{81}Fe_{19}$ 23Å/Cu 25Å/$Co_{81}Fe_{19}$ 23Å/$Mn_{76}Ir_{24}$ 80Å /Ta 30Å/$Ti_{10}W_{90}$ (N)150Å

STEP 1	**1st Exposure** – Spin Valve Definition	**Date:** 12/11/2012

Coating PR: Vapor Prime 30 min (Recipe - 0) coat 1.5 µm PR (Recipe 6/2)

Machine: Direct Write Laser (DWL)

Mask: uchipnewl1 **Map:** uchip

Die dimensions: X=7600 Y=6400

4 dies in wafer with 1inch **Alignment mark position:** X=168 Y=55.7

Energy: 75 %

Power: 120mW

Focus: 60

Develop: Recipe 6/2 **Development time:** 1 min

Optical Inspection:

Sample	Comments
SV976	OK

STEP 2	**Ion Milling** – Spin Valve Etching	**Date:** 13/11/2012

Machine: Nordiko 3000
385 A (etch rate: ~1 A/s −> time: 400s 30A of overetch)

Standard Etching Recipe (Etch Junction first)

Junction etch 70º

Assist Gun	Power (W)	V^+(V)	I^+(mA)	V^- (V)	I^- (mA)	Ar flux (sccm)	Pan (deg)	Rotation (%)
Set Values	-	735	105	350	-	10	70	30
Read Values	173	724.3	104.2	344.8	3.2	10.2	70	30

Optical Inspection:

Sample	Comments
SV976	OK

STEP 3 **Resist Stripping** **Date:** 13/11/2012

Hot µ-strip + ultrasonic
Rinse with IPA + DI water + dry compressed air

Started: 15h00 **Stopped:** 16h30

Total Time in hot µ-strip: 3x20min **Ultrasonic Time:** 3x10min

Optical Inspection:

Sample	Comments
SV976	OK. Spin valves are well defined

STEP 4 **2nd Exposure** – Contacts Leads Definition **Date:**19/11/2012

Coating PR: Vapor Prime 30 min (Recipe - 0) coat 1.5 µm PR (Recipe 6/2)

Pre-Development: 30 sec

Machine: Direct Write Laser (DWL)

Mask: uchipnewl2 **Map:** uchip

Alignment mark position: X=168 Y=55.7

Distance between alignment mark: X=6910

4 dies in wafer with 1inch **Energy:** 95%

Power: 120mW

Focus: 60

Develop: Recipe 6/2

Development time: 1 min

Optical Inspection:

Sample	Comments
SV976	OK

STEP 5 **Contacts Leads deposition** Date: 20-21/11/2012

Machine: Nordiko 3600
Al deposition: 3000 Å

Deposition Gun	Power (W)	V^+(V)	I^+(mA)	V^-(V)	I^-(mA)	Xe flow (sccm)	Pan (deg)	Rotation (%)
Set Values	170	1200	171	275		4	180	30
Read Values	156	1178	171	270	2	4.1	180	30

Optical Inspection:

Sample	Comments
SV976	OK

STEP 6 **Aluminium Lift-off** **Date:** 21/11/2012

Hot µ-strip + ultrasonic
Rinse with IPA + DI water + dry compressed air

Started: 12h00

Stopped: 13h40

Total Time in hot µ-strip: 4x20min

Ultrasonic Time: 2x10min

Optical Inspection:

Sample	Comments
SV976	Good definition of strips.

STEP 7	**3rd Exposure** – Passivation Layer Deposition	Date: 22/11/2012

Machine: Electrotech
SiN deposition: 3000 Å

1min 14 sec (3000 Å)
Holder: 300ºC
Showerhead: 350ºC

	Deposition Time	**NH_3 gas flow (sccm)**	**SiH_4 gas flow (sccm)**	**N_2 gas flow (sccm)**	**Pressure (mT)**	**Power Source RF (W)**
Read Values	1min 14sec	500	300	3500	850	500

Sample	**Comments**
SV976	It was necessary to find the deposition rate using different times and measuring samples with different thickness in ellipsometer to check. The ellipsometer only measures thicknesses until to 1000Å, we must find the deposition time to 1000Å, first. After we multiply the deposition time to 1000Å for three times and then we discover the deposition time to 3000Å - 40Å/sec.

STEP 8	**3rd Exposure** – Passivation Layer Definition	**Date:** 22/11/2013

Coating PR: Vapor Prime 30 min (Recipe - 0) coat 1.5 µm PR (Recipe 6/2)

Machine: DWL

Mask: uchipnewl3ninv

Map: uchip

Alignment mark position: X=168 Y=55.7

Distance between alignment mark: X=6910

4 dies in wafer with 1inch

Energy: 75 %

Power: 120mW

Focus: 60

Develop: Recipe 6/2

Development time: 1 min

Optical Inspection:

Sample	Comments
SV976	OK

STEP 9 **Ion Milling –** Passivation Layer Etching **Date:** 23/11/2012

Machine: Nordiko 3600
3000A (etch rate: assuming 2Å/s)

First step: Time - 8x230s
Second step: Time – 5x230s

Standard Etching Recipe (Etch Junction Stack all):

Assist Gun	Power (W)	V^+(V)	I^+(mA)	V^- (V)	I^- (mA)	Ar flux (sccm)	Pan (deg)	Rotation (%)
Set Values	-	735	105	350	-	10	70	30
Read Values	212	724.3	104.5	344.3	2.7	10.2	70	30

Sample	Comments
SV976	This step should be made by Reactive Ion Etching, in LAM. As LAM is off then we must perform in Nordiko 3600. The etch rate to SiN is not tested. Assuming that etch rate of SiN is equal that to the cooper, 2Å/s, then we did two steps of etch to not damage sample. The time of first step was 8x230''. After, we checked with the electrical probes if there was contact or not. A second etch step was performed during 5x230''.

Optical Inspection:

Sample	Comments
SV976	After first step by optical inspection was verified that the color presented is not metallic and measuring with electrical probes we checked that there not was contact. Then we proceeded to second step.

Electrical Probes Measurements

Sample	Comments
SV976	After two etching steps, it was checked that there was contact measuring with electric probes. Minimum resistance has values around 788 Ohm and maximum resistance about the 801 Ohm.

STEP 10 **Resist Stripping** **Date:** 26/11/2012

Hot µ-strip + ultrasonic
Rinse with IPA + DI water + dry compressed air

Started: 9h00 **Stopped:** 10h30

Total Time in hot µ-strip: 3x20min **Ultrasonic Time:** 3x10min

Optical Inspection:

Sample	Comments
SV976	OK

STEP 11 **4th Exposure** – Au pad definition **Date:** 26/11/2012

Coating PR: Vapor Prime 30 min (Recipe - 0) coat 1.5 µm PR (Recipe 6/2)

Machine: Direct Write Laser (DWL)

Mask: uchipnewl4 **Map:** uchip

Alignment mark position: X=168 Y=55.7

Distance between alignment mark: X=6910

4 dies in wafer with 1inch **Energy:** 77.5%

Power: 120mW

Focus: 60

Develop: Recipe 6/2 **Development time:** 1 min

Optical Inspection:

Sample	Comments
SV976	OK

STEP 12	Au Pad Deposition	Date: 28/11/2012

Machine: Alcatel

Cr Deposition: 50 Å
1min (50Å) 20W

Deposition Time	Cr thickness (A)	Ar gas flow (sccm)	Pressure (mT)	Power Source DC (W)
1m15s	50	20	24	20

Au Deposition: 400Å
3min (400Å) 20W

Deposition Time	Au thickness (A)	Ar gas flow (sccm)	Pressure (mT)	Power Source DC (W)
3m30s	400	20	24	20

STEP 13	Au Lift-off	Date: 29/11/2012

Hot µ-strip + ultrasonic
Rinse with IPA + DI water + dry compressed air

Started: 09h00

Stopped: 10h40

Total Time in hot µ-strip: 4x20min

Ultrasonic Time: 2x10min

Optical Inspection:

Sample	Comments
SV976	OK

Appendix II

Run Sheet Photoresist Profile Optimization

STEP 1	**1st Exposure** –Contact Leads Definition	**Date:** 27-28/09/2012

Coating PR: Vapor Prime 30 min (Recipe - 0) coat 1.5 µm PR (Recipe 6/2)

Machine: Direct Write Lase (DWL)

Mask: uchipnewl2 **Map:** uchip

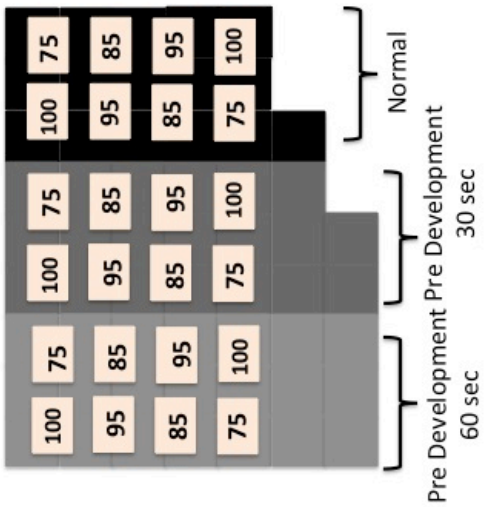

Die dimensions: X=7600 Y=6400

Alignment mark position: X=168 Y=55.7

Energy: Varying between 75%, 85%, 95% and 100%.

Power: 120mW

Focus: 60

Develop: Recipe 6/2

Development time: 1 min

Optimization Comments:

- In first sample the lithography process occurs normally just varying the energy between 75% and 100%.
- Second sample is submitted to pre-development, before of the exposure, during 30 seconds varying the energy between 75% and 100%.
- Third sample is submitted to pre-development, before of the exposure, during 60 seconds varying the energy between 75% and 100%.
- Dies position is presented in illustrative figure with respective energy that is applied.

Optical Inspection:

Sample	Comments
PR Profile	**Normal**: OK **Pre-development 30 sec**: One die not presents good development **Pre-development 60 sec**: Some dies present over development

STEP 2	Contacts Leads deposition	Date: 01/10/2012

Machine: Nordiko 3600
Al deposition: 3000 Å

Deposition Gun	Power (W)	V^+(V)	I^+(mA)	V^- (V)	I^- (mA)	Xe flow (sccm)	Pan (deg)	Rotation (%)
Set Values	170	1200	171	275	-	4	180	30
Read Values	156	1178	171	270	2	4.1	180	30

Optical Inspection:

Sample	Comments
SV976	OK

STEP 4	Aluminium Lift-off	**Date:** 03-08/10/2012

Hot µ-strip + ultrasonic
Rinse with IPA + DI water + dry compressed air

Started: 03/10/2012 **Stopped:** Depending of the sample

Total Time in hot µ-strip: 4x20 min **Ultrasonic Time:** 2x10 min

Optical Inspection:

Sample	Comments
PR Profile	**Normal**: With this time the lift-off is incomplete. It was necessary more two days. But when the lift-off was completed some contacts were lost in several dies. **Pre-development 30 sec**: With 80min in hot µ-strip and 20min of ultrasound the lift-off is completed in all dies. However the results are better in some dies than others depending of energy used in exposure. **Pre-development 60 sec**: With 80min in hot µ-strip and 20min of ultrasound the lift-off is completed in all dies. However the results are better in some dies than others depending of energy used in exposure.

Appendix III

Run Sheet Passivation Layer Optimization

STEP 1	**1st Exposure** – First Layer Mettalization	**Date:** 30/11/2012

Coating PR: Vapor Prime 30 min (Recipe - 0) coat 1.5 µm PR (Recipe 6/2)

Pre-development: 20 sec

Machine: Direct Write Laser (DWL)

Mask: testuchipL2

Map: uchip

Die dimensions: X=7600 Y=6400

Alignment mark position: X=168 Y=55.7

Distance between alignment mark: X=6978

Energy: 95%

Power: 120mW

Focus: 60

Develop: Recipe 6/2

Development time: 1 min 50 sec

Optical Inspection:

Sample	Comments
2	OK

STEP 2	**Aluminium Deposition**	**Date:**03/12/2012

Machine: Nordiko 3600
Al deposition: 3000 Å

Deposition Gun	Power (W)	V^+(V)	I^+(mA)	V^- (V)	I^- (mA)	Xe flow (sccm)	Pan (deg)	Rotation (%)
Set Values	170	1200	171	275	-	4	180	30
Read Values	156	1178	171	270	2	4.1	180	30

Optical Inspection:

Sample	Comments
SV976	OK

STEP 3 Aluminium Lift-off Date: 03/12/2012

Hot µ-strip + ultrasonic
Rinse with IPA + DI water + dry compressed air

Started: 12h00 **Stopped:** 13h40

Total Time in hot µ-strip: 4x20min **Ultrasonic Time:** 2x10min

Optical Inspection:

Sample	Comments
2	OK

STEP 4 Oxide Deposition **Date:** 04/12/2012

Machine: Electrotech

Sample 2			
SiO_2 (CVD)		**SiN (CVD)**	
Start	**End**	**Start**	**End**
04/12	04/12	04/12	04/12

- Must always use a calibration sample.

SiO_2 deposition: 3000 Å
Holder: 300ºC
Showerhead: 350ºC

	Deposition Time	**NH_3 gas flux (sccm)**	**SiH_4 gas flux (sccm)**	**N_2 gas flux (sccm)**	**Pressure (mT)**	**Power Source RF (W)**
Read Values						

SiN deposition: 3000 Å

1min 14 sec (3000 Å)
Holder: 300ºC
Showerhead: 350ºC

	Deposition Time	NH_3 gas flow (sccm)	SiH_4 gas flow (sccm)	N_2 gas flow (sccm)	Pressure (mT)	Power Source RF (W)
Read Values	1min 14sec	500	300	3500	850	500

STEP 5 **2nd Exposure** – Passivation Layer Definition **Date:** 04/12/2012

Coating PR: Vapor Prime 30 min (Recipe - 0) coat 1.5 µm PR (Recipe 6/2)

Machine: Direct Write Laser (DWL)

Mask: testuchipL3niv

Map: uchip

Die dimensions: X=7600 Y=6400

Alignment mark position: X=168 Y=55.7

Distance between alignment mark: X=6978

Energy: 75%

Power: 120mW

Focus: 60

Develop: Recipe 6/2

Development time: 1 min

Optical Inspection:

Sample	Comments
2	OK

STEP 6 **Ion Milling –** Passivation Layer Etching **Date:** 05/12/2012

Machine: Nordiko 3600
3000A (etch rate: assuming 2Å/s)
Time - 13x230s

Standard Etching Recipe (Etch Junction Stack all):

Assist Gun	Power (W)	V^+(V)	I^+(mA)	V^- (V)	I^- (mA)	Ar flux (sccm)	Pan (deg)	Rotation (%)
Set Values	-	735	105	350	-	10	60	30
Read Values	212	724.3	104.5	344.3	2.7	10.2	60	30

Optical Inspection:

Sample	Comments
2	OK

Electrical Probes Measurements

Sample	Comments
2	OK

STEP 7 **Resist Stripping** **Date:** 05/12/2012

Hot µ-strip + ultrasonic
Rinse with IPA + DI water + dry compressed air

Started: 16h00 **Stopped:** 17h30

Total Time in hot µ-strip: 3x20min **Ultrasonic Time:** 3x10min

Optical Inspection:

Sample	Comments
2	OK

STEP 8 **3rd Exposure -** Second Layer Metallization **Date:** 07/12/2012

Coating PR: Vapor Prime 30 min (Recipe - 0) coat 1.5 µm PR (Recipe 6/2)

Pre-development: 20 sec

Machine: Direct Write Laser (DWL)

Mask: testuchipL4 **Map:** uchip

Die dimensions: X=7600 Y=6400

Alignment mark position: X=168 Y=55.7

Distance between alignment mark: X=6978

Energy: 95%

Power: 120mW

Focus: 60

Develop: Recipe 6/2

Development time: 1 min 50 sec

Optical Inspection:

Sample	Comments
2	OK

STEP 9 Aluminium deposition **Date:** 10/12/2012

Machine: Nordiko 3600
Al deposition: 3000 Å

Deposition Gun	Power (W)	V^+(V)	I^+(mA)	V^- (V)	I^- (mA)	Xe flow (sccm)	Pan (deg)	Rotation (%)
Set Values	170	1200	171	275	-	4	180	30
Read Values	156	1178	171	270	2	4.1	180	30

Optical Inspection:

Sample	Comments
2	OK

STEP 8 Aluminum Lift-Off Date:

Hot µ-strip + ultrasonic
Rinse with IPA + DI water + dry compressed air

Started: 12h00

Stopped: 13h40

Total Time in hot µ-strip: 4x20min

Ultrasonic Time: 2x10min

Optical Inspection:

Sample	Comments
2	OK

Appendix IV

Run Sheet Passivation Layer Optimization Results

Oxide Breakdown	Date:

Test Goal: To find the oxide disruption voltage.

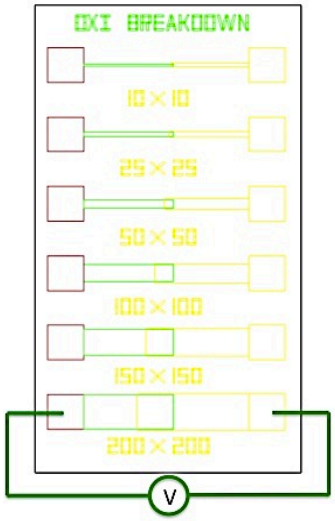

Procedure Test:

- Put the electrical probes in pads of different areas just like showed in figure.
- Verify if there is contact (short circuit) or not (open circuit).
- If open circuit is checked, apply a voltage in pads using an external voltage source.
- Increase the voltage until breakdown voltage.
- Do the same procedure for all pads with different areas.

Attention:

- Never put the electrical probes in pads with open circuit. The probes should always be short circuited in order to remove eventual charges accumulated on the leads.
- You have to ensure that the instrument is not in current controlled mode.

Results:

Sample:

Passivation Layer:
Machine:

Area [μm]	Disruption Voltage [V]			
200x200				
150x150				
100x100				
50x50				
25x25				
10x10				

Optical Inspection:

Sample	Comments

Graphic Results:

MET Overlay	Date:

Test Goal: To check metal overlay and voltage disruption corresponding.

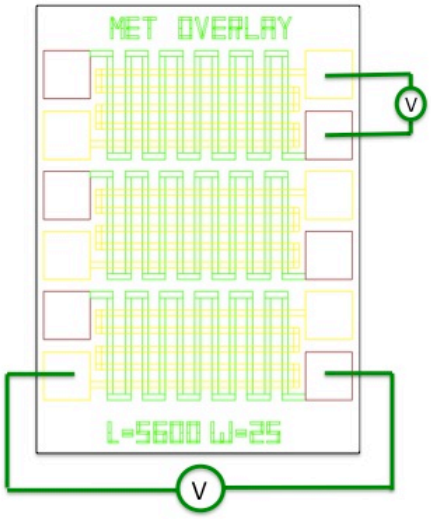

Procedure Test:

- Put the electrical probes in pads of each serpentine corresponding to each metallization layers.
- Verify if there is contact (short circuit) or not (open circuit).
- The expected case is to have an open circuit. This means that no current flows through passivation layer and the selected oxide is a good isolator.
- If an open circuit is observed inject a voltage until 10V to evaluate the operation mode of serpentines.

Attention:

- You should test all serpentines to obtain a statistical result.
- This measurement should be always made between pads of different serpentines.

Results

Sample:

Passivation Layer:
Machine:

Operation mode	MET Overlay											
Short Circuit Open Circuit												
Voltage												

Optical Inspection:

Sample	Comments

Results Appreciation:

Sample	Comments

Graphic Results:

Resistivity	Date:

Test Goal: To calculate the metal resistivity.

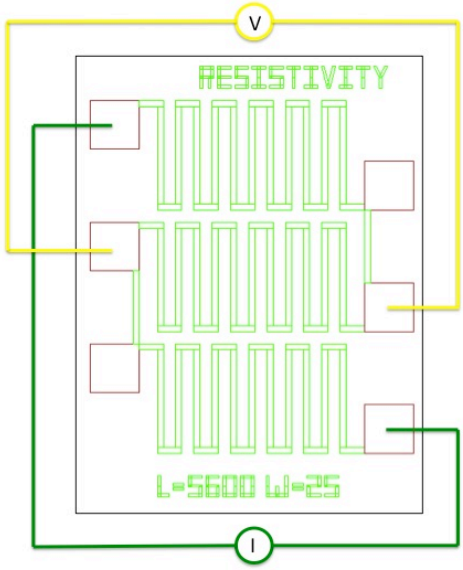

Procedure Test:

- Inject current on external pads and measure voltage on middle pads.
- Inject a current of 1mA.
- Register the voltage value.
- Calculate the resistance value using Ohm's Law:

$$R = \frac{V}{I}$$

- Then calculate the resistivity using this equation:

$$\rho = R\frac{t \times w}{L}$$

Results:

Sample:

Passivation Layer:
Machine:

Resistance [Ω]	Resistivity [Ω.m]

Optical Inspection:

Sample	Comments

Results Appreciation:

Sample	Comments

Graphic Results:

Fluid Tests	Date:

Test Goal: To evaluate the oxide in contact with a buffer solution, using or not UVO cleaner.

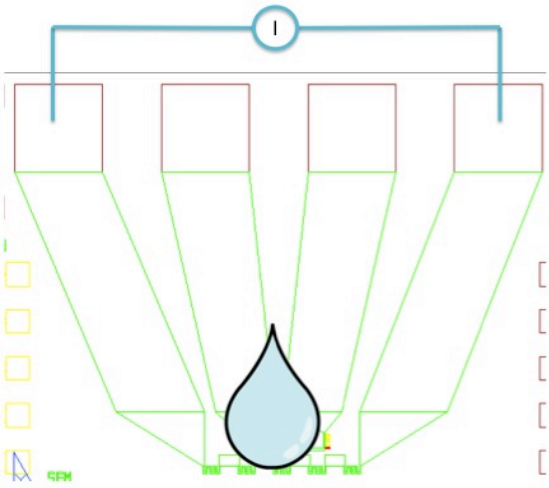

Procedure Test:

- Put the electrical probes in external pads.
- Verify if there is contact (short circuit) or not (open circuit).
- If a short circuit is observed apply a 6V voltage that corresponding a 150mA.
- Put the buffer solution (5µl/10µl (depending the surface) of phosphate buffer (PB) in contact with current lines and register the current variation during the time

Attention:

- When the current is zero means that current lines were disrupted.
- If the oxide holds the buffer phosphate during 1h30min should be made the same test with PBS, a solution more saline.
- Never put the biological fluid in contact with pads.
- Repeat the experience using UVO cleaner before tests.

Results: Sample non exposed to UVO cleaner

Sample:

Passivation Layer:
Machine:

	Phosphate Buffer	Phosphate Buffer Saline
Time (min)		

Results: Sample exposed to UVO cleaner:

Sample:

Passivation Layer:
Machine:

	Phosphate Buffer	Phosphate Buffer Saline
Time (min)		

Graphic Results: